Overlapping multidomain paired quasilinearization methods for solving boundary layer flow problems

---

Mpho Mendy Nefale

Supervisor(s):
Dr. Olumuyiwa Otegbeye
Dr. Shina Daniel Oloniiju

A dissertation submitted in fulfillment of the requirements for the degree of
Master of Science Computational and Applied Mathematics
in the school of
Computer Science and Applied Mathematics,
University of the Witwatersrand, Johannesburg
9 June 2024

Abstract

There is a constant and continuous need to refine current numerical approaches used to solve non-linear differential equations, which are employed to model real-world problems that often do not have analytical solutions. Spectral-based techniques have proven to be one of the most efficient numerical techniques for finding solutions of differential equations. Numerous spectral-based linearization techniques have been developed, such as the spectral relaxation (SRM), the spectral local linearization (SLLM), the spectral quasilinearization (SQLM), and the paired quasilinearization (PQLM) methods, among others. Previous research suggests that the PQLM is an efficient approach for solving complex non-linear systems of ordinary (ODEs) and partial differential equations (PDEs). However, it has been observed that this method requires further enhancement when utilized for problems described over a large domain, be it temporal or spatial. This research aims to address this limitation by proposing a modified version of the PQLM called the overlapping multi-domain paired quasilinearization method (OMD-PQLM), that enhances the accuracy and convergence speed of the original approach. The new approach entails solving a system by a technique that involves decoupling the system into pairs of equations and partitioning the large domain into smaller overlapping sub-domains. A comparison between the OMD-PQLM and the PQLM is conducted by solving systems of ODEs and PDEs. The proposed numerical approach is evaluated based on the norms of the residual and convergence errors, computational time, and the influence of the number of grid points and sub-domains on the convergence speed of the iterative scheme and the accuracy of the solutions. The findings demonstrate that the OMD-PQLM remarkably improves the accuracy of the solution compared to the PQLM, suggesting that partitioning the problem domain into overlapping multiple-domains optimizes the performance of the PQLM.

Declaration

I, Mpho Mendy Nefale, certify that this is entirely my work. It is being submitted for the degree of Master of Science Computational and Applied Mathematics at the University of the Witwatersrand, Johannesburg. It has not been submitted for any degree or examination at another university.

Mpho Mendy Nefale	Dr. O. Otegbeye	Dr. S.D. Oloniiju
Candidate	Supervisor	Co-supervisor
9 June 2024	9 June 2024	9 June 2024

Dedication

To my parents, Rudzani and Mpho, as well as my brothers, Livhuwani, Fhumulani, Omphilisa, and Mukhoro.

Acknowledgements

I begin by expressing my deepest gratitude to God—Father, Son (Jesus Christ, my Lord and Savior), and Holy Spirit, for His guidance, strength, and blessings throughout this journey. My heartfelt thanks to my supervisors, Dr. Olumuyiwa Otegbeye and Dr. Shina Daniel Oloniiju, for their exceptional guidance, encouragement, and unwavering support throughout the dissertation journey. Their expertise, patience, and unwavering dedication have been instrumental in shaping this work and helping me navigate the complexities of academic research. I am truly fortunate to have had the opportunity to learn from them and am deeply appreciative of their mentorship. I am also thankful to the School of Computer Science and Applied Mathematics, University of the Witwatersrand, for providing the necessary resources and facilities for conducting my research. I extend my gratitude to my family for their unwavering support and understanding during this journey. Special thanks to BANKSETA for the financial support that made this research possible. I also want to acknowledge my colleagues for their support and helpful discussions. Lastly, I would like to express my appreciation to all those who have contributed to this work in one way or another.

Contents

List of Figures

List of Tables

Chapter 1

Introduction

Real-world problems provide challenges that need to be addressed. A suitable approach is modelling such problems using mathematical equations. Mathematical models have proven to be invaluable in a variety of fields, including financial modelling, medical research, and engineering [1, 2, 3, 4], among others. The increasing complexities of these problems often result in systems of highly non-linear differential equations that are, in most cases, impossible or tedious to solve analytically [5]. Numerical methods transform continuous functions and their derivatives to their corresponding discrete form [6, 7, 8]. For non-linear differential equations, this might involve developing an iterative scheme [9]. Iterative methods work by using a previous solution to obtain an updated solution, and the process continues until a convergence or stopping condition is met [6].

The idea of numerical methods is not new. Numerical methods are almost as old as human civilization [10]. Archimedes of Syracuse between 287 and 212 BC created the method of estimating area, length, and volume for geometric figures, which is known as the method of exhaustion [10]. Some ancient Greek mathematicians made further advances in numerical approaches; in particular, Eudoxus of Cnidus improved the method of exhaustion for estimating areas, lengths, and volumes of geometric shapes [11]. This method of exhaustion is similar to modern numerical integration when used to find approximations. Newton and Leibniz had a significant impact on the formulation of calculus by developing numerical methods that led to an accurate understanding of mathematical models for real-world problems, beginning with physical sciences and progressing to engineering, medicine, business, and other sciences [10, 11]. Newton invented several numerical approaches for solving a range of problems, and his name is still associated with various extensions and modifications of his original concept [12]. Many notable mathematicians of the 18th and 19th centuries, such as Joseph-Louis Lagrange, Carl Friedrich Gauss, and Leonhard Euler, contributed significantly to the development of numerical methods [13, 14, 15]. In the year 1755, Euler [16] invented the difference method for one-spatial dimensional problems, which was later extended to two-dimensional problems by Runge in 1908 [17]. In the year 1928, Courant *et al.* [18] used the finite difference approach to estimate solutions to a mathematical physics problem. The discrete analogue of Dirichlet's theory was used in the research to apply a five-point approximation to discretize the Laplace equation [18]. The error of convergence was not computed in the study by Courant *et al.* [18] because the study's major goal was to prove the existence of numerical solutions. Marfurt [19] approximated the solution of the wave equation using the finite difference approach. The significance of this study's discoveries on the approximation of time-dependent problems has had a tremendous impact on numerical techniques for partial differential equations (PDEs). In the year 1930, the error bounds for difference approximation for elliptic problems were derived for the first time by Gerschgorin [20]. The study by Gerschgorin [20] was heavily based on a discrete counterpart of the maximum principle for the Laplace equation. Gerschorin's technique was used by Wasow *et al.* [21] in 1957 to analyze several elliptic equations and their boundary conditions.

After World War II, there was a huge improvement in time-dependent problems because computers enabled a multitude of practical applications. Crank and Nicolson [22] developed the use of implicit methods for solving initial boundary value problems in 1947. There was an increase in the development of finite difference methods for broad initial value problems in the 1950s and 1960s. The theorem of Lax equivalence was established during this period [23]. For hyperbolic functions, the finite difference was also used, specifically for non-linear differential equations [24]. Finite difference has continued to play an important role to date. Following these, mathematicians like Birkhoff *et al.* [25] analyzed the finite difference methods for piecewise polynomial functions and finite element methods for more complicated problems. In fluid dynamic problems and on higher-order elliptic equations, finite difference methods are useful and have been applied [26, 27, 28]. Using the idea of finite difference, other methods were developed shortly after; among them, the collocation method. Instead of an orthogonality condition, a collocation method searches for an approximation function in a space of finite elements by solving the differential equation at a finite number of collocation points [29]. For spectral methods, globally defined functions such as eigenvalue solutions of the Sturm–Liouville problem are used instead of piecewise polynomial functions [30].

In the last two decades, spectral methods have advanced rapidly. In several disciplines such as quantum mechanics, fluid dynamics, heat transfer, among others, these methods have been successfully applied [31, 32, 33, 34, 35]. Among numerical methods, spectral-based methods stand out as some of the highly effective numerical techniques for solving differential equations [36, 37]. In the year 1961, Steven Orszag developed spectral methods in a long series of papers [37, 38]. The fundamental idea of spectral methods is to represent solutions to differential equations as linear combinations of certain trial or basis functions. Spectral methods and finite difference methods are closely related, and they are both developed using a similar idea [39, 40]. What distinguishes these methods is the utilization of basis functions in spectral methods, which are non-zero global infinitely differentiable functions on the whole domain, whereas finite difference methods use them on small sub-domains [41, 42]. It is for this reason that spectral methods are called global methods because they approximate a function on its entire domain instead of in an infinitesimal domain. Spectral methods have been reported to have an exponential rate of convergence and good error properties, especially for differential equations with smooth solutions [43]. Various differential equations, viz., ordinary, partial, fractional, and similar problems involving differential equations have been solved through spectral methods [37, 38]. The hybridization of spectral methods with relaxation or linearization techniques has led to the creation and improvement of many numerical algorithms tailored for tackling highly non-linear differential equations. These methods include the spectral-based relaxation method (SRM), the spectral-based quasilinearization method (SQLM), the spectral-based local linearization method (SLLM), and the paired quasilinearization (PQLM), among others.

Motsa [44] introduced the SRM; which is a Chebyshev pseudospectral-based technique. The technique is shown to be highly effective in solving non-linear boundary layer flow problems [45, 46, 47]. The technique uses a concept akin to the Gauss-Seidel method to separate the differential equations via relaxation, leading to a decoupled set of linearized equations. The SRM converts a system of coupled equations into a sequence of decoupled equations, simplifying the process of solving the algebraic system. As a result, the SRM exhibits linear convergence and is computationally efficient [48]. The uncoupled system of linearized algebraic equations is then discretized through the Chebyshev pseudospectral technique. The SRM has been used for several problems [45, 49, 44]. Motsa *et al.* [48, 50] used the SRM for the solutions of time-dependent boundary layer flow problems and hyperchaotic systems. Compared to the SQLM and the Runge-Kutta-based MATLAB built-in solver, the SRM was shown to be more accurate and efficient. Motsa [45] applied the SRM to find a solution to a system of non-linear boundary layer flow equations and deduced that the technique is efficient, accurate, and straightforward to implement for such problems. Subba *et al.* [51] applied the SRM to solve solar energy problems and found that the method is significantly robust and more accurate than the Runge-Kutta method. Shateyi *et al.* [52] also found solutions to the thermal transfer and entropy emergence in the magnetohydrodynamic flow of Maxwell fluid, with the SRM, and verified that the method is accurate and converges rapidly.

The SQLM, as introduced by Motsa [48], is developed using the concept of Newton-Raphson's technique. The technique adopts the quasilinearization approach, proposed by Bellman and Kalaba [53], to linearize systems of non-linear equations, followed by numerical integration of the linearized equations through the Chebyshev spectral collocation approach. Magodoro *et al.* [54] employed the SQLM to resolve the equations characterizing the flow of a hydromagnetic nanofluid past a semi-infinite parallel plate and the technique was discovered to be accurate and rapidly convergent. Oyelakin *et al.* [55] employed the method to investigate the effect of non-linear thermal radiation in bioconvective Casson nanofluid flow. The approach demonstrated high efficiency and yielded precise results for the purpose of the study. The rate of convergence was improved by the successive overrelaxation method (SOR) [44]. The SLLM exhibits linear convergence as it transforms a system of coupled equations into a sequence of decoupled equations [56, 57].

There is a constant need for improving current numerical techniques. When seeking solutions to non-linear systems of ODEs and PDEs, the aforementioned spectral-based methods have proven to be effective and reliable. However, these methods also have limitations. The SRM exhibits computational efficiency, but a high number of iterations is required for convergence, compared to the SQLM. However, the SQLM converges quickly after a few iterations, although it is less computationally efficient. In an attempt to overcome the limitations, while maintaining speedy convergence and high accuracy, the paired quasilinearization method (PQLM) was introduced [58, 59]. The PQLM combines the advantages of both the SRM and the SQLM by transforming a coupled system into a decoupled paired sequence of equations. Additionally, it uses quasilinearization, enabling it to achieve quadratic convergence [59]. Using the PQLM, boundary layer flow problems, heat transfer in Casson nanofluids with Hall effects, and magnetohydrodynamic flow were successfully solved [59, 60]. The method gave more accurate results in some instances compared to the other methods, while achieving quick convergence. Otegbeye and Motsa [59] used the PQLM to solve a boundary layer problem, and the results were found to be very close to the exact solution when compared to the solution found using the SLLM. Otegbeye *et al.* [61, 62] applied the PQLM to double-diffusive convection flow over a cone embedded in a porous medium in the presence of nanoparticles. The PQLM has been proven to be effective, and capable of producing accurate numerical results with a rapid rate of convergence. Otegbeye [63] implemented the PQLM to approximate the solutions of ODEs and PDEs. The PQLM was found to be more accurate than the SLLM.

Studies such as [59] have shown that solving systems of ODEs and PDEs for large domains can be computationally demanding. In these situations, methods such as the SLLM [57], PQLM [58], and SQLM [48] are known for their computational expense. Domain decomposition-based spectral methods were introduced to overcome such challenges. Motsa and Animasun [58] developed the multi-domain quasilinearization method, and the multi-domain bivariate pseudo-spectral quasilinearization method (MD-BSQLM) [64, 65]. Magagula *et al.* [66] used the MD-BSQLM to solve non-linear PDEs, and the MD-BSQLM demonstrated the capability to produce accurate results in a few seconds for problems defined in a large domain.

Spectral collocation methods with overlapping grids are also applicable for solving problems with large domains. Mutua and Motsa [67] introduced the idea of splitting the interval of integration using the overlapping approach. The idea was used on the SQLM to determine the solution of the steady two-dimensional laminar flow of an electrically conducting, viscous fluid with constant density and volume over a continuously deformable sheet. The findings demonstrate the method's high level of accuracy and computational efficiency [67]. Mkhatshwa *et al.* [68] developed a method called the overlapping multi-domain bivariate spectral quasilinearization method (OMD-BSQLM). The method applies the technique of multi-domain in both time and space intervals. Mkhatshwa *et al.* [69] applied the OMD-BSQLM to magnetohydrodynamic mixed convection slip flow and the method was found to be accurate for this kind of boundary value problem. The OMD-BSQLM was used to determine solutions for systems of non-linear PDEs in fluid mechanics, demonstrating to be accurate and computationally efficient [70]. The utilization of the overlapping approach has been determined to enhance the accuracy of existing spectral-based methods [71]. Augmenting the number of overlapping intervals contributed to improved accuracy.

This dissertation aims to introduce the overlapping multidomain paired quasilinearization method (OMD-PQLM) for boundary value problems. The OMD-PQLM uses the concept of the PQLM, however, the problem's domain is subdivided into superimposed subintervals. The performance of the OMD-PQLM is compared to the PQLM. The objectives of this dissertation include

1. Formulating numerical schemes based on the OMD-PQLM for ODES.
2. Formulating numerical schemes based on the OMD-PQLM for PDEs that use overlapping approach in both space and time.
3. Performing a comparison analysis of the PQLM and OMD-PQLM using the infinity norm of the solution error and residual error to investigate their respective convergence speeds and method accuracies.
4. Investigating the combination of equations that yields a more accurate and quicker convergence speed for the solutions.

5. Investigating how the number of collocation points and overlapping intervals affects accuracy using the residual error's infinity norm.

The rest of this chapter outlines the general procedures we used throughout this dissertation. This chapter also describes the OMD-PQLM for a general system comprising M differential equations with M unknowns.

1.1 Taylor Series Expansion for Multivariable Functions

Consider a function $g(\omega_1, \omega_2, \ldots, \omega_N)$ that is infinitely differentiable within an open neighborhood around the point $(\omega_1, \omega_2, \ldots, \omega_N) = (\bar{a}_1, \bar{a}_2, \ldots, \bar{a}_N)$. In this context, g is defined within the domain of real-valued functions in N dimensions. The Taylor series expansion of $g(\omega_1, \omega_2, \ldots, \omega_N)$ centered at $(\bar{a}_1, \bar{a}_2, \ldots, \bar{a}_N)$ is the process of representing g using a first-order polynomial approximation. The expression for the Taylor series of $g(\omega_1, \omega_2, \omega_3, \ldots, \omega_N)$ is given by:

$$
\begin{aligned}
g(\omega_1, \omega_2, \omega_3, \ldots, \omega_N) &\approx g(\bar{a}_1, \bar{a}_2, \bar{a}_3, \ldots, \bar{a}_N) + \left.\frac{\partial g}{\partial \omega_1}\right|_{\bar{\mathbf{a}}} (\omega_1 - \bar{a}_1) \\
&+ \left.\frac{\partial g}{\partial \omega_2}\right|_{\bar{\mathbf{a}}} (\omega_2 - \bar{a}_2) + \cdots + \left.\frac{\partial g}{\partial \omega_N}\right|_{\bar{\mathbf{a}}} (\omega_N - \bar{a}_N) \\
&= g|_{\bar{\mathbf{a}}} + \sum_{i=0}^{N} \left.\frac{\partial g}{\partial \omega_i}\right|_{\bar{\mathbf{a}}} (\omega_i - a_i),
\end{aligned}
$$

where $\frac{\partial}{\partial \omega_i}$ represents the partial derivative in relation to ω_i ($i = 1, \ldots, N$).

1.2 Quasilinearization Method

The computational approach known as the quasilinearization method (QLM) integrates procedural algorithms with linear approximation techniques. The QLM was initially introduced by Bellman and Kalaba [72] as an advanced version of the traditional Newton-Raphson method. This method was developed to address non-linear ODEs and PDEs, providing solutions to the challenges posed by the complexities of non-linear models in physics [73]. One noticeable feature of the QLM is its second-order convergence often in a predictable manner [74]. A noteworthy observation by

Mandelzweig and Tabakin [73] is that the QLM starts by considering non-linearity from the beginning of each iteration, achieved by adjusting the differential operator.

The QLM's applicability is broad and versatile. It effectively addresses Lane-Emden equations [73] and extends its applicability to tackle problems like the Duffing, Blasius, and Thomas-Fermi equations [73]. Investigations in the field of quantum mechanics undertaken by Krivec and Mandelzweig [74] highlight the usefulness of the QLM, especially in ensuring numerical convergence and stability. Additionally, the QLM was used in solving multi-point boundary value problems [75], non-linear differential equations of order two [76, 77, 78, 79], periodic boundary value problems [80], convex functions [74], and non-linear optimal control problems [81], showcasing its versatility across various fields.

1.3 Gauss-Seidel Method

One of the most widely used methods for solving systems of linear equations is the Gauss-Seidel iterative numerical approach. It falls under the umbrella of iterative methods for solving non-linear systems and is known for its simplicity and efficiency, particularly when dealing with sparse matrices [82]. The method iteratively refines an initial guess for the solution until a certain convergence criterion is met. In each iteration, the Gauss-Seidel method updates each component of the solution vector using the most recent values of the other components [83]. The general formulation of the Gauss-Seidel method can be expressed as follows:

In the context of a system of linear equations represented as $M\mathbf{x} = \mathbf{b}$, where M is a square matrix, $\mathbf{x}$ denotes the solution vector, and $\mathbf{b}$ is the vector on the right-hand side, the Gauss-Seidel iteration for updating the components of x is given by:

$$x_i^{(k+1)} = \frac{1}{m_{ii}} \left(b_i - \sum_{j=1}^{i-1} m_{ij} x_j^{(k+1)} - \sum_{j=i+1}^{n} m_{ij} x_j^{(k)} \right) \tag{1.1}$$

Here, $x_i^{(k+1)}$ represents the $i - th$ element of the solution vector in the $(k+1) - th$ iteration, m_{ij} represent the elements of matrix M, and n signifies size of the system [84].

1.4 Residual Error and Solution Error

Approximating solutions to differential equations results in an occurrence of residual errors [85]. We consider an equation given by,

$$Kv = l, \tag{1.2}$$

with the approximate solution $\bar{v}$. The residual error is defined as

$$res(v) = K\bar{v} - l, \tag{1.3}$$

given that $\bar{v}$ is a sufficient approximation of Equation (1.2). For this study, the error residual's infinity norm is computed.

The solution error is obtained by measuring the discrepancy between consecutive approximations. The norm of the solution error is computed as follows:

$$\text{solution error } = \|\bar{v}_n - \bar{v}_{n-1}\|\,, \tag{1.4}$$

and for the purpose of this study, we take the infinity norm

$$\text{solution error } = \|\bar{v}_n - \bar{v}_{n-1}\|_\infty\,, \tag{1.5}$$

where $\bar{v}_n$ denotes the solution obtained in the current iteration, and $\bar{v}_{n-1}$ represents the solution obtained in the previous iteration. The double vertical bars $|| \cdot ||$ symbolize the norm, providing a scalar value that quantifies the magnitude of the difference between the solutions. Using the infinity norm to measure solution error effectively captures the error value with the largest absolute magnitude between consecutive approximations, ensuring precise control over the largest error component. This approach allows us to effectively investigate the convergence behavior of the iterative process. When we compare the solution from the current iteration with that of the previous iteration, we acquire valuable insights into the convergence of the solution.

1.5 Description of the OMD-PQLM

This segment outlines the implementation of the OMD-PQLM for a general system comprising M equations with M unknowns. We note that the method description caters to both PDEs and ODEs, though we exclude the time, μ, for the ODEs.

We consider a PDE given by the following:

$$g\Big[\mathbf{v}_1(\alpha,\mu)\Big] = 0, \quad \alpha \in [\alpha_0, \alpha_f], \quad \mu \in [\mu_0, \mu_f], \tag{1.6}$$

where $\mathbf{v_1}$ is the set of the unknown function and its spatial and temporal domains defined as

$$\mathbf{v}_1 = \left\{ v_1, \frac{\partial v_1}{\partial \alpha}, \ldots, \frac{\partial^{h-1} v_1}{\partial \alpha^{h-1}}, \frac{\partial^h v_1}{\partial \alpha^h}, \frac{\partial v_1}{\partial \mu}, \frac{\partial^2 v_1}{\partial \alpha \partial \mu} \right\}, \tag{1.7}$$

with h being the highest derivative. In Equation (1.7), $\mathbf{v_1}$ is assumed to be a continuously differentiable function.

Further consideration involves a system of M PDEs in M unknowns, given as

$$\mathbf{G}_l\Big[\mathbf{v}_1(\alpha,\mu), \mathbf{v}_2(\alpha,\mu), \ldots, \mathbf{v}_M(\alpha,\mu)\Big] = 0, \quad l = 1, 2, \ldots, M. \tag{1.8}$$

Equation (1.8) signifies a coupled non-linear system of PDEs, where M is a non-linear operator and $\mathbf{G}_l$ represents each equation for $l = 1, \cdots, M$. $\{\mathbf{v}_1, \mathbf{v}_2, \ldots, \mathbf{v}_M\}$ is a set that contains

$$\left[\left\{ v_1^{(0)}, v_1^{(1)}, \ldots, v_1^{(h_1)} \right\}, \ldots, \left\{ v_M^{(0)}, v_M^{(1)}, \ldots, v_M^{(h_M)} \right\} \right].$$

1.5.1 Paired Quasilinearization Method

This segment shows the implementation of the PQLM to the general system (1.8). Although random combinations can also be used for pairing, an ordered pairing will be used to demonstrate how the PQLM is implemented. Assume that $\mathbf{v}_1$ and $\mathbf{v}_2$ are the first pairing. In order to obtain a linearized pair, the QLM is applied to Equations $\mathbf{G}_1(\mathbf{v}_1, \mathbf{v}_2, \cdots, \mathbf{v}_M)$ and $\mathbf{G}_2(\mathbf{v}_1, \mathbf{v}_2, \cdots, \mathbf{v}_M)$. Similarly, the process is applied for successive pairs, incorporating improved solutions from preceding pairs to iteratively update the succeeding pairs. Generally, the pairing assumes the following structure:

$$\mathbf{G}_w\left[\alpha, \mathbf{v}_1, \cdots, \mathbf{v}_M\right] = 0, \quad w = \Big\{\{1,2\},\{3,4\},\dots,\{M-1,M\}\Big\}. \tag{1.9}$$

In order to linearize the system, a first-order Taylor series expansion is truncated for each pairing in the system using quasilinearization approach. This is achieved by selecting approximating points $(\mathbf{v}_1, \mathbf{v}_2, \cdots, \mathbf{v}_N)$ and then performing the expansion such that

$$\begin{aligned}\mathbf{G}_w\Big[\left(\mathbf{v}_{1,r},\dots,\mathbf{v}_{M,r}\right) + \Delta\left(\mathbf{v}_1,\dots,\mathbf{v}_M\right)\Big] &\approx \mathbf{G}_w\left[\mathbf{v}_{1,r},\dots,\mathbf{v}_{M,r}\right] \\ &+ \sum_{p=0}^{h_{w,w}} \frac{\partial^{(p)}\mathbf{G}_w\left[\mathbf{v}_{1,r},\dots,\mathbf{v}_{M,r}\right]}{\partial v_w^{(p)}}\left(\Delta\mathbf{v}_w^{(p)}\right),\end{aligned} \tag{1.10}$$

$$w = \Big\{\{1,2\},\{3,4\},\dots,\{M-1,M\}\Big\}, \tag{1.11}$$

where $\Delta\mathbf{v}_w^{(p)} = \mathbf{v}_{w,r+1}^{(p)} - \mathbf{v}_{w,r}^{(p)}$ and each pair $\frac{\partial^{(p)}\mathbf{G}_w\left(\mathbf{v}_{p,r}\right)}{\partial\mathbf{v}_w^{(p)}}$ represent a 2×2 Jacobian matrix. The complete representation of the expansion in Equation (1.10) is articulated in Equation (1.12) in the following manner:

$$\begin{aligned}&\mathbf{G}_w\Big[\left(\mathbf{v}_{1,r},\dots,\mathbf{v}_{M,r}\right) + \Delta\left(\mathbf{v}_1,\dots,\mathbf{v}_M\right)\Big] \approx \\ &\qquad \mathbf{G}_w\left[\mathbf{v}_{1,r},\dots,\mathbf{v}_{M,r}\right] + \sum_{p=0}^{h_{w,w}} \frac{\partial^{(p)}\mathbf{G}_w\left[\mathbf{v}_{1,r},\dots,\mathbf{v}_{M,r}\right]}{\partial v_w^{(p)}}\left(\mathbf{v}_{w,r+1}^{(p)}\right) \\ &\qquad - \sum_{p=0}^{h_{w,w}} \frac{\partial^{(p)}\mathbf{G}_w\left[\mathbf{v}_{1,r},\dots,\mathbf{v}_{M,r}\right]}{\partial v_w^{(p)}}\left(\mathbf{v}_{w,r}^{(p)}\right), \\ &w = \Big\{\{1,2\},\{3,4\},\dots,\{M-1,M\}\Big\}.\end{aligned} \tag{1.12}$$

The expansion given in Equation (1.12) is incorporated into the system (1.9), resulting in the derivation of

$$\sum_{p=0}^{h_{w,w}} \frac{\partial^{(p)} \mathbf{G}_w \left[\mathbf{v}_{1,r}, \cdots \cdots \mathbf{v}_{M,r}\right]}{\partial v_w^{(p)}} \left(\mathbf{v}_{w,r+1}^{p}\right) = R_{w,r},$$
$$w = \Big\{ \{1,2\}, \{3,4\}, \ldots \{M-1, M\} \Big\} \tag{1.13}$$

where

$$R_{w,r} = \sum_{p=0}^{h_{w,w}} \frac{\partial^{(p)} \mathbf{G}_w \left[\mathbf{v}_{1,r}, \ldots, \mathbf{v}_{M,r}\right]}{\partial v_w^{(p)}} \left(\mathbf{v}_{w,r}^{(p)}\right) - \mathbf{G}_w \left[\mathbf{v}_{1,r}, \ldots, \mathbf{v}_{M,r}\right].$$

1.5.2 Overlapping Grids

The overlapping approach is applied to both spatial and temporal domains. The spatial interval of integration $[\alpha_0, \alpha_f]$ is split into z overlapping sub-domains, each of length L_α represented as

$$I_\psi = [x_0^\psi, x_{N_\alpha}^\psi] \quad \psi = 1, 2, 3, \ldots, z. \tag{1.14}$$

Each of these intervals is then discretized into a set of $N_\alpha + 1$ collocation points. Similarly, the time interval of integration $[\mu_0, \mu_f]$ is divided into κ overlapping subdomains, each of length L_μ denoted by

$$I_u = [t_0^u, t_{N_\mu}^u] \quad u = 1, 2, 3, \ldots, \kappa. \tag{1.15}$$

Within the I_ψ and I_u subintervals, the last two points overlap with the initial two points of the subsequent $I_{\psi+1}$ and I_{u+1} subintervals. These subintervals' lengths are consistently defined as

$$L_\alpha = \frac{\alpha_f - \alpha_0}{z + \frac{1}{2}(1-z)\left(1 - \cos\left(\frac{\pi}{N_\alpha}\right)\right)}, \tag{1.16}$$

$$L_\mu = \frac{\mu_f - \mu_0}{\kappa + \frac{1}{2}(1-\kappa)\left(1 - \cos\left(\frac{\pi}{N_\mu}\right)\right)}. \tag{1.17}$$

$N_\alpha + 1$ and $N_\mu + 1$ represent the collocation points used in each respective subinterval. We observe that the spatial domain's total length is given by

$$\alpha_f - \alpha_0 = 2L_\alpha - \rho + (2L_\alpha - 2\rho)\left(\frac{z}{2} - 1\right) = 2L_\alpha - \rho + (L_\alpha - \rho)(z-2). \tag{1.18}$$

Equation (1.18) is used to derive the formula in Equation (1.16), where the parameter ρ represents the overlapping distance.

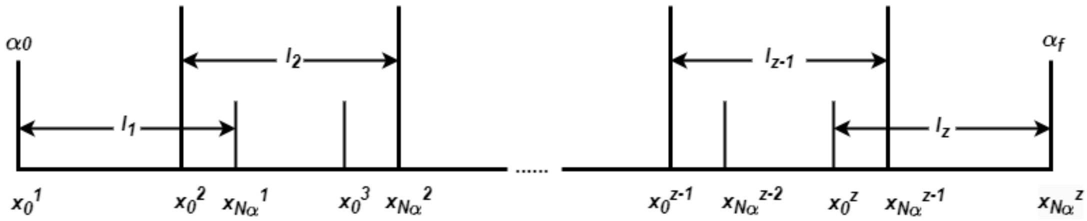

Figure 1.1: Overlapping grid on the spatial domain

Figure 1.1 shows the overlapping grid on the spatial domain. Notably, a comparable configuration is used for the temporal domain. It is observed that $\rho = x_0 - x_1$. Focusing on the initial interval I_1, where $\alpha \in \left[\alpha_0, x^1_{N_\alpha}\right]$ and the length $L_\alpha = x^1_{N_\alpha} - \alpha_0$, the application of the linear transformation $x = \frac{L_\alpha}{2}\zeta + \frac{\alpha_0 + x^1_{N_\alpha}}{2}$ facilitates the conversion of the interval $\left[\alpha_0, x^1_{N_\alpha}\right]$ into the standardized form $[-1, 1]$. Consequently, using the Gauss-Lobatto collocation points $\zeta_m = \cos\left(\frac{\pi m}{N_\alpha}\right)$, where $m = 0, 1, 2, 3, \ldots, N_\alpha$, we derive

$$\rho = x_0 - x_1 = \frac{L_\alpha}{2}(\zeta_0 - \zeta_1) = \frac{L_\alpha}{2}\left(1 - \cos\left(\frac{\pi}{N_\alpha}\right)\right). \tag{1.19}$$

As a result, Equation (1.18) transforms to

$$\alpha_f - \alpha_0 = \rho(1-z) + zL_\alpha = \frac{L_\alpha}{2}\left(1 - \cos\left(\frac{\pi}{N_\alpha}\right)\right)(1-z) + zL_\alpha. \tag{1.20}$$

Upon rearrangement, with L_α as the subject, it yields Equation (1.16). A similar approach is used to derive the expression representing the length of the temporal interval. Subsequently, in each sub-domain, we solve

$$\begin{aligned} &\sum_{p=0}^{h_{w,w}} \frac{\partial^{(p)} \mathbf{G}_w \left[\mathbf{v}_{1,r}^{(\psi,u)}, \ldots, \mathbf{v}_{M,r}^{(\psi,u)} \right]}{\partial v_w^{(p)}} \left(\mathbf{v}_{w,r+1}^{(p,\psi,u)} \right) = R_{w,r}, \\ &w = \Big\{ \{1,2\}, \{3,4\}, \ldots, \{M-1, M\} \Big\}, \end{aligned} \tag{1.21}$$

where

$$R_{w,r} = \sum_{p=0}^{h_{w,w}} \frac{\partial^{(p)} \mathbf{G}_w \left[\mathbf{v}_{1,r}^{(\psi,u)}, \ldots, \mathbf{v}_{M,r}^{(\psi,u)} \right]}{\partial v_w^{(p)}} \left(\mathbf{v}_{w,r}^{(p,\psi,u)} \right) - \mathbf{G}_w \left[\mathbf{v}_{1,r}^{(\psi,u)}, \ldots, \mathbf{v}_{M,r}^{(\psi,u)} \right]. \tag{1.22}$$

Prior to utilizing the spectral collocation technique within each distinct subinterval, the intervals I_ψ and I_u are converted to $\zeta \in [-1,1]$ and $\epsilon \in [-1,1]$ using

$$x_m^{\psi} = \frac{x_{N_\alpha}^{\psi} - x_0^{\psi}}{2} \zeta + \frac{x_{N_\alpha}^{\psi} + x_0^{\psi}}{2}, \quad \{\zeta_m\}_{m=0}^{N_\alpha} = \cos\left(\frac{\pi m}{N_\alpha} \right), \tag{1.23}$$

$$t_n^{u} = \frac{t_{N_\mu}^{u} - t_0^{u}}{2} \epsilon + \frac{t_{N_\mu}^{u} + t_0^{u}}{2}, \quad \{\epsilon_n\}_{n=0}^{N_\mu} = \cos\left(\frac{\pi n}{N_\mu} \right). \tag{1.24}$$

The overall number of collocation points across both the spatial and temporal domains, respectively, as derived by Mutua and Motsa [67] are given by

$$\begin{aligned} \tilde{M}_x &= N_\alpha + (N_\alpha - 1)(z - 1), \\ \tilde{M}_t &= N_\mu + \big(N_\mu - 1\big)(\kappa - 1), \end{aligned} \tag{1.25}$$

1.5.3 Spectral Collocation Method

This segment shows the implementation of the Chebyshev spectral collocation technique for addressing the system of Equations (1.21) in both spatial and temporal domains. We have the overlapping intervals I_ψ and I_u linearly transformed into $\zeta \in [-1,1]$ and $\epsilon \in [-1,1]$, respectively. The process of determining solutions $v_{1,r}(\zeta,\epsilon), \ldots, v_{M,r}(\zeta,\epsilon)$ for the system (1.21) involves utilizing bivariate Lagrange interpolation polynomials in the following form

$$
\begin{aligned}
v_1(\zeta,\epsilon) &\approx \sum_{m=0}^{N_\alpha}\sum_{n=0}^{N_\mu} v_1\left(\zeta_m,\epsilon_n\right)\mathbf{L}_m(\zeta)\mathbf{L}_n(\epsilon),\\
v_2(\zeta,\epsilon) &\approx \sum_{m=0}^{N_\alpha}\sum_{n=0}^{N_\mu} v_2\left(\zeta_m,\epsilon_n\right)\mathbf{L}_m(\zeta)\mathbf{L}_n(\epsilon),\\
&\vdots\\
v_M(\zeta,\epsilon) &\approx \sum_{m=0}^{N_\alpha}\sum_{n=0}^{N_\mu} v_M\left(\zeta_m,\epsilon_n\right)\mathbf{L}_m(\zeta)\mathbf{L}_n(\epsilon),
\end{aligned}
\tag{1.26}
$$

$\mathbf{L}_m$ and $\mathbf{L}_n$ signify the Lagrange cardinal functions given by

$$
\begin{aligned}
L_m(\zeta) &= \prod_{m=0,m\neq w}^{N_\alpha}\frac{\zeta-\zeta_w}{\zeta_m-\zeta_w},\\
L_n(\epsilon) &= \prod_{n=0,n\neq w}^{N_\mu}\frac{\epsilon-\epsilon_w}{\epsilon_n-\epsilon_w},
\end{aligned}
\tag{1.27}
$$

where

$$
\begin{aligned}
L_m\left(\zeta_w\right) = \delta_{mw} &= \begin{cases} 0 \text{ if } m\neq w\\ 1 \text{ if } m = w\end{cases},\\
L_n\left(\epsilon_w\right) = \delta_{nw} &= \begin{cases} 0 \text{ if } n\neq w\\ 1 \text{ if } n = w\end{cases}.
\end{aligned}
\tag{1.28}
$$

The grid points used are Chebyshev-Gauss-Lobatto points, denoted by ζ_m and ϵ_n as shown in Equations (1.29) and (1.30).

$$
\zeta_m = \cos\frac{\pi m}{N_\alpha},\quad m = 0,1,\ldots,N_\alpha, \tag{1.29}
$$

$$
\epsilon_n = \cos\frac{\pi n}{N_\mu},\quad n = 0,1,\ldots,N_\mu. \tag{1.30}
$$

The differentiation matrices $\bar{\mathbf{D}}$ and $\bar{\mathbf{d}}$, as per Trefethen [42] are transformed just as the domains are transformed. The transformed differentiation matrices takes the form

$$\mathbf{D} = \frac{2}{L_\alpha}\bar{\mathbf{D}}, \tag{1.31}$$

$$\mathbf{d} = \frac{2}{L_\mu}\bar{\mathbf{d}}. \tag{1.32}$$

Using corresponding differentiation matrices, we approximate the derivatives of the dependent variables in space and time, respectively, in the following manner:

$$\begin{aligned}
\left.\frac{\partial v_1^{(p)}}{\partial \zeta^{(p)}}\right|_{\zeta_m,\epsilon_n} &= \mathbf{D}^{(p)}V_{1,m}, \quad \left.\frac{\partial v_1}{\partial \epsilon}\right|_{\zeta_m,\epsilon_n} = \sum_{n=0}^{N_\mu}\mathbf{d}_{mn}V_{1,n},\\
\left.\frac{\partial v_2^{(p)}}{\partial \zeta^{(p)}}\right|_{\zeta_m,\epsilon_n} &= \mathbf{D}^{(p)}V_{2,m}, \quad \left.\frac{\partial v_2}{\partial \epsilon}\right|_{\zeta_m,\epsilon_n} = \sum_{n=0}^{N_\mu}\mathbf{d}_{mn}V_{2,n},\\
\left.\frac{\partial v_3^{(p)}}{\partial \zeta^{(p)}}\right|_{\zeta_m,\epsilon_n} &= \mathbf{D}^{(p)}V_{3,m}, \quad \left.\frac{\partial v_3}{\partial \epsilon}\right|_{\zeta_m,\epsilon_n} = \sum_{n=0}^{N_\mu}\mathbf{d}_{mn}V_{3,n},\\
&\vdots\\
\left.\frac{\partial v_M^{(p)}}{\partial \zeta^{(p)}}\right|_{\zeta_m,\epsilon_n} &= \mathbf{D}^{(p)}V_{M,m}, \quad \left.\frac{\partial v_M}{\partial \epsilon}\right|_{\zeta_m,\epsilon_n} = \sum_{n=0}^{N_\mu}\mathbf{d}_{mn}V_{M,n},
\end{aligned} \tag{1.33}$$

where $V_1, V_2, V_3 \ldots, V_M$ are vectors of the form

$$\begin{aligned}
V_1 &= \left[v_1\left(\zeta_0, \epsilon_n\right), v_1\left(\zeta_1, \epsilon_n\right), \ldots, v_1\left(\zeta_{N_\alpha}, \epsilon_n\right)\right]^T,\\
V_2 &= \left[v_2\left(\zeta_0, \epsilon_n\right), v_2\left(\zeta_1, \epsilon_n\right), \ldots, v_2\left(\zeta_{N_\alpha}, \epsilon_n\right)\right]^T,\\
V_3 &= \left[v_3\left(\zeta_0, \epsilon_n\right), v_3\left(\zeta_1, \epsilon_n\right), \ldots, v_3\left(\zeta_{N_\alpha}, \epsilon_n\right)\right]^T,\\
&\vdots\\
V_M &= \left[v_M\left(\zeta_0, \epsilon_n\right), v_M\left(\zeta_1, \epsilon_n\right), \ldots, v_M\left(\zeta_{N_\alpha}, \epsilon_n\right)\right]^T.
\end{aligned} \tag{1.34}$$

The system in Equation (1.21) is solved by implementing the Chebyshev spectral collocation approach in the following manner:

$$\sum_{p=0}^{h_{w,w}} \operatorname{diag}\left[\frac{\partial^{(p)}\mathbf{G}_w\left(\mathbf{v}_{1,n,r}^{(\psi,u)}, \ldots, \mathbf{v}_{M,n,r}^{(\psi,u)}\right)}{\partial v_{w,n}^{(p,\psi,u)}}\right]\left(\mathbb{V}_{w,r+1}^{(p,\psi,u)}\right) = \mathbf{R}_{w,r}, \tag{1.35}$$

where

$$\text{diag}\left[\frac{\partial^{(p)}\mathbf{G}_w\left(\mathbf{v}^{\psi,u}_{1,n,r},\ldots,\mathbf{v}^{\psi,u}_{M,n,r}\right)}{\partial v^{(p)}_{w,n}}\right] \text{ is given by}$$

$$\begin{bmatrix} \frac{\partial^{(p)}\mathbf{G}_w\left(\mathbf{v}^{\psi,u}_{1,n,r}(\zeta_0,\epsilon_n),\ldots,\mathbf{v}^{\psi,u}_{M,n,r}(\zeta_0,\epsilon_n)\right)}{\partial v^{(p,\psi,u)}_{w,n}} & 0 & \cdots & 0 \\ 0 & \frac{\partial^{(p)}\mathbf{G}_w\left(\mathbf{v}^{\psi,u}_{1,n,r}(\zeta_1,\epsilon_n),\ldots,\mathbf{v}^{\psi,u}_{M,n,r}(\zeta_1,\epsilon_n)\right)}{\partial v^{(p,\psi,u)}_{w,n}} & \ddots & 0 \\ \vdots & & \ddots & \vdots \\ 0 & 0 & \cdots & \frac{\partial^{(p)}\mathbf{G}_w\left(\mathbf{v}^{\psi,u}_{1,n,r}(\zeta_M,\epsilon_n),\ldots,\mathbf{v}^{\psi,u}_{M,n,r}(\zeta_M,\epsilon_n)\right)}{\partial v^{(p,\psi,u)}_{w,n}} \end{bmatrix}, \tag{1.36}$$

and

$$\mathbb{V}^{(p,\psi,u)}_{w,r+1} = \mathbf{D}^p \mathbf{v}^{(\psi,u)}_{w,r+1}.$$

1.6 Structure of Dissertation

Chapter 2 investigates a system of ODEs representing mixed convection within a nanoliquid film driven by gravity. This film contains both nanoparticles and gyrotactic microorganisms. The problem was solved using the OMD-PQLM and the PQLM. We conducted an investigation to analyze the impact of using various sets of the OMD-PQLM on accuracy and convergence. The investigation also looks at the effects of an augmentation in the size of the domain. We further analyze the impact of the number of overlapping intervals on the accuracy.

In Chapter 3, we expand the OMD-PQLM to address the solution of partial differential equations (PDEs). The system of PDEs represents the dynamic behavior of a micropolar fluid flowing across a stretching sheet in the presence of magnetic fields. The equations are solved by applying the OMD-PQLM and the PQLM. We analyze the impact of the overlapping grid approach on accuracy and convergence compared to the standard PQLM. The investigation also looks at the effects of augmentation in the size of the temporal domain.

Chapter 4 investigates a novel model of the MHD Williamson-nanofluid flow over an exponentially stretched. The solution is obtained through the implementation of the OMD-PQLM. The results are evaluated by analyzing the accuracy and the convergence rate. The influence of various parameters on the velocity, temperature, and concentration profiles is investigated using a set of equations that yields solutions with a higher accuracy and a faster rate of convergence. The investigated parameters include the Williamson, porosity, Hall, chemical reaction, and magnetic parameters, among others.

Chapter 5 concludes and summarises the dissertation.

Chapter 2

OMD-PQLM for a System of ODEs

This chapter introduces the application of the OMD-PQLM to solve a system of ordinary differential equations (ODEs) modeling the gravity-driven flow of a nano-liquid film. The chapter compares the performance of the OMD-PQLM with that of the PQLM in terms of accuracy, convergence, and computational efficiency. The analysis covers different solution pairings to determine their effects on the methods' effectiveness. These findings are crucial for practical applications such as enhanced oil recovery (EOR) [86] and heat transfer systems [87], demonstrating the method's potential in solving complex fluid dynamics problems.

2.1 Gravity-Driven Flow of a Liquid Film Immersed with Nanoparticles and Gyrotactic Microorganisms

For the purpose of implementing the OMD-PQLM, consider a system of ODEs representing mixed convection in a gravity-propelled nanoliquid infused with nanoparticles and gyrotactic microorganisms. Raees *et al.* [88] originally investigated this problem. The model used the Buongiorno's model and considers two types of boundary conditions namely, passive and active. The model has relevance to mass and heat transfer equipment configurations such as evaporators, coolers, and trickling filters [89, 87]. Furthermore, it has the potential applications of nanofluids in enhancing heat transfer, particularly in enhanced oil recovery (EOR), a technology used in the oil and gas industries to augment oil recovery [90, 86]. The inclusion of gyrotactic microorganisms is tied to applications in microbial EOR [91].

Other notable authors have investigated problems related to film flow phenomena, nanofluids, and bioconvection. A study by Kuznetsov and Nield [92], among others, have delved into various aspects of nanofluid flow, heat transfer, and bioconvection. According to Nield and Kuznetsov [92], it might be physically impossible to actively control the volume fraction of nanoparticles at the boundary as Buongiorno [93] did for various natural and induced convection problems. In response to this, Nield and Kuznetsov [94] updated the model by replacing the actively controlled boundary condition with a passively controlled one. This modification aims to enhance the model's physical realism in certain scenarios.

The research by Raees *et al.* [88] compared nanofluid models that were actively and passively controlled. The passively controlled model was found to be more accurate and more in line with how the system works in reality. The passively controlled nanofluid model is viewed as a more accurate representation of nanofluid in practical terms. [95].

Otegbeye [59] studied the same problem by Raees *et al.* [88] using the PQLM and the SLLM. The PQLM has proven to converge quicker than the SLLM yet conserving higher accuracy. The study also concluded that the PQLM could be a valuable tool for solving comparable complex problems. In this segment, we implement the newly introduced numerical technique, the OMD-PQLM for a comparative analysis with the PQLM, assessing its efficacy based on accuracy, convergence, and computational cost. The model is represented by the following equations:

$$g''' + \frac{2}{3}\left(1 - g'^2\right) + gg'' + Grh - Nr\theta + Rb\phi = 0, \tag{2.1}$$

$$h'' + Prgh' + Nbh'\theta' + Nth'^2 = 0, \tag{2.2}$$

$$\theta'' + \frac{Nt}{Nb}h'' + Leg\theta' = 0, \tag{2.3}$$

$$\phi'' + Scg\phi' - Pe\phi'\theta' - Pe\phi\theta'' = 0, \tag{2.4}$$

with boundary conditions

$$\begin{aligned} &h(\infty) = \phi(\infty) = \theta(\infty) = 0, \quad g'(\infty) = 1, \\ &h'(0) - \gamma h(0) = -\gamma, \quad \phi(0) = 1, \quad \theta(0) = 1, \quad g(0) = 0, \quad g'(0) = 0, \end{aligned} \tag{2.5}$$

where $g(\zeta), h(\zeta), \theta(\zeta)$ and $\phi(\zeta)$ represent the unitless stream function, nanoparticle volume fraction, temperature, and the microorganisms density respectively. The following parameters describe the system: Pe and Rb are the Peclet and Rayleigh numbers for bioconvection; Pr stands for Prandtl number; Le stands for Lewis number; Gr stands for Grashof number; Sc stands for Schmidt number; γ is a constant parameter with no units; and Nt, Nb, together with Nr are the parameters for thermophoresis, Brownian motion, and buoyancy, respectively.

2.2 Methods of Solution

There are three different ways to pair the system of Equations (2.1) to (2.4). These combinations will be considered to determine how various pairing sets affect the convergence and accuracy of the solution. The pairings are defined as follows:

i. case 1: involves the pairings ($\{g, \phi\}$ and $\{h, \theta\}$) corresponding to the Equations $\{2.1, 2.4\}$ and $\{2.2, 2.3\}$,

ii. case 2: involves the pairings ($\{g, h\}$ and $\{\theta, \phi\}$) corresponding to the Equations $\{2.1, 2.2\}$ and $\{2.3, 2.4\}$, and

iii. case 3: involves the pairings ($\{g, \theta\}$ and $\{h, \phi\}$) corresponding to the Equations $\{2.1, 2.3\}$ and $\{2.2, 2.4\}$.

2.2.1 Case 1: involves the pairings ($\{g, \phi\}$ and $\{h, \theta\}$) corresponding to the Equations $\{2.1, 2.4\}$ and $\{2.2, 2.3\}$

The linearization of the non-linear terms, g'^2, gg'' and $g\phi'$, involves making use of a first-order Taylor series expansion, resulting in the linearized pair

$$\begin{aligned} &g'''_{r+1} + \frac{2}{3} - \frac{4}{3}g'_r g'_{r+1} + \frac{2}{3}g'^2_r + g_r g''_{r+1} + g''_r g_{r+1} - g_r g''_r + Grh_r - Nr\theta_r \\ &\quad + Rb\phi_{r+1} = 0, \end{aligned} \tag{2.6}$$

$$\phi''_{r+1} + Scg_r\phi'_{r+1} + Sc\phi'_r g_{r+1} - Sc\phi'_r g_r - Pe\theta'_r\phi'_{r+1} - Pe\theta''_r\phi_{r+1} = 0. \tag{2.7}$$

The implementation of the Chebyshev spectral collocation method with an overlapping grid is implemented, as expressed by the following equations:

$$\Big[\mathbf{D}^3 + [g_r]\,\mathbf{D}^2 - \Big[\frac{4}{3}g'_r\Big]\,\mathbf{D} + [g''_r]\,\mathbf{I}\Big]\,\mathbf{G}_{r+1} + \Big[[Rb]\mathbf{I}\Big]\,\mathbf{\Phi}_{r+1} = -\frac{2}{3} - \frac{2}{3}g'^2_r + g_r g''_r \\ - Grh_r + Nr\theta_r, \tag{2.8}$$

$$\Big[\,[Sc\boldsymbol{\phi}'_r]\;\mathbf{I}\Big]\,\mathbf{G}_{r+1} + \Big[\mathbf{D}^2 + [Scg_r - Pe\theta'_r]\,\mathbf{D} - [Pe\theta''_r]\;\mathbf{I}\Big]\,\mathbf{\Phi}_{r+1} = Scg_r\phi'_r, \tag{2.9}$$

where $\mathbf{I}$ is the identity matrix of the same size as $\mathbf{D}$.

The updated solutions of g and ϕ are incorporated into the next couple of equations. Non-linear terms, $h'\theta'$ and h'^2, in the subsequent pair are linearized thorough a first-order Taylor series expansion. The Chebyshev spectral collocation and overlapping approaches are then applied in the following manner:

$$\Big[\mathbf{D}^2 + [Prg_{r+1} + Nb\theta'_r + 2Nth'_r]\,\mathbf{D}\Big]\,\boldsymbol{H}_{r+1} + \big[[Nbh'_r]\,\mathbf{D}\big]\,\mathbf{\Theta}_{r+1} = Nbh'_r\theta'_r + Nth'^2_r, \tag{2.10}$$

$$\Big[\frac{Nt}{Nb}\mathbf{D}^2\Big]\,\boldsymbol{H}_{r+1} + \Big[\mathbf{D}^2 + [Leg_{r+1}]\,\mathbf{D}\Big]\,\mathbf{\Theta}_{r+1} = 0. \tag{2.11}$$

2.2.2 Case 2: involves the pairings ($\{g, h\}$ and $\{\theta, \phi\}$) corresponding to the Equations $\{2.1, 2.2\}$ and $\{2.3, 2.4\}$

The linearized pair is obtained by linearizing the non-linear components, g'^2, gg'', gh' and h'^2, by the use of the first-order Taylor series expansion, resulting in

$$g'''_{r+1} - \frac{4}{3}g'_r g'_{r+1} + g_r g''_{r+1} + g''_r g_{r+1} + Grh_{r+1} = Nr\theta_r - Rb\phi_r - \frac{2}{3} - \frac{2}{3}g'^2_r + g_r g''_r, \tag{2.12}$$

$$h''_{r+1} + Prg_r h'_{r+1} + Prh'_r g_{r+1} + Nb\theta'_r h'_{r+1} + 2Nth'_r h'_{r+1} = Prg_r h_r + Nth'^2_r. \tag{2.13}$$

The Chebyshev spectral collocation method and the overlapping approach are applied in the following manner:

$$\left[\mathbf{D}^3 + [g_r]\,\mathbf{D}^2 - \left[\frac{4}{3}g_r'\right]\mathbf{D} + [g_r'']\,\mathbf{I}\right]\mathbf{G}_{r+1} + \left[[Gr]\mathbf{I}\right]\boldsymbol{H}_{r+1} = \\ -\frac{2}{3} - \frac{2}{3}g_r'^2 + g_r g_r'' + Nr\theta_r - Rb\phi_r, \tag{2.14}$$

$$\left[\,[Prh_r']\,\mathbf{I}\right]\mathbf{G}_{r+1} + \left[\mathbf{D}^2 + [Prg_r + Nb\theta_r' + 2Nth_r']\,\mathbf{D}\right]\boldsymbol{H}_{r+1} = Prg_r h_r' + Nth_r'^2. \tag{2.15}$$

The revised solutions of g and h from Equations (2.14) and (2.15) are incorporated into the subsequent pair of Equations (2.16) and (2.17). The non-linear terms, $\phi'\theta'$ and $\phi\theta''$, within the second pair are linearized to get

$$\theta_{r+1}'' + Leg_{r+1}\theta_{r+1}' = -\frac{Nt}{Nb}h_{r+1}'', \tag{2.16}$$

$$\phi_{r+1}'' + Scg_{r+1}\phi_{r+1}' - Pe\phi_r'\theta_{r+1}' - Pe\theta_r'\phi_{r+1}' - Pe\phi_r\theta_{r+1}'' - Pe\theta_r''\phi_{r+1} = \\ -Pe\phi_r'\theta_r' - Pe\theta_r''\phi_r. \tag{2.17}$$

We implement the Chebyshev spectral collocation technique with an overlapping grid to integrate the pair of Equations (2.16) and (2.17) in the form

$$\left[\mathbf{D}^2 + [Leg_{r+1}]\,\mathbf{D}\right]\boldsymbol{\Theta}_{r+1} + [\mathbf{0}]\boldsymbol{\Phi}_{r+1} = -\frac{Nt}{Nb}h_{r+1}'', \tag{2.18}$$

$$\left[[-Pe\phi_r]\,\mathbf{D}^2 - [Pe\phi_r']\,\mathbf{D}\right]\boldsymbol{\Theta}_{r+1} + \left[\mathbf{D}^2 + [Scg_{r+1} - Pe\theta_r']\,\mathbf{D} - [Pe\theta_r'']\,\mathbf{I}\right]\boldsymbol{\Phi}_{r+1} = \\ -Pe\phi_r'\theta_r' - Pe\theta_r''\phi_r, \tag{2.19}$$

where $\mathbf{0}$ denotes a zero matrix of the same size as $\mathbf{I}$ and $\mathbf{D}$.

2.2.3 Case 3: involves the pairings ($\{g, \theta\}$ and $\{h, \phi\}$) corresponding to the Equations $\{2.1, 2.3\}$ and $\{2.2, 2.4\}$

The linearized pair is obtained by linearizing the non-linear components, g'^2, gg'' and $g\theta'$, through the Taylor series expansion of order one, resulting in expansion

$$\begin{aligned} g'''_{r+1} - \frac{4}{3}g'_r g'_{r+1} + g_r g''_{r+1} + g''_r g_{r+1} - Nr\theta_{r+1} &= -\frac{2}{3} - \frac{2}{3}g'^2_r + g_r g''_r \\ &\quad - Grh_r - Rb\phi_r, \end{aligned} \tag{2.20}$$

$$\theta''_{r+1} + Leg_r\theta'_{r+1} + Le\theta'_r g_{r+1} = Leg_r\theta'_r - \frac{Nt}{Nb}h''_r. \tag{2.21}$$

The Chebyshev spectral collocation technique with an overlapping grid is implemented to the pair of Equations (2.20) and (2.21) to obtain

$$\begin{aligned} \left[\mathbf{D}^3 + [g_r]\,\mathbf{D}^2 - \left[\frac{4}{3}g_r\right]\mathbf{D} + [g''_r]\,\mathbf{I}\right]\mathbf{G}_{r+1} + \Big[[-Nr]\mathbf{I}\Big]\mathbf{\Theta}_{r+1} &= -\frac{2}{3} - \frac{2}{3}g'^2_r + g_r g''_r \\ &\quad - Grh_r - Rb\phi_r, \end{aligned} \tag{2.22}$$

$$\Big[\,[Le\theta'_r]\,\mathbf{I}\Big]\mathbf{G}_{r+1} + \Big[\mathbf{D}^2 + [Leg_r]\,\mathbf{D}\Big]\,\mathbf{\Theta}_{r+1} = -\frac{Nt}{Nb}h''_r + Leg_r\theta'_r. \tag{2.23}$$

The solutions for g and θ are updated based on the pair of Equations (2.22) and (2.23), and these updated solutions are then used in the subsequent pair of equations. The non-linear term, h'^2, within the second pair is linearized to get

$$h''_{r+1} + Prg_{r+1}h'_{r+1} + Nb\theta'_{r+1}h'_{r+1} + 2Nth'_r h'_{r+1} = Nth'^2_r, \tag{2.24}$$

$$\phi''_{r+1} + Scg_{r+1}\phi'_{r+1} - Pe\theta'_{r+1}\phi'_{r+1} - Pe\theta''_{r+1}\phi_{r+1} = 0. \tag{2.25}$$

We implement the Chebyshev spectral collocation technique with an overlapping grid to integrate the pair of Equations (2.24) and (2.25) in the form

$$\Big[\mathbf{D}^2 + \left[Prg_{r+1} + Nb\theta'_{r+1} + 2Nth'_r\right]\mathbf{D}\Big]\,\boldsymbol{H}_{r+1} + [\mathbf{0}]\mathbf{\Phi}_{r+1} = Nth'^2_r, \tag{2.26}$$

$$[\mathbf{0}]\boldsymbol{H}_{r+1} + \Big[\mathbf{D}^2 + \left[Scg_{r+1} - Pe\theta'_{r+1}\right]\mathbf{D} - \left[Pe\theta''_{r+1}\right]\mathbf{I}\Big]\,\mathbf{\Phi}_{r+1} = \mathbf{0}, \tag{2.27}$$

where $\mathbf{0}$ denotes a zero matrix of the same size as $\mathbf{I}$ and $\mathbf{D}$.

2.3 Findings and Analysis

In this segment, we discuss the solution obtained by the application of the OMD-PQLM and the PQLM. The most efficient case of the PQLM was used in the comparison, while all cases were considered for the OMD-PQLM. The convergence and accuracy of the solutions are evaluated by carrying out solution and residual errors analyses. Moreover, a comparison was conducted between the iterations required to reach convergence.

The parameters within the differential equations system were assigned specific values, unless explicitly stated otherwise. The Prandtl number (Pr), bioconvection Rayleigh number (Rb), Schmidt number (Sc), Lewis number (Le), constant λ, and reduced heat transfer parameter γ are all assigned a value of 1. The buoyancy ratio parameter (Nr), the thermophoresis parameter (Nt), and the Brownian motion parameter (Nb) are assigned values of 0.1, 0.3, and 0.1, respectively. Convergent results were achieved using 30 grid points for the PQLM and 8 grid points for the OMD-PQLM. The number of overlapping sub-intervals was set to 6, and the domain was defined as $[0, 20]$. The preliminary approximations complying with all boundary constraints are

$$\begin{aligned} g_0 &= \zeta - \frac{1}{\lambda}\left(\exp^{-\lambda\zeta} - \exp^{-2\lambda\zeta}\right), \quad h_0 = \exp^{-\lambda\zeta} - \left(\frac{\lambda}{\gamma + 2\lambda}\right)\exp^{-2\lambda\zeta}, \\ \phi_0 &= \theta_0 = \exp^{-\lambda\zeta}. \end{aligned} \tag{2.28}$$

The present study involves an investigation into the influence of different numbers of overlapping grids on the accuracy of solutions, along with an evaluation of the impact of expanding the domain truncation. In the context of the Spectral-based methods, the concept of overlapping grids has exhibited enhanced accuracy [67]. The idea of overlapping is expected to optimize the PQLM similarly.

Table 2.1: Achieving convergence using the PQLM and the OMD-PQLM for localized fluid-surface friction, $-g''(0)$, alongside the computational time taken for 40 iterations of the scheme

Iterations	PQLM	OMD-PQLM 1	OMD-PQLM 2	OMD-PQLM 3
1	1.83349	1.83349	1.87430	1.88681
2	1.83078	1.83078	1.82835	1.82191
3	1.83324	1.83324	1.83331	1.83606
4	1.83310	1.83310	1.83310	1.83244
5	1.83311	1.83311	1.83311	1.83325
6	1.83310	1.83310	1.83310	1.83307
7	1.83310	1.83310	1.83310	1.83311
8	1.83310	1.83310	1.83310	1.83310
9	1.83310	1.83310	1.83310	1.83311
10	1.83310	1.83310	1.83310	1.83310
11	1.83310	1.83310	1.83310	1.83310
$\vdots$	$\vdots$	$\vdots$	$\vdots$	$\vdots$
40	1.83310	1.83310	1.83310	1.83310
Time (secs)	0.31817	0.13166	0.29775	0.21797

Table 2.2: Achieving convergence using the PQLM and the OMD-PQLM for the local flux of motile microorganisms adjacent to the wall, -$h'(0)$, and computational time required to compute 40 iterations of the scheme

Iterations	PQLM	OMD-PQLM 1	OMD-PQLM 2	OMD-PQLM 3
1	0.3575368484	0.3575367812	0.3534512412	0.3599893987
2	0.3560754788	0.3560754834	0.3558119605	0.3556049868
3	0.3561932566	0.3561932564	0.3562091464	0.3563218573
4	0.3561859693	0.3561859694	0.3561855505	0.3561558052
5	0.3561864279	0.3561864280	0.3561864385	0.3561933085
6	0.3561863991	0.3561863991	0.3561863989	0.3561848380
7	0.3561864019	0.3561864010	0.3561864009	0.35618675396
8	0.3561864011	0.3561864008	0.3561864008	0.3561863209
9	0.3561864008	0.3561864008	0.3561864008	0.3561864188
10	0.3561864008	0.3561864008	0.3561864008	0.3561863967
11	0.3561864008	0.3561864008	0.3561864008	0.3561864008
$\vdots$	$\vdots$	$\vdots$	$\vdots$	$\vdots$
40	0.3561864008	0.3561864008	0.3561864008	0.3561864008
Time (secs)	0.138625	0.0803180	0.222967	0.259167

Table 2.3: Achieving convergence using the PQLM and the OMD-PQLM for the local flux of motile microorganisms adjacent to the wall, $-\theta'(0)$, and computational time required to compute 40 iterations of the scheme

Iteration	PQLM	OMD-PQLM 1	OMD-PQLM 2	OMD-PQLM 3
1	0.2528181611	0.2528179573	0.2767272338	0.3203705008
2	0.2477337923	0.2477337958	0.2480429023	0.2389700963
$\vdots$	$\vdots$	$\vdots$	$\vdots$	$\vdots$
7	0.2478389418	0.2478389418	0.2478389417	0.2478437665
8	0.2478389417	0.2478389417	0.2478389417	0.2478378513
9	0.2478389417	0.2478389417	0.2478389417	0.2478391882
10	0.2478389417	0.2478389417	0.2478389417	0.2478388859
11	0.2478389417	0.2478389417	0.2478389417	0.2478389417
$\vdots$	$\vdots$	$\vdots$	$\vdots$	$\vdots$
40	0.2478389417	0.2478389417	0.2478389417	0.2478389417
Time (secs)	0.270773	0.115535	0.253668	0.198569

Table 2.4: Achieving convergence using the PQLM and the OMD-PQLM for the local flux of motile microorganisms adjacent to the wall, $-\phi'(0)$, and computational time required to compute 40 iterations of the scheme

Iteration	PQLM	OMD-PQLM 1	OMD-PQLM 2	OMD-PQLM 3
1	1.4037974504	1.4037984019	0.8073354409	0.8528074166
2	0.7850167022	0.7850165384	0.7805901771	0.7726468801
3	0.7808984543	0.7808984555	0.7809594988	0.7826111816
$\vdots$	$\vdots$	$\vdots$	$\vdots$	$\vdots$
8	0.7809399589	0.7809399589	0.7809399588	0.7809389496
9	0.7809399588	0.7809399588	0.7809399588	0.7809401870
10	0.7809399588	0.7809399588	0.7809399588	0.7809399073
11	0.7809399588	0.7809399588	0.7809399588	0.7809399705
15	0.7809399588	0.7809399588	0.7809399588	0.7809399588
$\vdots$	$\vdots$	$\vdots$	$\vdots$	$\vdots$
40	0.7809399588	0.7809399588	0.7809399588	0.7809399588
Time (secs)	0.173668	0.109560	0.319594	0.249988

Tables 2.1 to 2.4 show an analysis of the convergence together with the computational time taken to compute 40 iterations of cases 1 to 3 of the OMD-PQLM and the PQLM case. The PQLM case used in this study is the most efficient case within the PQLM cases. The findings according to Tables 2.1 to 2.4 show that cases 1 and 2 of the OMD-PQLM have faster convergence in comparison to the PQLM and case 3 of the OMD-PQLM. Moreover, the OMD-PQLM cases 2 and 3 have the slowest convergence. Poor performance in cases 2 and 3 could be attributed to a lesser application of the quasilinearization method, particularly in equations with fewer non-linear terms. This limited use of quasilinearization might lead to slower convergence and decreased accuracy compared to cases where the method is more extensively employed, in equations with higher non-linearity. However, it is worth noting that all methods achieve convergence in a relatively short period of time, with each method converging in less than 0.5 seconds.

Figures 2.1 to 2.4 show the error norm between consecutive iterations with an increase in the iterations' number. The error computation involves subtracting the results from the present iteration and the preceding iteration as the iteration number increases. The OMD-PQLM case 1 shows the quickest convergence, as it achieves the fastest convergence at the $14th$ iteration. Overall, OMD-PQLM cases 1 and 2 show quicker convergence in comparison to case 3 of the OMD-PQLM and the PQLM case. Case 3 of the OMD-PQLM shows the slowest convergence compared to the other cases under consideration.

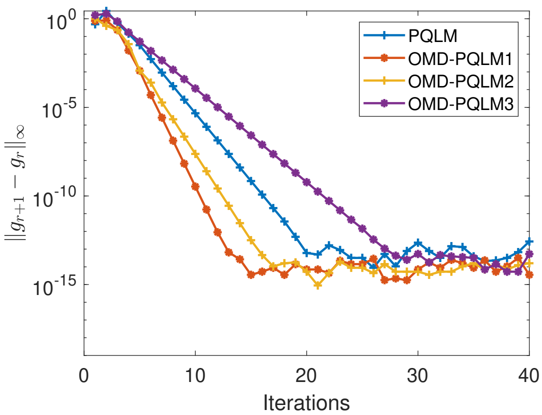

Figure 2.1: Error in g across consecutive iterations

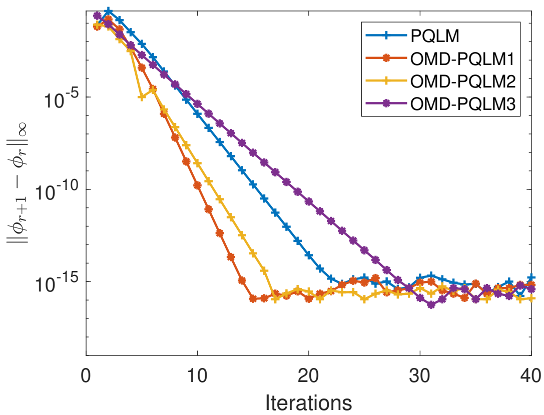

Figure 2.2: Error in ϕ across consecutive iterations

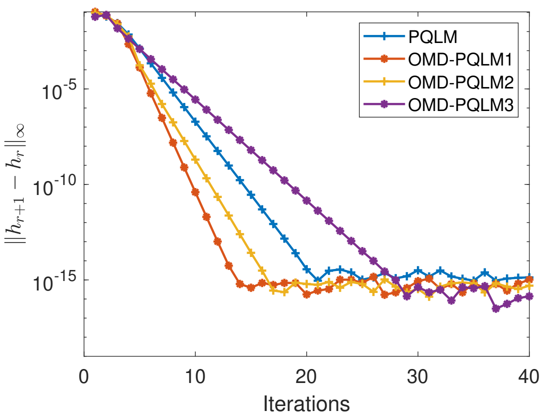

Figure 2.3: Error in h across consecutive iterations

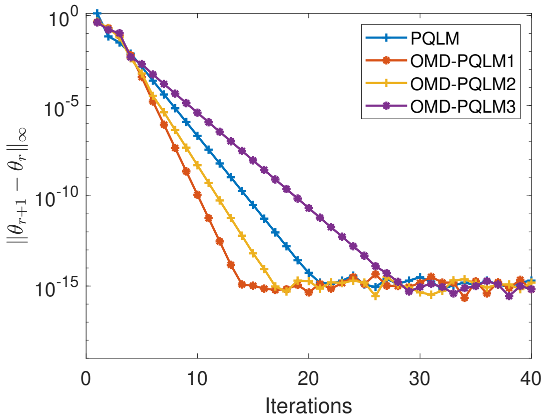

Figure 2.4: Error in θ across consecutive iterations

The residual error's infinity norm is shown in Figures 2.5 to 2.8. The residual error norm indicates the level of accuracy of the approximated solution. In order to calculate the residual error, the estimated solution acquired from the numerical results is substituted into the initial system of equations. The residual error is expressed as

$$\begin{aligned}
\mathrm{Res}(\boldsymbol{g}) &= \boldsymbol{g}''' + \frac{2}{3}\left(1 - \boldsymbol{g}'^2\right) + \boldsymbol{g}\boldsymbol{g}'' + Gr\boldsymbol{h} - Nr\boldsymbol{\theta} + Rb\boldsymbol{\phi}, \\
\mathrm{Res}(\boldsymbol{h}) &= \boldsymbol{h}'' + Pr\boldsymbol{g}\boldsymbol{h}' + Nb\boldsymbol{h}'\boldsymbol{\theta}' + Nt\boldsymbol{h}'^2, \\
\mathrm{Res}(\boldsymbol{\theta}) &= \boldsymbol{\theta}'' + \frac{Nt}{Nb}\boldsymbol{h}'' + Le\boldsymbol{g}\boldsymbol{\theta}', \\
\mathrm{Res}(\boldsymbol{\phi}) &= \boldsymbol{\phi}'' + Sc\boldsymbol{g}\boldsymbol{\phi}' - Pe\boldsymbol{\phi}'\boldsymbol{\theta}' - Pe\boldsymbol{\phi}\boldsymbol{\theta}'',
\end{aligned} \tag{2.29}$$

The system of Equations in (2.29) consists of the approximated solutions acquired from cases 1 to 3 of the OMD-PQLM and the PQLM case.

From Figures 2.5 to 2.8, it is observed that all cases of the OMD-PQLM show greater accuracy as compared to the PQLM case. However, certain OMD-PQLM cases have slower convergence compared to the PQLM. Overall, all methods reach a comparable level of accuracy of 10^{-15} to 10^{-16}.

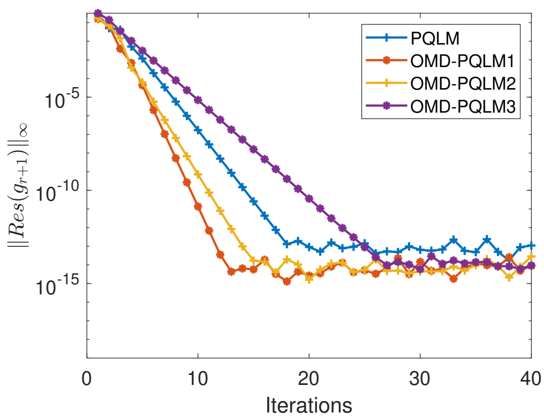

Figure 2.5: The relationship between $\|Res(g_{r+1})\|_\infty$ and iteration steps

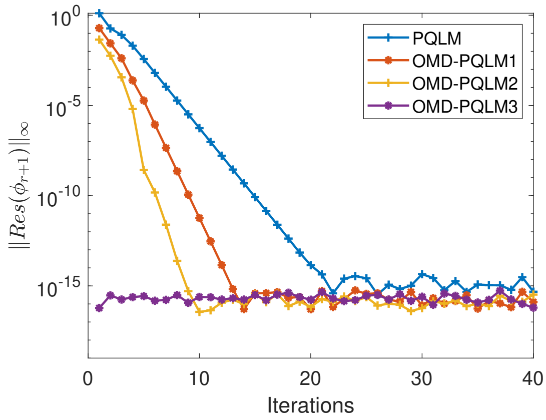

Figure 2.6: The relationship between $\|Res(\phi_{r+1})\|_\infty$ and iteration steps

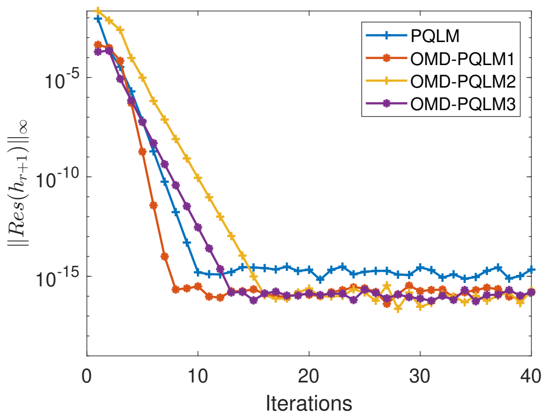

Figure 2.7: The relationship between $\|Res(h_{r+1})\|_\infty$ and iteration steps

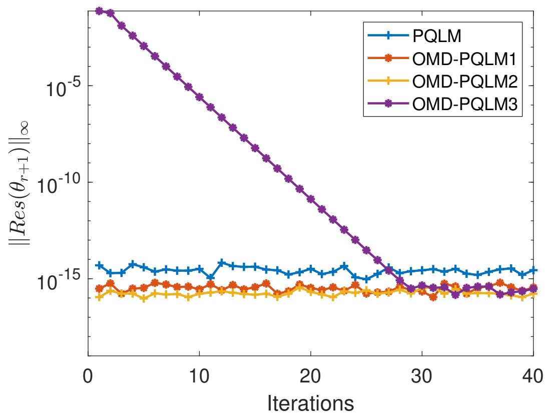

Figure 2.8: The relationship between $\|Res(\theta_{r+1})\|_\infty$ and iteration steps

Figures 2.9 to 2.16 show the errors in the solution and residual when the domain is expanded to $[0, 50]$. As per Otegbeye [63], while the PQLM demonstrates higher accuracy within certain limits, as the domain expands, the method reaches a threshold where it ceases to produce convergent and accurate results.

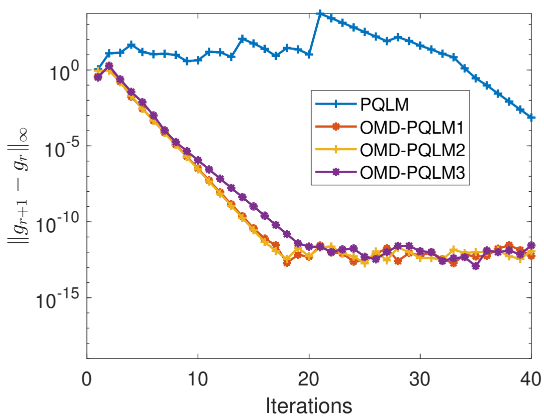

Figure 2.9: Error in g across consecutive iterations

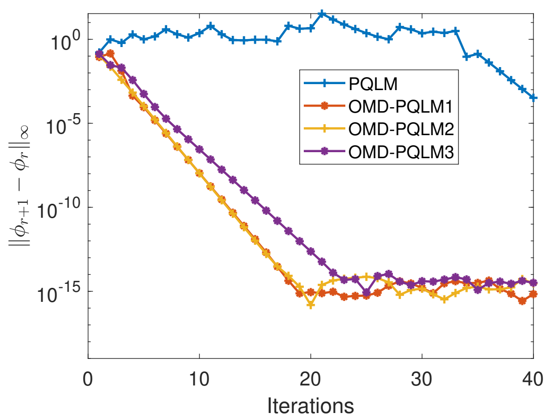

Figure 2.10: Error in ϕ across consecutive iterations

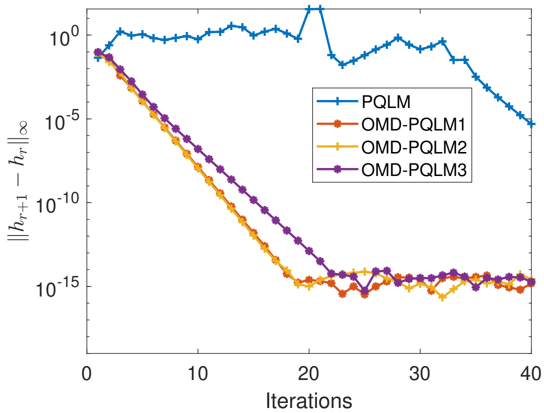

Figure 2.11: Error in h across consecutive iterations

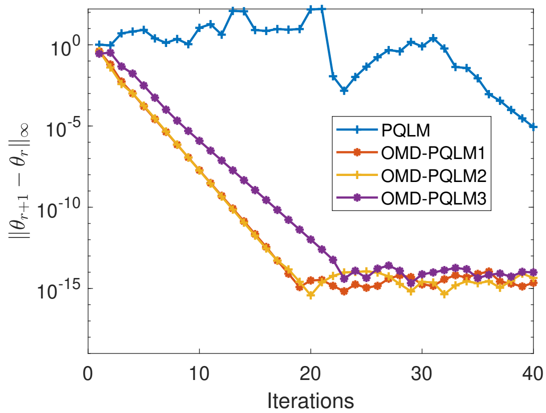

Figure 2.12: Error in θ across consecutive iterations

It is observed from Figures 2.13 to 2.12 that expanding the domain leads the PQLM to fail to produce convergent results. However, cases 1 to 3 of the OMD-PQLM maintain a faster rate of convergence and highly accurate results, even with domain expansion.

From Figures 2.13 to 2.16, it is observed that expanding the domain does not impact the accuracy of all cases of the OMD-PQLM. However, PQLM is impacted and fails to yield convergent and accurate results.

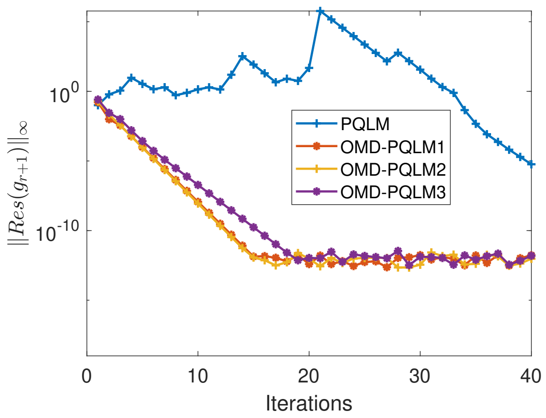

Figure 2.13: The relationship between $\|Res(g_{r+1})\|_\infty$ and iteration steps.

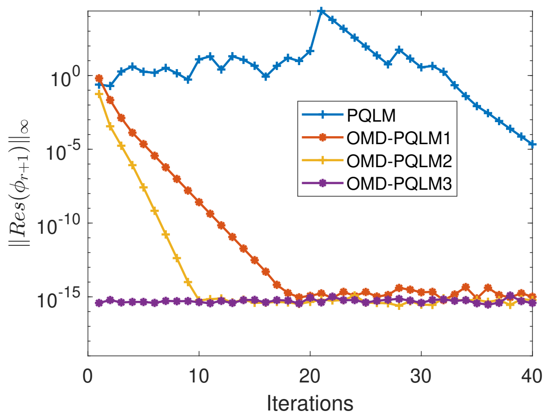

Figure 2.14: The relationship between $\|Res(\phi_{r+1})\|_\infty$ and iteration steps

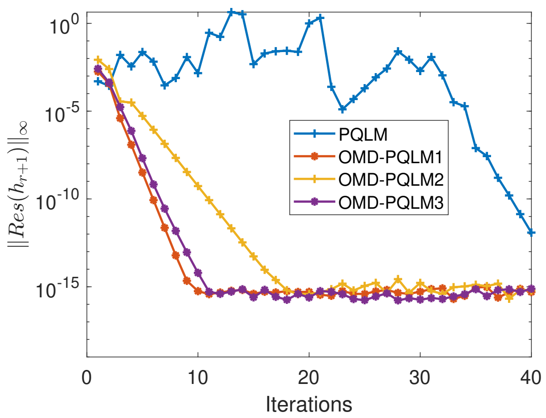

Figure 2.15: The relationship between $\|Res(h_{r+1})\|_\infty$ and iteration steps

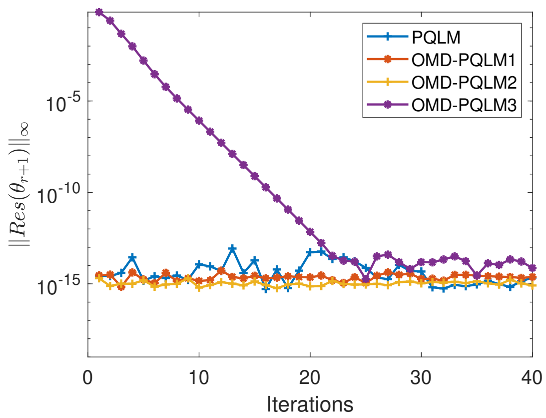

Figure 2.16: The relationship between $\|Res(\theta_{r+1})\|_\infty$ and iteration steps

The number of collocation points is fixed at $N_\alpha = 8$. Table 2.5 displays the impact when changing the number of overlapping intervals while maintaining a consistent number of collocation points in each sub-interval. The results indicate that the accuracy of solutions is higher for a few overlapping intervals. Nevertheless, when the quantity of overlapping sub-intervals increases, the method exhibits an ability to converge in a fewer number of iterations.

Table 2.5: Influence of overlapping sub-intervals on the iteration of convergence and accuracy

z	$\tilde{M}_x$	No. of iterations for f	Convergence value for f	No. of iterations for ϕ	Convergence value for ϕ	No. of iterations for h	Convergence value for h	No. of iterations for θ	Convergence value for θ
4	13	18	3.8×10^{-14}	19	4.0×10^{-16}	10	1.29×10^{-16}	1	3.19×10^{-16}
5	21	18	8.1×10^{-13}	18	5.0×10^{-16}	10	3.7×10^{-16}	1	3.05×10^{-16}
10	41	12	7.1×10^{-13}	18	9.2×10^{-16}	8	4.3×10^{-16}	1	4.1×10^{-16}
$\vdots$	$\vdots$	$\vdots$	$\vdots$	$\vdots$	$\vdots$	$\vdots$	$\vdots$	$\vdots$	$\vdots$
20	81	10	3.06×10^{-12}	12	5.9×10^{-14}	6	1.39×10^{-14}	1	2.4×10^{-14}
25	101	10	8.4×10^{-12}	10	7.61×10^{-13}	6	1.26×10^{-14}	1	1.7×10^{-14}

2.4 Summary

The OMD-PQLM was used successfully in this chapter to solve a set of ODEs in three distinct permutations. The results acquired from the various permutations of the OMD-PQLM were compared to those obtained from the PQLM. It was noted that two of the OMD-PQLM cases displayed faster convergence compared to the PQLM and achieved higher accuracy. The investigation of the OMD-PQLM reveals noteworthy observations across its three cases. Both cases 1 and 2 exhibit rapid convergence and enhanced accuracy across all four equations when compared to case 3. This improved performance is attributed to the presence of a higher number of nonlinear terms in cases 1 and 2, necessitating more frequent application of the quasilinearization technique. Furthermore, computational efficiency analysis demonstrates that all three cases achieve converged solutions in less than 1 second. These findings underscore the ability of cases 1 to 3 of the OMD-PQLM cases to enhance the accuracy of the PQLM while maintaining computational efficiency. The OMD-PQLM requires fewer collocation points and overlapping intervals. The PQLM fails to attain convergent and precise results in a larger domain, while all OMD-PQLM cases produce convergent and accurate results even in a large domain. The utilization of overlapping sub-intervals enhances the efficiency of the PQLM. This chapter has presented a technique that improves the speed of convergence of the PQLM while simultaneously enhancing its accuracy.

Chapter 3

OMD-PQLM for a System of PDEs

This chapter introduces the iterative schemes of the OMD-PQLM and the PQLM applied to a system of PDEs, which describes the spatio-temporal dynamics of mass and thermal transfer in time-dependent MHD motion of a micropolar fluid across a deformable sheet. The efficiency of the OMD-PQLM will be compared to that of the PQLM in terms of accuracy against iteration, accuracy against the temporal domain, and the speed of convergence against iteration.

3.1 Mass and Thermal Transfer in Time-Dependent MHD Motion of a Micropolar Fluid Across a Deformable Sheet

For the purpose of implementing the OMD-PQLM, consider a system of ODEs representing a mathematical analysis of the combined impact of thermal and mass flux in a time-dependent flow of a micropolar fluid over a dilating sheet. Hayat and Qasim [96] have previously studied this model. Non-Newtonian fluids, including micropolar fluids, exhibit complex and complicated behavior that cannot be explained by a basic directly proportional relationship between stress and how much the substance deforms [97]. The model of micropolar fluid applied in this model has extra factors like microrotation and gyration, which helps explain how fluids behave in different industrial and engineering situations [98]. The model incorporates the impact of thermal radiation and magnetic fields on fluid dynamics. The model applies to various real-world scenarios involving non-Newtonian fluids, specifically micropolar fluids. Examples include the flow of molten polymers, pulps, foods, fossil fuels, and naturally occurring fluids like animal blood. The results have implications for many industries, including extrusion, food processing, electrical power generation, astrophysical flows, solar power technology, spacecraft re-entry, and the movement of biological fluids [99, 100, 101, 102, 103, 104, 105, 106]. Previous research has addressed similar micropolar fluid flow problems using a variety of numerical techniques. For instance, Takhar *et al.* [107] used finite element solutions for axisymmetric flow between porous disks. Chang [108] performed numerical analysis for mixed heat transfer flow alongside a vertical flat plate using the finite difference with cubic spline collocation. Hayat and Qasim [96] used the homotopy analysis method (HAM) proposed by Liao [109] for solving the non-linear problems. The method is reported to be powerful and has been applied in various studies [110, 111, 112, 113, 114]. Otegbeye [59] solved the same problem as Hayat and Qasim [96] by applying PQLM and SLLM. The PQLM outperforms the SLLM in terms of both accuracy and convergence. It was also observed that in the case of the PQLM, cases including more non-linear terms result in faster convergence and higher accuracy. The model is represented by the following equations:

$$(1+K)g''' + (1-\epsilon)\left(\frac{\zeta}{2}g'' - \epsilon\frac{\partial g'}{\partial \epsilon}\right) + \epsilon\left(gg'' - (g')^2 - M^2 g'\right) + Kh' = 0 \tag{3.1}$$

$$\left(1+\frac{K}{2}\right)h'' + (1-\epsilon)\left(\frac{1}{2}h + \frac{\zeta}{2}h' - \epsilon\frac{\partial h}{\partial \epsilon}\right) + \epsilon\left(gh' - g'h - 2Kh - Kg''\right) = 0 \tag{3.2}$$

$$(1+N_R)\,\omega'' + Pr(1-\epsilon)\left(\frac{\zeta}{2}\omega' - \epsilon\frac{\partial \omega}{\partial \epsilon}\right) + Pr\epsilon g\omega' = 0, \tag{3.3}$$

$$\theta'' + Sc(1-\epsilon)\left(\frac{\zeta}{2}\theta' - \epsilon\frac{\partial \theta}{\partial \epsilon}\right) + Sc\epsilon g\theta' - \gamma Sc\epsilon\theta = 0, \tag{3.4}$$

with associated conditions

$$\begin{aligned} &g(\epsilon,0) = 0, \quad g'(\epsilon,0) = \omega(\epsilon,0) = \theta(\epsilon,0) = 1, \quad h(\epsilon,0) = -m_0 g''(\epsilon,0), \\ &g'(\epsilon,\infty) = h(\epsilon,\infty) = \omega(\epsilon,\infty) = \theta(\epsilon,\infty) = 0. \end{aligned} \tag{3.5}$$

The following parameters describe the system: K is the material parameter, M is the Hartman number, Pr is the Prandtl number, N_R is the radiation parameter, Sc is the Schmidt number, and γ is the chemical reaction parameter.

3.2 Methods of Solution

There are three different ways to pair the systems of Equations (3.1) to (3.4). These combinations will be considered to determine how the different sets of pairings affect the convergence speed and accuracy of the solution. The pairings are defined as follows:

i. case 1: involves the pairings ($\{g, h\}$ and $\{\omega, \theta\}$) corresponding to the Equations $\{3.1, 3.2\}$ and $\{3.3, 3.4\}$,

ii. case 2: involves the pairings ($\{g, \omega\}$ and $\{h, \theta\}$) corresponding to the Equations $\{3.1, 3.3\}$ and $\{3.2, 3.4\}$, and

iii. case 3: involves the pairings ($\{g, \theta\}$ and $\{h, \omega\}$) corresponding to the Equations $\{3.1, 3.4\}$ and $\{3.2, 3.3\}$.

3.2.1 Case 1: involves the pairings ($\{g, h\}$ and $\{\omega, \theta\}$) corresponding to the Equations $\{3.1, 3.2\}$

The non-linear terms in Equations (3.1) and (3.2) undergo linearization through the first-order Taylor series expansion, resulting in

$$[a_1 r]\, g'''_{r+1} + [a_2 r]\, g''_{r+1} + [a_3 r]\, g'_{r+1} + [a_4 r]\, g_{r+1} - \epsilon(1-\epsilon)\frac{\partial g'_{r+1}}{\partial \epsilon} + K h'_{r+1} = a_5 r, \tag{3.6}$$

$$\begin{aligned} &[b_1 r]\, g''_{r+1} + [b_2 r]\, g'_{r+1} + [b_3 r]\, g_{r+1} + [b_4 r]\, h''_{r+1} + [b_5 r]\, h'_{r+1} + [b_6 r]\, h_{r+1} \\ &\quad - \epsilon(1-\epsilon)\frac{\partial h_{r+1}}{\partial \epsilon} = b_7 r, \end{aligned} \tag{3.7}$$

where

$$\begin{aligned}
&a_1r = 1 + K, \quad a_2r = (1-\epsilon)\frac{\zeta}{2} + \epsilon g_r, \quad a_3r = -2\epsilon g_r' - \epsilon M^2, \quad a_4r = \epsilon g_r'', \\
&a_5r = \epsilon g_r g_r'' - \epsilon g_r'^2, \quad b_1r = -\epsilon K, \quad b_2r = -\epsilon h_r, \quad b_3r = \epsilon h_r', \quad b_4r = 1 + \frac{K}{2}, \\
&b_5r = \frac{\zeta}{2}(1-\epsilon) + \epsilon g_r, \quad b_6r = \frac{1}{2}(1-\epsilon) - \epsilon\left(g_r' + 2K\right), \\
&b_7r = \epsilon\left(g_r h_r' - g_r' h_r\right).
\end{aligned}$$

The latest updated solutions of g and h are used in the subsequent couple of equations. Equations (3.3) and (3.4) are linear, hence they may be represented as

$$[c_1r]\,\omega_{r+1}'' + [c_2r]\,\omega_{r+1}' - Pr\epsilon(1-\epsilon)\frac{\partial \omega_{r+1}}{\partial \epsilon} = 0, \tag{3.8}$$

$$\theta_{r+1}'' + [e_1r]\,\theta_{r+1}' - [e_2r]\,\theta_{r+1} - Sc\epsilon(1-\epsilon)\frac{\partial \theta_{r+1}}{\partial \epsilon} = 0, \tag{3.9}$$

where

$$\begin{aligned}
&c_1r = 1 + N_R, \quad c_2r = Pr(1-\epsilon)\frac{\zeta}{2} + Pr\epsilon g_{r+1}, \\
&e_1r = Sc(1-\epsilon)\frac{\zeta}{2} + Sc\epsilon g_{r+1}, \quad e_2r = \gamma Sc\epsilon.
\end{aligned}$$

The Chebyshev spectral collocation method and the overlapping approach are applied to linear pairs of Equations (3.8) and (3.9) in the following manner:

$$A_{1,1}^m \mathbf{G}_{r+1,m} - \epsilon_m(1-\epsilon_m)\sum_{n=0}^{\tilde{M}_{t-1}} d_{mn}\mathbf{D}\mathbf{G}_{r+1,n} + A_{1,2}^m \mathbf{H}_{r+1,m} = \mathbf{R}_{1,m}, \tag{3.10}$$

$$A_{2,1}^m \mathbf{G}_{r+1,m} + A_{2,2}^m \mathbf{H}_{r+1,m} - \epsilon_m(1-\epsilon_m)\sum_{n=0}^{\tilde{M}_{t-1}} d_{mn}\mathbf{H}_{r+1,n} = \mathbf{R}_{2,m}, \tag{3.11}$$

where

$$\begin{aligned}
&A_{1,1}^m = [a_1r]\,\mathbf{D}^3 + (a_2r)\,\mathbf{D}^2 + [a_3r]\,\mathbf{D} + [a_4r]\,\mathbf{I}, \quad A_{1,2}^m = K\mathbf{D}, \\
&A_{2,1}^m = [b_1r]\,\mathbf{D}^2 + [b_2r]\,\mathbf{D} + [b_3r]\,\mathbf{I}, \quad A_{2,2}^m = [b_4r]\,\mathbf{D}^2 + [b_5r]\,\mathbf{D} + [b_6r]\,\mathbf{I} \\
&\mathbf{R}_{1,m} = \epsilon(1-\epsilon)\mathbf{d}_{m\tilde{M}_t}\mathbf{D}\mathbf{G}_{\tilde{M}_t,r} + a_5r, \quad \mathbf{R}_{2,m} = \epsilon(1-\epsilon)\mathbf{d}_{m\tilde{M}_t}\mathbf{H}_{\tilde{M}_t,r} + b_7r,
\end{aligned}$$

and

$$E^{m}_{1,1}\mathbf{\Omega}_{r+1,m} - Pr\epsilon_m\left(1-\epsilon_m\right)\sum_{n=0}^{\tilde{M}_{t-1}} d_{mn}\mathbf{\Omega}_{r+1,n} + E^{m}_{1,2} = \mathbf{R}_{3,m}, \tag{3.12}$$

$$E^{m}_{2,1} + E^{m}_{2,2}\mathbf{\Theta}_{r+1,m} - Sc\epsilon_m\left(1-\epsilon_m\right)\sum_{n=0}^{\tilde{M}_{t-1}} d_{mn}\mathbf{\Theta}_{r+1,n} = \mathbf{R}_{4,m}, \tag{3.13}$$

where

$$E^{m}_{1,1} = [c_1r]\,\mathbf{D}^2 + [c_2r]\,\mathbf{D}, \quad E^{m}_{1,2} = 0, \quad E^{m}_{2,1} = 0, \quad E^{m}_{2,2} = \mathbf{D}^2 + [e_1r]\,\mathbf{D} - [e_2r]\,\mathbf{I}$$
$$\mathbf{R}_{3,m} = Pr\epsilon(1-\epsilon)\mathbf{d}_{m\tilde{M}_t}\mathbf{\Omega}_{\tilde{M}_t,r}, \quad \mathbf{R}_{4,m} = Sc\epsilon(1-\epsilon)\mathbf{d}_{m\tilde{M}_t}\mathbf{\Theta}_{M_t,r}$$

Here, $\mathbf{I}$ represent an identity matrix of size $\left(\tilde{M}_x+1\right)\times\left(\tilde{M}_x+1\right)$.

3.2.2 Case 2: involves the pairings ($\{g,\omega\}$ and $\{h,\theta\}$) corresponding to the Equations $\{3.1, 3.3\}$ and $\{3.2, 3.4\}$

The non-linear terms in Equations (3.1) and (3.3) undergo linearization through the first-order Taylor series expansion, resulting in

$$[a_1r]\,g'''_{r+1} + [a_2r]\,g''_{r+1} + [a_3r]\,g'_{r+1} + [a_4r]\,g_{r+1} - \epsilon(1-\epsilon)\frac{\partial g'_{r+1}}{\partial\epsilon} = a_5r, \tag{3.14}$$

$$[b_1r]\,g_{r+1} + [b_2r]\,\omega''_{r+1} + [b_3r]\,\omega'_{r+1} - Pr\epsilon(1-\epsilon)\frac{\partial\omega_{r+1}}{\partial\epsilon} = b_4r, \tag{3.15}$$

where

$$a_1r = 1+K, \quad a_2r = (1-\epsilon)\frac{\zeta}{2} + \epsilon g_r, \quad a_3r = -2\epsilon g'_r - \epsilon M^2,$$
$$a_4r = \epsilon g''_r, \quad a_5r = \epsilon g_r g''_r - \epsilon g'^2_r - Kh'_r, \quad b_1r = Pr\epsilon\omega'_r,$$
$$b_2r = 1+N_R, \quad b_3r = Pr\left((1-\epsilon)\frac{\zeta}{2} + \epsilon g_r\right), \quad b_4r = Pr\epsilon g_r\omega'_r.$$

The latest updated solutions of g and ω are used in the subsequent couple of equations. Equations (3.2) and (3.4) exhibit linearity. Applying the Chebyshev spectral collocation and overlapping approaches, we solve the decoupled linearized pairs of equations in the following manner:

$$\Big[[a_1r]\,\mathbf{D}^3 + [a_2r]\,\mathbf{D}^2 + [a_3r]\,\mathbf{D} + [a_4r]\,\mathbf{I}\Big]\,\mathbf{G}_{r+1,m} - \epsilon_m\,(1-\epsilon_m)\sum_{n=0}^{\tilde{M}_t-1}\mathbf{d}_{mn}\mathbf{D}\mathbf{G}_{r+1,n} = \mathbf{R}_{1,m}, \tag{3.16}$$

$$\Big[[b_1r]\,\mathbf{I}\Big]\mathbf{G}_{r+1,m} + \Big[[b_2r]\,\mathbf{D}^2 + [b_3r]\,\mathbf{D}\Big]\,\mathbf{\Omega}_{r+1,m} - Pr\epsilon_m\,(1-\epsilon_m)\sum_{n=0}^{M_{t-1}}\mathbf{d}_{mn}\mathbf{\Omega}_{r+1,n} = \mathbf{R}_{2,m}, \tag{3.17}$$

$$\Big[[c_1r]\,\mathbf{D}^2 + [c_2r]\,\mathbf{D} + [c_3r]\,\mathbf{I}\Big]\,\mathbf{H}_{r+1,m} - \epsilon_m\,(1-\epsilon_m)\sum_{n=0}^{\tilde{M}_{t-1}}\mathbf{d}_{mn}\mathbf{H}_{r+1,n} = \mathbf{R}_{3,m}, \tag{3.18}$$

$$\Big[\mathbf{D}^2 + [e_1r]\,\mathbf{D} + [e_2r]\,\mathbf{I}\Big]\,\mathbf{\Theta}_{r+1,m} - Sc\epsilon_m\,(1-\epsilon_m)\sum_{n=0}^{\tilde{M}_{t-1}}\mathbf{d}_{mn}\mathbf{\Theta}_{r+1,n} = \mathbf{R}_{4,m}, \tag{3.19}$$

where

$$c_1r = 1 + \frac{K}{2}, \quad c_2r = (1-\epsilon)\frac{\zeta}{2} + \epsilon g_{r+1}, \quad c_3r = (1-\epsilon)\frac{1}{2} - \epsilon g'_{r+1} - 2\epsilon K,$$
$$c_4r = \epsilon K g''_{r+1}, \quad e_1r = Sc\left((1-\epsilon)\frac{\zeta}{2} + \epsilon g_{r+1}\right), \quad e_2r = \gamma Sc\epsilon,$$

and

$$\mathbf{R}_{1,m} = \epsilon_m\,(1-\epsilon_m)\,\mathbf{d}_{m\tilde{M}_t}\mathbf{D}\mathbf{G}_{\tilde{M}_t,r} + \mathbf{a}_5r, \tag{3.20}$$
$$\mathbf{R}_{2,m} = Pr\epsilon_m\,(1-\epsilon_m)\,\mathbf{d}_{m\tilde{M}_t}\mathbf{\Omega}_{\tilde{M}_t,r} + \mathbf{b}_4r, \tag{3.21}$$
$$\mathbf{R}_{3,m} = \epsilon_m\,(1-\epsilon_m)\,\mathbf{d}_{m\tilde{M}_t}\mathbf{H}_{\tilde{M}_t,r} + \mathbf{c}_4r, \tag{3.22}$$
$$\mathbf{R}_{4,m} = Sc\epsilon_m\,(1-\epsilon_m)\,\mathbf{d}_{m\tilde{M}_t}\mathbf{\Theta}_{\tilde{M}_t,r}. \tag{3.23}$$

3.2.3 Case 3: involves the pairings ($\{g, \theta\}$ and $\{h, \omega\}$) corresponding to the Equations $\{3.1, 3.4\}$ and $\{3.2, 3.3\}$

The non-linear terms in Equations (3.1) and (3.4) undergo linearization through the first-order Taylor series expansion, resulting in the expansion

$$[a_1r]\, g'''_{r+1} + [a_2r]\, g''_{r+1} + [a_3r]\, g'_{r+1} + [a_4r]\, g_{r+1} - \epsilon(1-\epsilon)\frac{\partial g'_{r+1}}{\partial \epsilon} = a_5r, \tag{3.24}$$

$$[b_1r]\, g_{r+1} + \theta''_{r+1} + [b_2r]\, \theta'_{r+1} + [b_3r]\, \theta_{r+1} - Sc\epsilon(1-\epsilon)\frac{\partial \theta_{r+1}}{\partial \epsilon} = b_4r, \tag{3.25}$$

where

$$\begin{aligned}
&a_1r = 1 + K, \quad a_2r = (1-\epsilon)\frac{\zeta}{2} + \epsilon g_r, \quad a_3r = -2\epsilon g'_r - \epsilon M^2, \\
&a_4r = \epsilon g''_r, \quad a_5r = \epsilon g_r g''_r - \epsilon g'^2_r - Kh'_r, \quad b_1r = Sc\epsilon\theta'_r, \\
&b_2r = Sc\left((1-\epsilon)\frac{\zeta}{2} + \epsilon g_r\right), \quad b_3r = -\gamma Sc\epsilon, \quad b_4r = Sc\epsilon g_r \theta'_r.
\end{aligned}$$

The updated solutions of g and θ are incorporated into the next couple of equations. Equations (3.2) and (3.3) exhibit linearity. The Chebyshev spectral collocation and overlapping approaches are then applied to all pairs in the following manner:

$$\Big[[a_1r]\,\mathbf{D}^3 + [a_2r]\,\mathbf{D}^2 + [a_3r]\,\mathbf{D} + [a_4r]\,\mathbf{I}\Big]\,\mathbf{G}_{r+1,m} - \epsilon_m\,(1-\epsilon_m)\sum_{n=0}^{\tilde{M}_t-1}\mathbf{d}_{mn}\mathbf{D}\mathbf{G}_{r+1,n} = \mathbf{R}_{1,m}, \tag{3.26}$$

$$\Big[\,[b_1r]\,\mathbf{I}\Big]\mathbf{G}_{r+1,m} + \Big[\mathbf{D}^2 + [b_2r]\,\mathbf{D} + [b_3r]\,\mathbf{I}\Big]\,\mathbf{\Theta}_{r+1,m} - Sc\epsilon_m\,(1-\epsilon_m)\sum_{n=0}^{\tilde{M}_t-1}\mathbf{d}_{mn}\mathbf{\Theta}_{r+1,n} = \mathbf{R}_{2,m}, \tag{3.27}$$

and

$$\Big[[c_1r]\,\mathbf{D}^2 + [c_2r]\,\mathbf{D} + [c_3r]\,\mathbf{I}\Big]\,\mathbf{H}_{r+1,m} - \epsilon_m\,(1-\epsilon_m)\sum_{n=0}^{\tilde{M}_t-1}\mathbf{d}_{mn}\mathbf{H}_{r+1,n} = \mathbf{R}_{3,m}, \tag{3.28}$$

$$\Big[[e_1r]\,\mathbf{D}^2 + [\mathbf{e}_2r]\,\mathbf{D}\Big]\,\mathbf{\Omega}_{r+1,m} - Pr\epsilon_m\,(1-\epsilon_m)\sum_{n=0}^{\tilde{M}_t-1}\mathbf{d}_{mn}\mathbf{\Omega}_{r+1,n} = \mathbf{R}_{4,m}, \tag{3.29}$$

where

$$
\begin{aligned}
&c_1r = 1 + \frac{K}{2}, \quad c_2r = (1-\epsilon)\frac{\zeta}{2} + \epsilon g_{r+1}, \quad c_3r = (1-\epsilon)\frac{1}{2} - \epsilon g'_{r+1} - 2\epsilon K, \\
&c_4r = \epsilon K g''_{r+1}, \quad e_1r = 1 + N_R, \quad e_2r = Pr\left(\frac{\zeta}{2}(1-\epsilon) + \epsilon g_{r+1}\right),
\end{aligned} \tag{3.30}
$$

$$\mathbf{R}_{1,m} = \epsilon_m\left(1-\epsilon_m\right)\mathbf{d}_{m\tilde{M}_t}\mathbf{DG}_{\tilde{M}_t,r} + \mathbf{a}_5r, \tag{3.31}$$

$$\mathbf{R}_{2,m} = Sc\epsilon_m\left(1-\epsilon_m\right)\mathbf{d}_{m\tilde{M}_t}\mathbf{\Theta}_{\tilde{M}_t,r} + \mathbf{b}_4r, \tag{3.32}$$

$$\mathbf{R}_{3,m} = \epsilon_m\left(1-\epsilon_m\right)\mathbf{d}_{m\tilde{M}_t}\mathbf{H}_{\tilde{M}_t,r} + \mathbf{c}_4r, \tag{3.33}$$

$$\mathbf{R}_{4,m} = Pr\epsilon_m\left(1-\epsilon_m\right)\mathbf{d}_{m\tilde{M}_t}\mathbf{\Omega}_{\tilde{M}_t,r}. \tag{3.34}$$

3.3 Results and Discussions

The numerical solutions of Equations (3.1) to (3.4), along with the boundary conditions in Equation (3.5), is obtained using the OMD-PQLM and the PQLM. Both the OMD-PQLM and the PQLM have three cases each. Unless stated otherwise, the predefined numerical values for the parameters remain constant: $Nr = 0.5$, $\gamma = 1$, $M = 0.5$, $m_0 = 0.5$, $Sc = 0.7$, and $Pr = 0.7$. The OMD-PQLM used $N_\alpha = 6$ and $N_\mu = 4$ grid points, with $z = 5$ and $\kappa = 3$ sub-intervals for spatial and temporal domains, respectively. The PQLM used 30 and 10 spatial and temporal grid points, respectively, to achieve convergence.

Solution errors obtained between two successive iterations are shown in Figures 3.1 to 3.4.

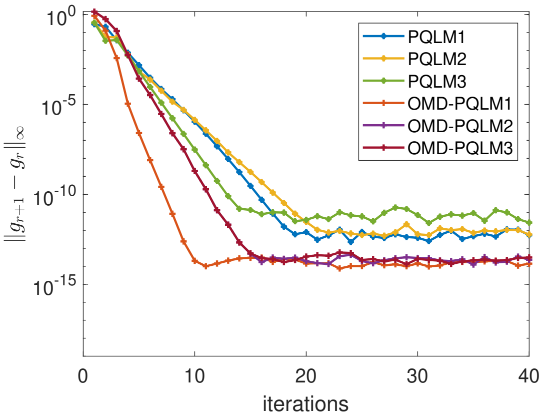

Figure 3.1: Error in g across consecutive iterations

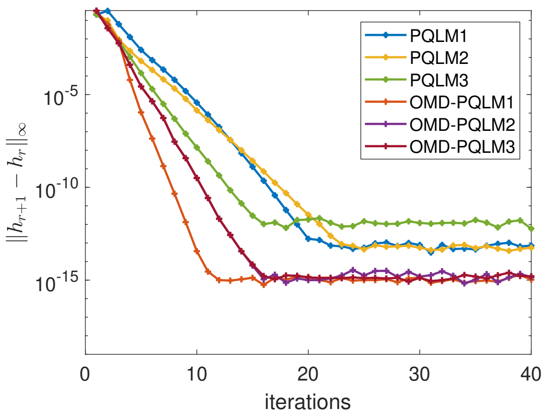

Figure 3.2: Error in h across consecutive iterations

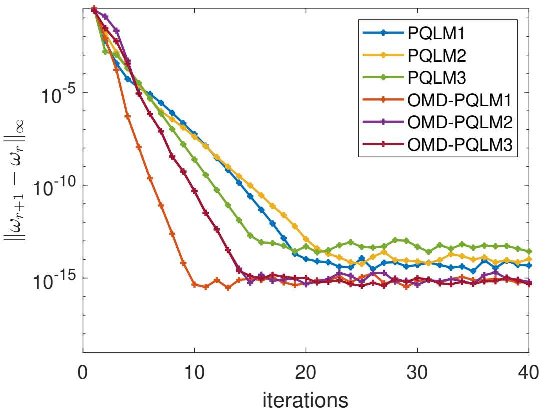

Figure 3.3: Error in ω across consecutive iterations

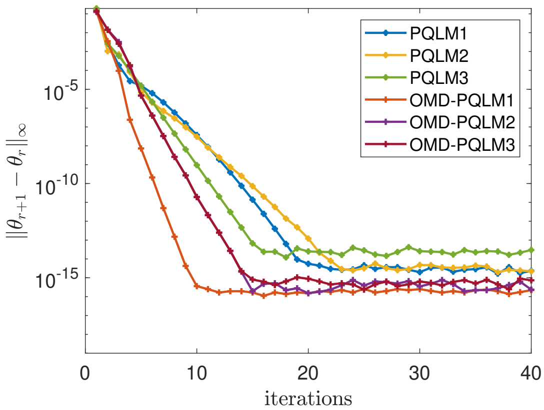

Figure 3.4: Error in θ across consecutive iterations

OMD-PQLM cases 1 to 3 demonstrate faster convergence compared to the PQLM cases 1 to 3. This distinction becomes evident when examining the slopes of OMD-PQLM cases 1 to 3, which are more steep in comparison to their PQLM counterparts. Further analysis shows that among the OMD-PQLM cases, the first case stands out for its quick convergence.

Figures 3.5 to 3.8 display the residual errors obtained using cases 1 to 3 of both the OMD-PQLM and the PQLM against the number of iterations. The residual error is used to evaluate accuracy by assessing the proximity of the estimated solution to zero.

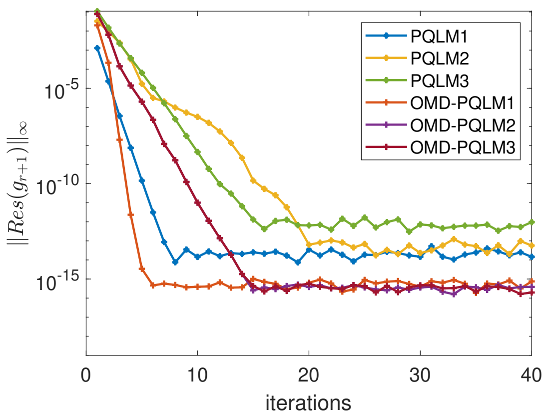

Figure 3.5: The impact of iterations on $\|Res(g_{r+1})\|_\infty$

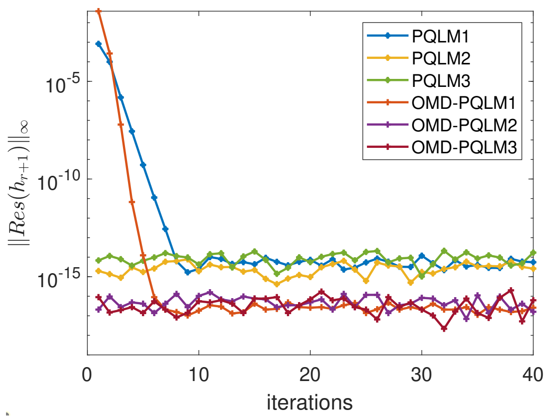

Figure 3.6: The impact of iterations on $\|Res(h_{r+1})\|_\infty$

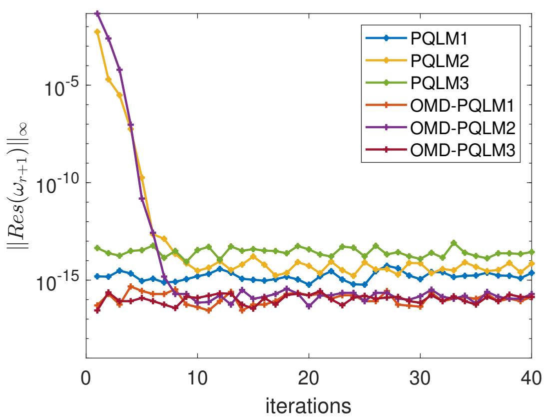

Figure 3.7: The impact of iterations on $\|Res(\omega_{r+1})\|_\infty$

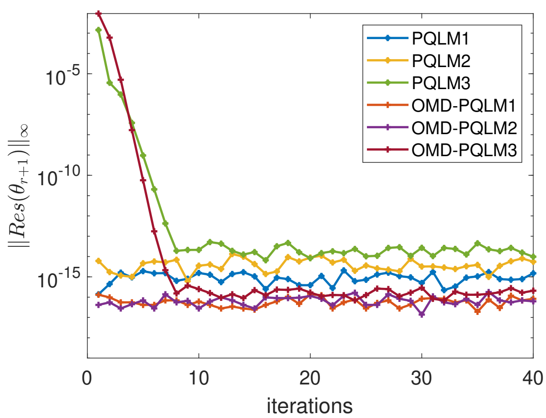

Figure 3.8: The impact of iterations on $\|Res(\theta_{r+1})\|_\infty$

It can be noted that with an increasing number of iterations, there is an improvement in accuracy. The accuracies of all OMD-PQLM cases 1 to 3 surpass those of the PQLM cases 1 to 3. OMD-PQLM cases 1 to 3 demonstrate a comparable residual error of 10^{-16}.

Figures 3.9 to 3.12 present the residual errors of cases 1 to 3 of the OMD-PQLM and cases 1 to 3 of the PQLM against the temporal domain, $[0, 1]$.

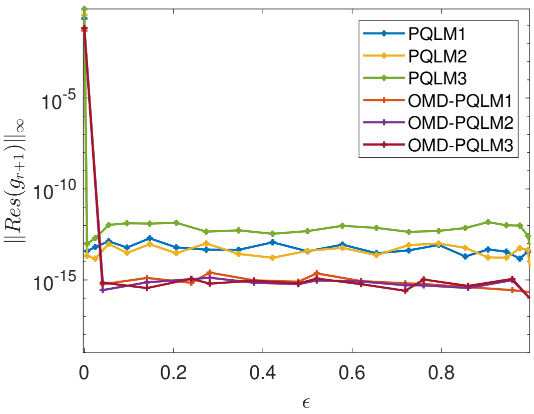

Figure 3.9: Investigating accuracy within the temporal domain using the residual error's norm with respect to g

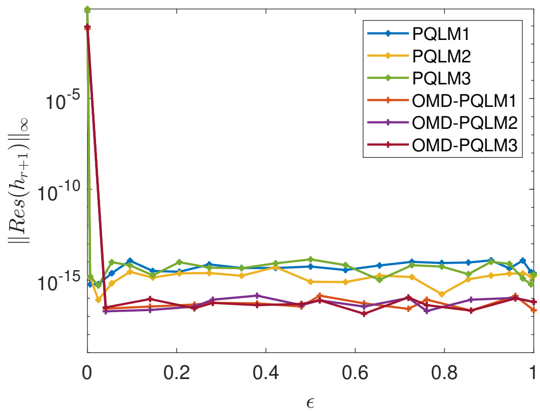

Figure 3.10: Investigating accuracy within the temporal domain using the residual error's norm with respect to h

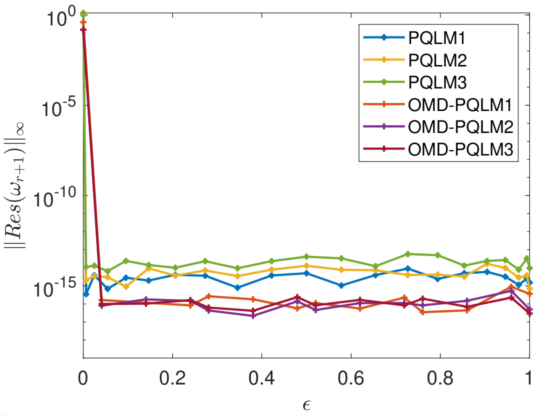

Figure 3.11: Investigating accuracy within the temporal domain using the residual error's norm with respect to ω

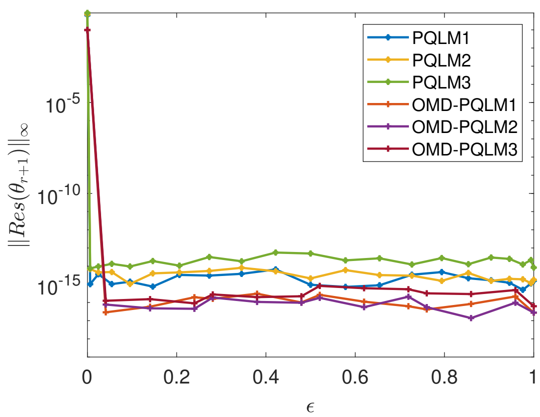

Figure 3.12: Investigating accuracy within the temporal domain using the residual error's norm with respect to θ

Notably, the residual errors consistently maintain a low level across the temporal domain, suggesting a sustained accuracy of the methods throughout the considered temporal domain. The OMD-PQLM cases 1 to 3 outperform all the PQLM cases in terms of accuracy. The OMD-PQLM cases 1 to 3 demonstrate a remarkable level of accuracy, as evidenced by a residual error of 10^{-16}, which is comparable.

Figures 3.13 to 3.16 present the residual errors obtained in both the PQLM and the OMD-PQLM over the time interval of $[0, 2]$.

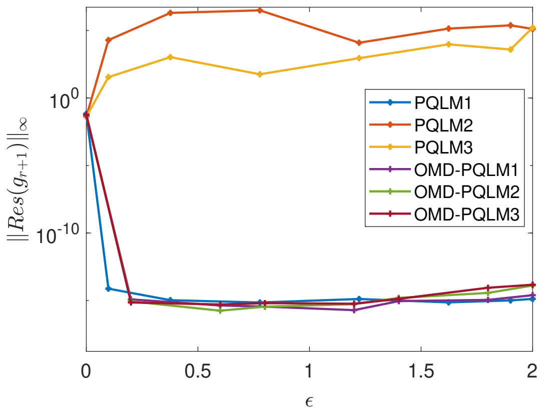

Figure 3.13: Investigating accuracy within the temporal domain using the residual error's norm with respect to g

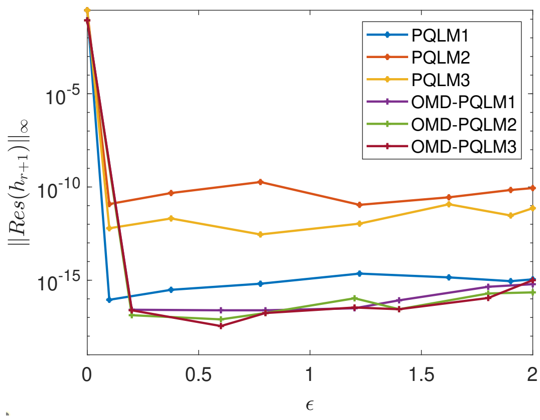

Figure 3.14: Investigating accuracy within the temporal domain using the residual error's norm with respect to h

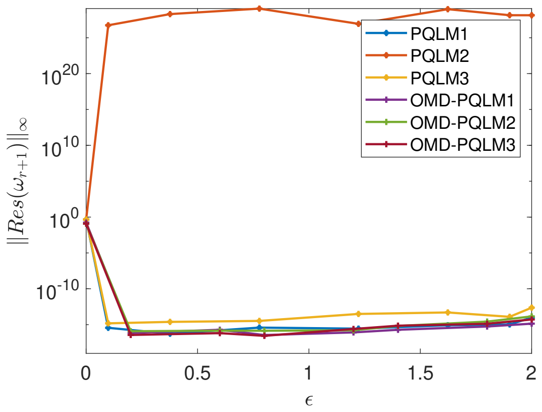

Figure 3.15: Investigating accuracy within the temporal domain using the residual error's norm with respect to ω

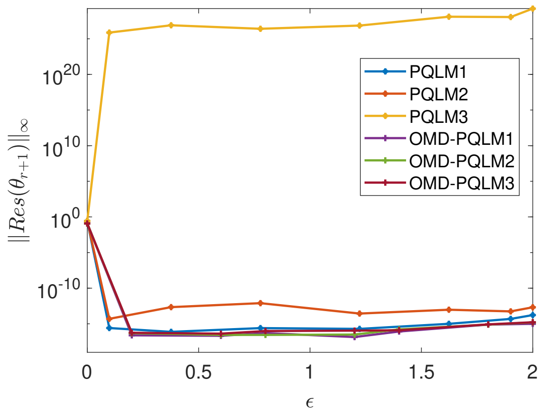

Figure 3.16: Investigating accuracy within the temporal domain using the residual error's norm with respect to θ

Case 1 of the PQLM shows higher accuracy, whereas PQLM cases 2 and 3 fall short in delivering accurate solutions. The OMD-PQLM consistently performs better with higher accuracy in all three cases. The PQLM exhibits enhanced accuracy through the application of the overlapping technique, particularly in problems characterized by large domains.

3.4 Summary

In this chapter, the implementation and comparative analysis of the OMD-PQLM cases 1 to 3 and PQLM cases 1 to 3 for the system of PDEs are outlined. The OMD-PQLM cases 1 to 3 display a faster rate of convergence while comparing all of them to the PQLM cases 1 to 3. Among the OMD-PQLM cases, case 1 exhibits the fastest rate of convergence. This may well be attributed to the existence of more nonlinear terms in their respective pairings, which allows for more implementation of quasilinearization. In addition, OMD-PQLM cases 1 to 3 are more accurate as compared to PQLM cases 1 to 3. It is worth mentioning that when using the OMD-PQLM, while identifying the optimum cases, more importance must be given to a combination with more non-linear terms. Such a strategy would make the process of quasilinearization more complete, leading to a more efficient combination of equations, quick convergence, and also improvement in accuracy. The results by Otegbeye [59] support the results in this chapter where it was found that in the case of the PQLM, cases including more non-linear terms result in faster convergence and higher accuracy. Based on the observation that OMD-PQLM cases 1 to 3 exhibit higher efficiency in comparison to PQLM cases 1 to 3, it can be concluded that solving the system on overlapping partitioned domains effectively optimizes the PQLM.

Chapter 4

Overlapping Multi-Domain Paired Quasilinearization Method for the Solution of the MHD Williamson-Nanofluid Flow over an Exponentially Stretching Surface

4.1 Introduction

Williamson [115] developed the Williamson fluid model, a non-Newtonian fluid exhibiting shear-thinning properties. The Williamson fluid model is applied in diverse biological and industrial settings, particularly in the production of emulsion sheets such as photographic films, as well as in the study of plasma and blood flow [116, 117, 118, 119]. Nadeem and Akbar [120] investigated the peristaltic transport of Williamson fluid in an endoscope using the homotopy analysis method. Their findings revealed that an increase in the non-Newtonian Williamson parameter resulted in a decrease in the velocity of the flow. Similarly, Nadeem and Hussain [121] examined the impact of nanoparticles on the boundary layer flow of Williamson fluid over a dilating surface using the homotopy analysis method. Their study demonstrated that both the width of the boundary layer and the velocity decrease as the Williamson parameter is increased. Gorla and Gireesha [122] numerically investigated heat transfer characteristics on a linearly stretching surface in Williamson nanofluids. The analysis applied the Runge-Kutta–Felhberg fourth-fifth order method along with the Shooting approach. The findings revealed that higher values of the Williamson parameter corresponded to an increased thermal boundary thickness.

To enhance the thermal properties of the fluid, Choi [123] proposed the addition of nanofluid, and this attracted many researchers. The concept proposed by Choi [123] has been used to improve the heat transfer rate in liquids. Mkhatshwa *et al.* [124] studied the MHD mixed convective nanofluid flow about a vertical slender cylinder and reported that augmentation to the nanoparticle volume fraction also enhances the skin friction. They used the OMD-BSQLM, and the method was accurate and the authors were able to carry out the desired investigation on different parameters. Shehzad *et al.* [125] investigated the stagnation point flow of nanofluid over a heated shirking sheet using finite difference technique in consideration of RKF45 method with a shooting technique and it was reported that mass transfer improves with the augmentation of the thermophoresis parameter.

In astrophysical, geophysical, nanotechnological and engineering problems, magnetohydrodynamic (MHD) flows has become common in the recent years. Srinivasacharya [126] studied Hall and ion-slip current effects for flow in a pipe and reported that Hall and ion-slip parameters increased in both flow velocity and microrotation. A sinusoidally heated wavy cavity in porous medium nanofluid applying inclined magnetic field studied by Sameh *et al.* [127] reported an increase in Hartmann number decreases the Nusselt numbers. For the improvement of heat transfer through dispersion, Nawaz [128] investigated three-dimensional heat transfer in the flow of micro-polar liquid subject to four types of nanoparticles, taking into account Hall and ion-slip effects using the finite difference method, the finite element method, and the finite volume method, and reported that Hall current enhancement influences the main flow.

No investigations have been conducted on the combined effect of Hall and Williamson nanofluid on a stretching sheet, as per existing literature. The non-linear system of equations that governs the flow is solved using the OMD-PQLM and individual interest of parameters including the Williamson, porosity, Hall, chemical reaction, and magnetic parameters is studied.

4.2 Formulation and Mathematical Description of the Dynamical System

We examine the steady mixed convective, laminar flow of an electrically conducting nanoparticle-immersed Williamson fluid with constant density and volume past a vertically linearly dilating sheet in a porous medium, influenced by a perpendicularly applied magnetic field B_0. Additionally, the dynamical accounts for the effects of Hall current, assuming a small magnetic Reynolds number. The plate is exponentially stretched along the horizontal axes of the three-coordinate system, while the z axis remains perpendicular to the xy plane. The mass and momentum conservation equations of the flow are as follows:

$$\bigtriangledown \cdot \mathbf{V} = 0, \tag{4.1}$$

$$(\mathbf{V} \cdot \bigtriangledown)\mathbf{V} = \bigtriangledown \cdot \mathbf{S} + \rho \mathbf{b}. \tag{4.2}$$

In this context, $\mathbf{V}$ denotes the velocity vector, ρ represents the fluid density, $\mathbf{S}$ stands for the Cauchy stress tensor, and $\mathbf{b}$ is the specific body force vector. The definition of the Cauchy stress tensor, $\mathbf{S}$, is as follows:

$$\mathbf{S} = -p\mathbf{I} + \tau, \tag{4.3}$$

and τ is the Williamson fluid model defined as

$$\tau = \left[\mu_\infty + \frac{\mu_0 - \mu_\infty}{1 - \Gamma\dot{\gamma}}\right] A_1, \tag{4.4}$$

where p $\mathbf{I}$, τ, $\mu_0, \mu_\infty, \Gamma, A_1$ are pressure, identity vector, extra stress tensor, zero viscosity, infinite shear rate viscosity, time constant, and the Rivlin-Erickson tensor, respectively. $\dot{\gamma}$ is given by

$$\dot{\gamma} = \sqrt{\frac{1}{2}\pi}, \quad \text{where} \quad \pi = trace(A_1)^2. \tag{4.5}$$

In this context, we considered the scenario for which $\mu_\infty = 0$ and $\Gamma\dot{\gamma} << 1$. Therefore, τ_1 can be expressed as

$$\tau = \left(\frac{\mu_0}{1-\Gamma\dot{\gamma}}\right)A_1. \tag{4.6}$$

Through the application of binomial expansion, the expression yields

$$\tau = \mu_0(1+\Gamma\dot{\gamma})A_1. \tag{4.7}$$

Under the assumptions above and following Nadeem [120], Srinivas [126], the conservation equations describing the thermal and mass flux in the flow are expressed as:

$$\frac{\partial u}{\partial x} + \frac{\partial v}{\partial y} + \frac{\partial w}{\partial z} = 0, \tag{4.8}$$

$$\begin{aligned} u\frac{\partial u}{\partial x} + v\frac{\partial u}{\partial y} + w\frac{\partial u}{\partial z} &= \nu\frac{\partial^2 u}{\partial y^2} + \sqrt{2}\Gamma\frac{\partial u}{\partial z}\frac{\partial^2 u}{\partial z^2} - \frac{\nu_f}{k}u - \frac{\sigma B_0^2}{1+\beta^2}(u+\beta v) \\ &+ g^*[\beta_T(T-T_\infty) + (C-C_\infty)], \end{aligned} \tag{4.9}$$

$$u\frac{\partial v}{\partial x} + v\frac{\partial v}{\partial y} + w\frac{\partial v}{\partial z} = \nu\frac{\partial^2 v}{\partial z^2} + \sqrt{2}\Gamma\frac{\partial v}{\partial z}\frac{\partial^2 v}{\partial z^2} - \frac{\nu}{k}w - \frac{\sigma B_0^2}{1+\beta^2}(\beta u + v), \tag{4.10}$$

$$u\frac{\partial T}{\partial x} + v\frac{\partial T}{\partial y} + w\frac{\partial T}{\partial z} = \alpha\frac{\partial^2 T}{\partial z^2} + \Lambda\left(D_B\left(\frac{\partial C}{\partial z}\right)\left(\frac{\partial T}{\partial z}\right) + \frac{D_T}{T_\infty}\left(\frac{\partial T}{\partial y}\right)^2\right) + Q(T-T_\infty), \tag{4.11}$$

$$u\frac{\partial C}{\partial x} + v\frac{\partial C}{\partial y} + w\frac{\partial C}{\partial z} = D_B\frac{\partial^2 C}{\partial z^2} + \frac{D_T}{T_\infty}\frac{\partial^2 T}{\partial z^2} - k_1(C-C_\infty). \tag{4.12}$$

The boundary conditions are

$$\begin{aligned} u = U_w, \quad v = V_w, \quad w = 0, \quad T = T_w, \quad C = C_w \text{ at } \quad z = 0, \\ u \to 0, \quad v \to 0, \quad T = T_\infty, \quad C = C_\infty \quad \text{as} \quad z \to \infty. \end{aligned} \tag{4.13}$$

Here, u, v, w represent the velocity components, β is the Hall parameter, T is the

temperature of the nanofluid, γ porosity parameter, C is the concentration of nanoparticles, g^* is the gravity, σ is electric conductivity of a fluid, D_T and B_D are the coefficient of thermophoretic diffusion and Brownian diffusion, $\Lambda = \frac{(\rho C)_p}{(\rho C)_f}$ is the ratio between the effective heat capacity of the nanoparticles and base fluid, k_1 is the chemical reaction, T_∞ and C_∞ ambient temperature and concentration, U_w and V_w are the surface stretching velocities, T_w and C_w are temperature and concentration, and assumed the form
$U_w = U_0 e^{\frac{x+y}{L}}, \quad V_w = V_0 e^{\frac{x+y}{L}}, \quad T_w = T_\infty + T_0 e^{\frac{A(x+y)}{2L}}, \quad C_w = C_\infty + C_0 e^{\frac{A(x+y)}{2L}},$
where U_0, V_0, T_0, C_0 are constants, and L is the reference length.
Applying the similarity transformation

$$u = U_0 e^{\frac{x+y}{L}} g'(\eta), \quad v = V_0 e^{\frac{x+y}{L}} h'(\eta), \quad w = \left(\frac{U_0}{2\nu L}\right)^{1/2} e^{\frac{x+y}{2L}} (g' + \eta g' + h + \eta h'),$$

$$T = T_\infty + T_0 e^{\frac{x+y}{2L}} \omega(\eta), \quad C = C_\infty + C_0 e^{\frac{x+y}{2L}} \theta(\eta), \; \eta = z\sqrt{\frac{U_0}{2\nu L}}, \tag{4.14}$$

and substituting Equation (4.14) into Equations (4.8) to (4.12), we get the following non-dimensional equations

$$(1+\chi g'')g''' + (g+h)g'' - 2(g'+h)g' + \lambda(\omega + N_r\theta) - \gamma g' - \frac{M}{1+\beta^2}(g' + \beta h') = 0, \tag{4.15}$$

$$(1+\chi h')h''' + (g+h)h'' - 2(g'+h')h' - \gamma h' - \frac{M}{1+\beta^2}(\beta g' - h') = 0, \tag{4.16}$$

$$\omega'' + Pr[(g+h)\omega' - A(g'+h')\omega + Nb\omega'\theta' + Nt\omega'^2] + Q\omega = 0, \tag{4.17}$$

$$\theta'' + PrLe[(g+h)\theta' - A(g'+h')\theta] + \frac{N_t}{N_b}\omega'' - K\theta = 0, \tag{4.18}$$

where $\chi = \Gamma U_0 \sqrt{\frac{U_w}{\nu L}}$ is the Williamson parameter, $G_r = \frac{h^* \beta_T (T_w - T_\infty) x^3}{\nu^2}$ is the temperature Grashof number, $Re_x = \frac{U_0 L}{\nu} e^{\frac{x+y}{L}}$ is the Reynolds numbers, $\lambda = \frac{G_r}{Re^2}$ is mixed convection parameter, $M = \frac{2L\sigma B_0^2}{U_w \rho}$ is the magnetic parameter, $\gamma = \frac{\nu_f}{Ka}$ is the porosity parameter, the buoyancy ratio parameter $Nr = \frac{\beta_c (C_w - C_\infty)}{\beta_T (T_w - T_\infty)}$, $Nb = \frac{\Lambda D_B (C_w - C_\infty)}{\nu_f}$ is the Brownian motion parameter, $Nt = \frac{\Lambda D_T (T_w - T_\infty)}{T_\infty \nu}$ is the thermophoresis parameter, $Pr = \frac{\nu}{\alpha}$ is the Prandtl number, $K = \frac{2k_1}{U_w}$ is the chemical reaction parameter and $Le = \frac{\alpha}{D_B}$ is the Lewis number.

The boundary conditions now take the form

$$g = 0, \quad g' = 1, \quad h = 0, \quad h' = S, \quad \omega = 1 \quad \theta = 1, \text{ at } \quad \eta = 0$$

$$g' \to 0, \quad h' \to 0, \quad \omega \to 0 \quad \theta \to 0, \quad \text{as} \quad \eta \to \infty, \tag{4.19}$$

where $S = \frac{V_0}{U_0}$ is the stretching ratio.
The engineering parameters of interest are the Skin friction coefficients C_{fx} and C_{fz}, the Sherwood number Sh_x, and the local Nusselt number Nu_x given by

$$C_{fx} = \frac{\tau_{ux}}{\rho U_w^2}, \quad C_{fz} = \frac{\tau_{wx}}{\rho U_w^2}, \quad Nu_x = \frac{x q_w}{k(T_w - T_\infty)}, \qquad Sh_x = \frac{x q_m}{D_B(C_w - C_\infty)}, \tag{4.20}$$

where

$$\tau_{ux} = \mu \left(\frac{\partial u}{\partial z} + \frac{\Gamma}{\sqrt{2}} \left(\frac{\partial u}{\partial z} \right)^2 \right)_{z=0}, \quad \tau_{wz} = \mu \left(\frac{\partial w}{\partial y} + \frac{\Gamma}{\sqrt{2}} \left(\frac{\partial w}{\partial y} \right)^2 \right)_{z=0},$$

$$q_w = -k \left(\frac{\partial T}{\partial z} \right)_{z=0}, \quad q_m = -D_B \left(\frac{\partial C}{\partial z} \right)_{z=0}. \tag{4.21}$$

The non-dimensional form is written as

$$Re_x^{1/2} C_{fx} = g''(0) + \frac{\chi}{2} g''^2(0), \quad Re_x^{1/2} C_{fz} = h''(0) + \frac{\chi}{2} h''^2(0),$$

$$Re_x^{-1/2} Nu_x = \omega'(0), \quad Re_x^{-1/2} Sh_x = \theta'(0) \tag{4.22}$$

4.3 Numerical Discretization of the Fluid Flow System

This section describes the application of the OMD-PQLM as detailed in Chapter 1 to solve the system of non-linear Equations (4.15) to (4.18). There are three different ways to pair the systems of Equations (4.15) to (4.18). These combinations will be considered to determine how the various sets of pairing affect the speed of convergence and solutions. The pairings are defined as follows:

i. case 1: involves the pairings ($\{g, h\}$ and $\{\omega, \theta\}$) corresponding to the Equations $\{4.15, 4.16\}$ and $\{4.17, 4.18\}$,

ii. case 2: involves the pairings ($\{g,\omega\}$ and $\{h,\theta\}$) corresponding to the Equations $\{4.15, 4.17\}$ and $\{4.16, 4.18\}$, and

iii. case 3: involves the pairings ($\{g,\theta\}$ and $\{h,\omega\}$) corresponding to the Equations $\{4.15, 4.18\}$ and $\{4.16, 4.17\}$.

4.3.1 Case 1: involves the pairing ($\{g,h\}$ and $\{\omega,\theta\}$) corresponding to the Equations $\{4.15, 4.16\}$ and $\{4.17, 4.18\}$

The non-linear components, $\chi g'' g''', gg'', hg'', -2g'^2, -2hg'$, $\chi h' h'''$, $(g+h)h''$, and $-2\left(g'+h'\right)h'$, undergo linearization through the first-order Taylor series expansion. The Chebyshev spectral collocation and overlapping approaches are then applied to the linearized pair in the following manner:

$$\Big[[a_0]\mathbf{D}^3 + [a_1]\mathbf{D}^2 + [a_2]\mathbf{D} + [a_3]\mathbf{I}\Big]\mathbf{G}_{r+1} + \Big[[a_4]\mathbf{D} + [a_5]\mathbf{I}\Big]\mathbf{H}_{r+1} = R_1, \tag{4.23}$$

$$\Big[[b_0]\mathbf{D} + [b_1]\mathbf{I}\Big]\mathbf{G}_{r+1} + \Big[[b_2]\mathbf{D}^3 + [b_3]\mathbf{D}^2 + [b_4]\mathbf{D} + [b_5]\mathbf{I}\Big]\mathbf{H}_{r+1} = R_2. \tag{4.24}$$

where

$$a_0 = 1 + \chi g_r'', \quad a_1 = \chi g_r''' + g_r + h_r, \quad a_2 = -4g_r' - 2h_r' - \gamma - \frac{M}{1+\beta^2},$$
$$a_3 = g_r'', \quad a_4 = -\frac{M\beta}{1+\beta^2}, \quad a_5 = g_r'' - 2g_r', \quad b_0 = -2h_r' - \frac{M\beta}{1+\beta^2}, \quad b_1 = h_r'',$$
$$b_2 = 1 + \chi h_r', \quad b_3 = g_r + h_r, \quad b_4 = \chi h_r''' - 2g_r' - 4h_r' - \gamma - \frac{M}{1+\beta^2}, \quad b_5 = h_r'',$$
$$R_1 = \chi g_r'' g_r''' + (g_r + h_r)\, g_r'' - 2\left(g_r' + h_r'\right) g_r' - \lambda\left(\omega_r + N_r\theta_r\right),$$
$$R_2 = \chi h_r' h_r''' + (g_r + h_r)\, h_r'' - 2\left(g_r' + h_r'\right) h_r'.$$

The second set of equations integrates the revised solutions for g and h. The linearized pair is obtained by linearizing the non-linear components, $PrNb\omega'\theta'$ and $PrNt\omega'^2$, by the use of the first-order Taylor series expansion.

$$\omega_{r+1}'' + Pr\Big(\left(g_{r+1} + h_{r+1}\right) + Nb\theta_r + 2Nt\omega_r'\Big)\omega_{r+1}' + \Big(Pr\left(-A\left(g_{r+1}' + h_{r+1}'\right)\right) + Q\Big)$$
$$\cdot\, \omega_{r+1} + \left[PrNb\omega_r'\right]\theta_{r+1}' = PrNb\omega_r'\theta_r' + PrNt\omega_r'^2, \tag{4.25}$$

$$\left(\frac{Nt}{Nb}\right)\omega_{r+1}'' + \theta_{r+1}'' + \Big(PrLe\left(g_{r+1} + h_{r+1}\right)\Big)\theta_{r+1}' + \Big(PrLe\left(-A\left(g_{r+1}' + h_{r+1}'\right)\right) - K\Big)\theta_{r+1} = 0. \tag{4.26}$$

The Chebyshev spectral collocation method and the overlapping approach are applied in the following manner:

$$\Big[\mathbf{D}^2 + [c_0]\,\mathbf{D} + [c_1]\mathbf{I}\Big]\,\mathbf{\Omega}_{r+1} + \Big[\,[c_2]\,\mathbf{D}\Big]\mathbf{\Theta}_{r+1} = R_3, \tag{4.27}$$

$$\left[\left(\frac{N_t}{Nb}\right)\mathbf{D}^2\right]\mathbf{\Omega}_{r+1} + \Big[\mathbf{D}^2 + [e_0]\,\mathbf{D} + [e_1]\,\mathbf{I}\Big]\,\mathbf{\Theta}_{r+1} = R_4, \tag{4.28}$$

where

$$c_0 = Pr\left[\left(g_{r+1} + h_{r+1}\right) + Nb\theta_r' + 2Nt\omega_r'\right], \quad c_1 = Pr\left(-A\left(g_{r+1}' + h_{r+1}'\right)\right) + Q,$$
$$c_2 = PrNb\omega_r', \quad e_0 = PrLe\left(g_{r+1} + h_{r+1}\right), \quad e_1 = PrLe\left(-A\left(g_{r+1}' + h_{r+1}'\right)\right) - K$$
$$R_3 = PrNb\omega_r'\theta_r' + PrNt\omega_r'^2, \quad R_4 = \mathbf{0}.$$

4.3.2 Case 2: involves the pairings ($\{g, \omega\}$ and $\{h, \theta\}$) corresponding to the Equations $\{4.15, 4.17\}$ and $\{4.16, 4.18\}$

The linearized pair is obtained by linearizing the non-linear components, $\chi g'' g'''$, gg'', $-2g'^2$, and $Pr(g\omega' - Ag'\omega' - Nt\omega'^2)$, by the use of the first-order Taylor series expansion. The Chebyshev spectral collocation and overlapping approaches are then applied in the following manner:

$$\Big[[a_0]\mathbf{D}^3 + [a_1]\mathbf{D}^2 + [a_2]\mathbf{D} + [a_3]\mathbf{I}\Big]\,\mathbf{G}_{r+1} + \Big[[\lambda]\mathbf{I}\Big]\,\mathbf{\Omega}_{r+1} = R_1, \tag{4.29}$$

$$\Big[[b_0]\mathbf{D} + [b_1]\mathbf{I}\Big]\,\mathbf{G}_{r+1} + \Big[\mathbf{D}^2 + [b_2]\mathbf{D} + [b_3]\mathbf{I}\Big]\,\mathbf{\Omega}_{r+1} = R_2, \tag{4.30}$$

where

$$a_0 = 1 + \chi g_r'', \quad a_1 = \chi g_r''' + g_r + h_r, \quad a_2 = -4g_r' - 2h_r - \gamma - \frac{M}{1+\beta^2}$$
$$a_0 = g_r'', \quad b_0 = -PrA\omega_r, \quad b_1 = Pr\omega_r',$$
$$b_2 = Pr(g_r + h_r + Nb\theta_r + 2Nt\omega_r'), \quad b_3 = -PrA\left(g_r' + h_r'\right) + Q,$$
$$R_1 = \chi g_r'' g_r''' + g_r'' g_r'' - 2g_r'^2 - \lambda Nr\theta_r - \frac{M\beta h_r'}{1+\beta^2},$$
$$R_2 = Pr\left(g_r\omega_r' - Ag_r'\omega_r + Nt\omega_r'^2\right).$$

The second set of equations integrates the revised solutions for g and ω. The linearized pair is obtained by linearizing the non-linear components, $\chi h'h''', hh''$, $PrLe(h\theta' - Ah'\theta)$, and h'^2, by the use of the first-order Taylor series expansion. The Chebyshev spectral collocation and overlapping approaches are then applied in the following manner:

$$\left[[c_0]\mathbf{D}^3 + [c_1]\mathbf{D}^2 + [c_2]\mathbf{D} + [h_r'']\mathbf{I}\right]\mathbf{H}_{r+1} + \left[[\mathbf{0}]\right]\mathbf{\Theta}_{r+1} = R_3 \tag{4.31}$$
$$\left[[e_0]\mathbf{D} + [e_1]\mathbf{I}\right]\mathbf{H}_{r+1} + \left[\mathbf{D}^2 + [e_2]\mathbf{D} + [e_3]\mathbf{I}\right]\mathbf{\Theta}_{r+1} = R_4 \tag{4.32}$$

where

$$c_0 = 1 + \chi h_r', \quad c_1 = g_{r+1} + h_r, \quad c_2 = \chi h_r''' - 4h_r' - 2g_{r+1}' - \gamma - \frac{M}{1+\beta^2},$$
$$e_0 = PrLe(-A\theta_{r+1}), \quad e_1 = PrLe\theta_r', \quad e_2 = PrLe(g_{r+1} + h_r),$$
$$e_3 = PrLe(-A(g_{r+1}' + h_r')) - K,$$
$$R_3 = \chi h_r' h_r''' + h_r h_r'' - 2h_r^2 + \frac{M\beta g_{r+1}'}{1+\beta^2},$$
$$R_4 = PrLe\left(h_r\theta_r' - Ah_r'\theta_r\right) - \frac{Nt}{Nb}\omega_{r+1}'',$$

where $\mathbf{0}$ denotes a zero matrix of the same size as $\mathbf{I}$ and $\mathbf{D}$.

4.3.3 Case 3: involves the pairings $(\{g, \theta\}$ and $\{h, \omega\})$ corresponding to the Equations $\{4.15, 4.18\}$ and $\{4.16, 4.17\}$

The linearized pair is obtained by linearizing the non-linear components, $\chi g'' g'''$, gg'', $-2g'^2$, and, $PrLe(g\theta' - Ag'\theta)$, by the use of the first-order Taylor series expansion. The Chebyshev spectral collocation and overlapping approaches are then applied in the following manner:

$$\Big[[a_0]\mathbf{D}^3 + [a_1]\mathbf{D}^2 + [a_2]\mathbf{D} + [g_r'']\mathbf{I}\Big]\mathbf{G}_{r+1} + \Big[[\lambda Nr]\mathbf{I}\Big]\mathbf{\Theta}_{r+1} = R_1, \tag{4.33}$$

$$\Big[[b_0]\mathbf{D} + [b_1]\mathbf{I}\Big]\mathbf{G}_{r+1} + \Big[\mathbf{D}^2 + [b_2]\mathbf{D} + [b_3]\mathbf{I}\Big]\mathbf{\Theta}_{r+1} = R_2, \tag{4.34}$$

where

$$\begin{aligned}
&a_0 = 1 + \chi g_r'', \quad a_1 = \chi g_r''' + g_r + h_r, \quad a_2 = -4g_r' - 2h_r' - \gamma - \frac{M}{1+\beta^2}, \\
&b_0 = -PrLeA\theta_r, \quad b_1 = PrLe\theta_r', \quad b_2 = PrLe(g_r + h_r), \\
&b_3 = -PrLeA(g_r' + h_r') - K, \\
&R_1 = \chi g_r'' g_r''' + g_r g_r'' - 2g_r'^2 - \lambda\omega_r - \frac{M\beta h_r'}{1+\beta^2} \\
&R_2 = PrLe\left(g_r\theta_r' - Ag_r'\theta_r\right) - \frac{Nt}{Nb}\omega_r''.
\end{aligned}$$

The subsequent pair of equations make use of the improved solutions for g and θ. The linearized pair is obtained by linearizing the non-linear components $\chi h' h'''$, hh'', $-2h'^2$, $Prh\omega'$, $-PrAh'\omega$, and $PrNt\omega'^2$, by the use of the first-order Taylor series expansion. The Chebyshev spectral collocation and overlapping approaches are then applied in the following manner:

$$\Big[[c_0]\mathbf{D}^3 + [c_1]\mathbf{D}^2 + [c_2]\mathbf{D} + [h_r'']\mathbf{I}\Big]\mathbf{H}_{r+1} + \Big[[\mathbf{0}]\Big]\mathbf{\Omega}_{r+1} = R_3 \tag{4.35}$$

$$\Big[[e_0]\mathbf{D} + [e_1]\mathbf{I}\Big]\mathbf{H}_{r+1} + \Big[\mathbf{D}^2 + [e_2]\mathbf{D} + [e_3]\mathbf{I}\Big]\mathbf{\Omega}_{r+1} = R_4 \tag{4.36}$$

where

$$c_0 = 1 + \chi h'_r, \quad c_1 = g_{r+1} + h_r, \quad c_2 = \chi h'''_r - 4h'_r - 2g'_{r+1} - \gamma - \frac{M}{1+\beta^2},$$
$$e_0 = -PrA\omega_r, \quad e_1 = Pr\omega'_r, \quad e_2 = Pr(g_{r+1} + h_r) + Nb\theta'_{r+1} + 2Nt\omega'_r,$$
$$e_3 = Pr(-A(g'_{r+1} - Ah'_r) + Q),$$
$$R_3 = \chi h'_r h'''_r + h_r h''_r - 2h'^2_r + \frac{M\beta g'_{r+1}}{1+\beta^2},$$
$$R_4 = Pr\left(g_r\omega'_r - Ah'_r\omega_r + N_t\omega'^2_r\right),$$

0 denotes a zero matrix of the same size as **I** and **D**.

4.4 Findings and Analysis

The numerical solution of Equations (4.15) to (4.18), along with the boundary conditions in Equation (4.19), is obtained using the OMD-PQLM and the PQLM. Unless stated otherwise, the predefined numeric values for the parameters remain constant, $\chi = 0.3$, $\lambda = Nb = Nt = Q = Le = 0.5$, $Nr = \gamma = K = 1$, $M = 3$, $\beta = 2$, and $Pr = A = 5$.

The solution error analysis is undertaken to analyze the convergence. The solution error is determined by computing the subtraction of consecutive iterations of the approximate solutions.

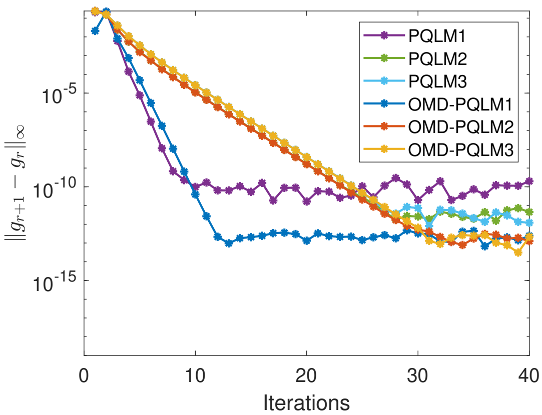

Figure 4.1: Error in g between consecutive iterations

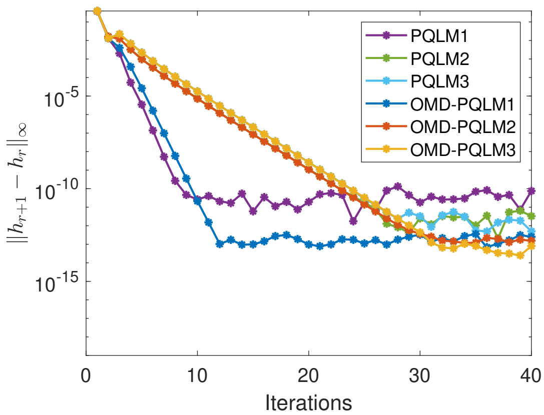

Figure 4.2: Error in h between consecutive iterations

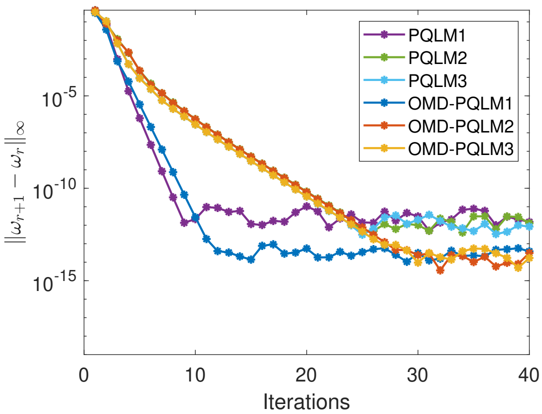

Figure 4.3: Error in ω between consecutive iterations

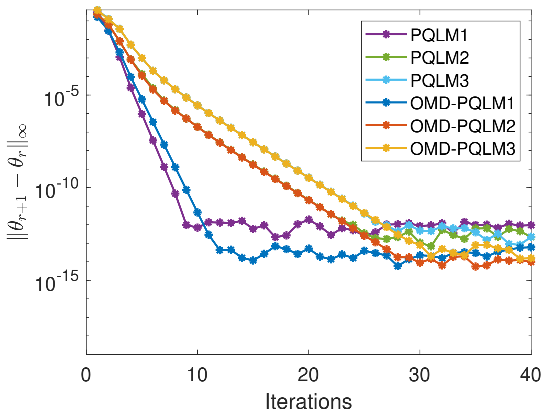

Figure 4.4: Error in θ between consecutive iterations

The errors in solutions for Equations (4.15) to (4.18) can be observed in Figures 4.1 to 4.4. It has been noted that as the number of iterations increases, the error between two successive approximate solutions decreases until it reaches a point where further improvement is not possible. Once the error has reached its minimum and cannot be further decreased, it denotes that the method has converged. The OMD-PQLM cases demonstrate the smallest error in solutions, whereas the PQLM cases attain convergence more quickly than the OMD-PQLM cases. Case 1 of both the PQLM and the OMD-PQLM exhibits rapid convergence, as evidenced by the steep incline of the slope. In both Case 1 of the PQLM and the OMD-PQLM, the solution errors for $g(\eta)$, $h(\eta)$, $\omega(\eta)$, and $\theta(\eta)$ exhibit convergence between the 8th and 12th iterations. The OMD-PQLM cases exhibit all desirable characteristics and demonstrate rapid convergence to a greater level of accuracy in comparison to other cases.

The estimated solutions obtained through the OMD-PQLM are then substituted into the transformed model equations to obtain the residual norm, in the following manner:

$$\begin{aligned}\mathbf{Res}(\mathbf{G}) &= (1+\chi\mathbf{g}'')\mathbf{g}''' + (\mathbf{g}+\mathbf{h})\mathbf{g}'' - 2(\mathbf{g}'+\mathbf{h})\mathbf{g}' + \lambda(\boldsymbol{\omega}+N_r\boldsymbol{\theta}) \\ &- \gamma\mathbf{g}' + \frac{M}{1+\beta^2}(\mathbf{g}'+\beta\mathbf{h}'),\end{aligned} \tag{4.37}$$

$$\mathbf{Res}(\mathbf{H}) = (1+\chi\mathbf{h}')\mathbf{h}''' + (\mathbf{g}+\mathbf{h})\mathbf{h}'' - 2(\mathbf{g}'+\mathbf{h}')\mathbf{h}' - \gamma\mathbf{h}' - \frac{M}{1+\beta^2}(\beta\mathbf{g}'-\mathbf{h}'), \tag{4.38}$$

$$\boldsymbol{Res}(\boldsymbol{\Omega}) = \boldsymbol{\omega}'' + Pr[(\mathbf{g}+\mathbf{h})\boldsymbol{\omega} - A(\mathbf{g}'+\mathbf{h}')\boldsymbol{\omega}' + Nb\boldsymbol{\omega}'\boldsymbol{\theta}' + Nt\boldsymbol{\omega}'^2] + Q\boldsymbol{\omega}, \tag{4.39}$$

$$\boldsymbol{Res}(\boldsymbol{\Theta}) = \boldsymbol{\theta}'' + PrLe[(\mathbf{g}+\mathbf{h})\boldsymbol{\theta}' - A(\mathbf{g}'+\mathbf{h}')\boldsymbol{\theta}] + \frac{N_t}{N_b}\boldsymbol{\omega}'' - K\boldsymbol{\theta}. \tag{4.40}$$

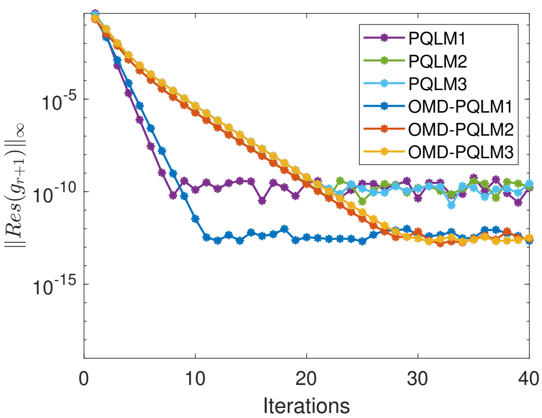

Figure 4.5: The impact of iterations on $\|Res(g_{r+1})\|_\infty$

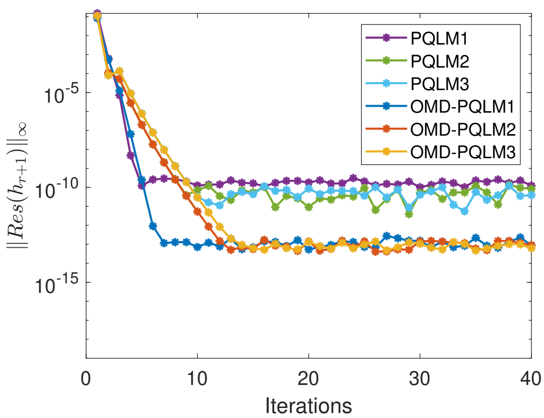

Figure 4.6: The impact of iterations on $\|Res(h_{r+1})\|_\infty$

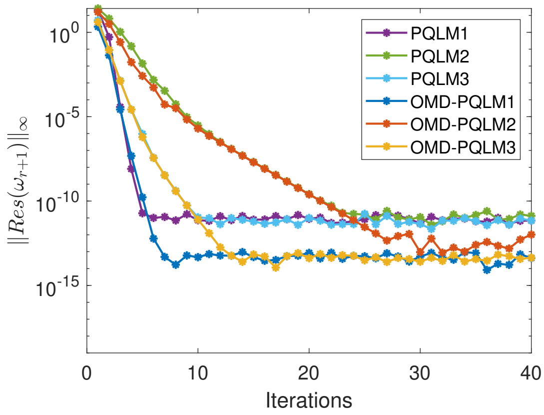

Figure 4.7: The impact of iterations on $\|Res(\omega_{r+1})\|_\infty$

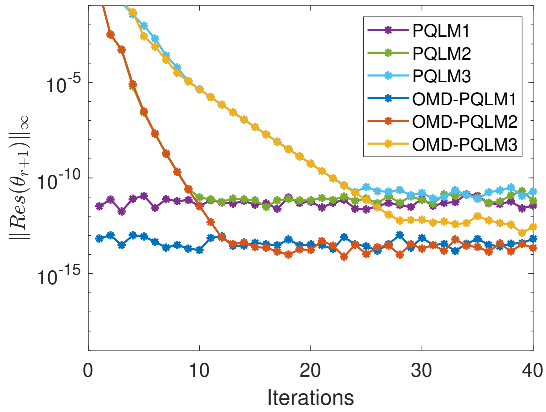

Figure 4.8: The impact of iterations on $\|Res(\theta_{r+1})\|_\infty$

Figures 4.5 to 4.8 show the effect of the number of iterations on accuracy. As the number of iterations increases, it is noteworthy that the accuracy for Figures 4.5 to 4.7 improves until it reaches its optimum level and cannot be further improved. The OMD-PQLM cases exhibit higher accuracy compared to all the PQLM cases. While the PQLM cases converge faster, they reach a lower accuracy compared to the OMD-PQLM cases. Specifically, Case 1 of the PQLM demonstrates the fastest convergence but achieves the lowest accuracy levels, with the residual error for $h(\eta)$ being the highest compared to the other cases. Conversely, OMD-PQLM Case 1 embodies all desirable characteristics, demonstrating both higher accuracy and faster convergence. The residual errors for the OMD-PQLM fall within the range of 10^{-13} to 10^{-14}, indicating that the OMD-PQLM is highly effective in solving comparable problems discussed in this study.

The OMD-PQLM case 1 was used to carry out the analysis of different parameters of interest since it embodies both higher accuracy and faster convergence.

4.4.1 Combined Effects of the Williamson and Hall Parameters

Figures 4.9 to 4.12 show the combined effects of the Hall and Williamson parameters on the flows' velocities in the x and y direction, $g'(\eta)$ and $h'(\eta)$, the concentration, $\theta(\eta)$, and the temperature distribution, $\omega(\eta)$.

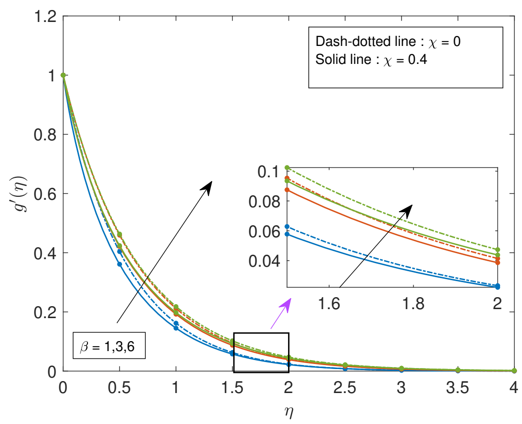

Figure 4.9: Impact of the Williamson, χ, and the Hall parameter, β, on $g'(\eta)$

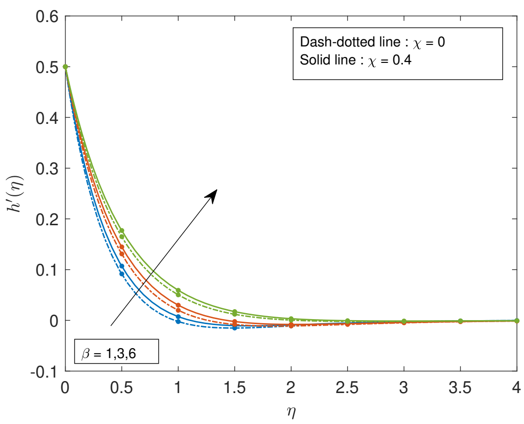

Figure 4.10: Impact of the Williamson, χ, and the Hall parameter, β, on $h'(\eta)$

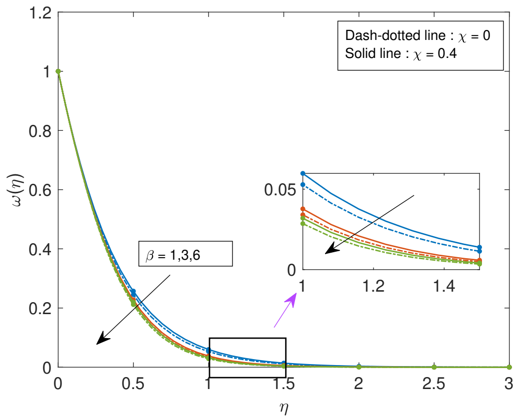

Figure 4.11: Impact of the Williamson, χ, and the Hall parameter, β, on $\omega(\eta)$

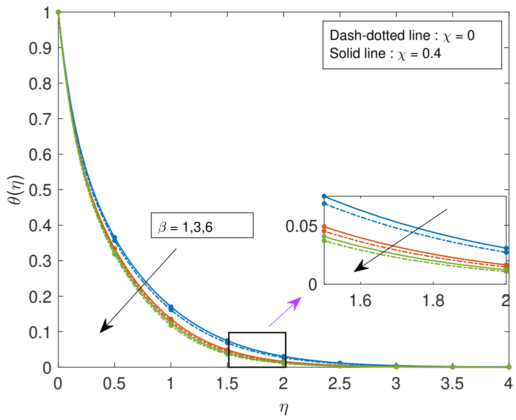

Figure 4.12: Impact of the Williamson, χ, and the Hall parameter, β, on $\theta(\eta)$

The Williamson parameter significantly influences the flows' velocities, temperature distribution, and concentration. It is observed that both $g'(\eta)$ and $h'(\eta)$ increase as the Hall parameter, β, increases, indicating heightened velocity components in the x and y directions. When the Williamson parameter, χ, is set to 0.4, $g'(\eta)$ consistently remains below the case of a viscous fluid ($\chi = 0$). For $h'(\eta)$ with $\chi = 0$, the velocity in the y-direction consistently remains lower compared to $\chi = 0.4$, implying that the shear-thinning effects enhance the speed in the y-direction. As the Hall parameter, β, increases, the temperature distribution, $\omega'(\eta)$, and concentration, $\theta'(\eta)$, both decrease, showing an inverse relationship. The evidence suggests that a larger β value leads to a cooling impact and modifies the behavior of nanoparticles within the nanofluid. In the absence of the Williamson parameter, lower temperatures and concentrations are constantly observed, suggesting that the shear-thinning features of the Williamson parameter lead to an increased concentration and temperature.

4.4.2 Combined Effect of the Williamson and the Porosity Parameter

Figures 4.13 to 4.16 show the combined effect of the porosity and the Williamson parameter on the velocity profiles, $g'(\eta)$ and $h'(\eta)$, the concentration, $\theta(\eta)$, and the temperature distribution, $\omega(\eta)$.

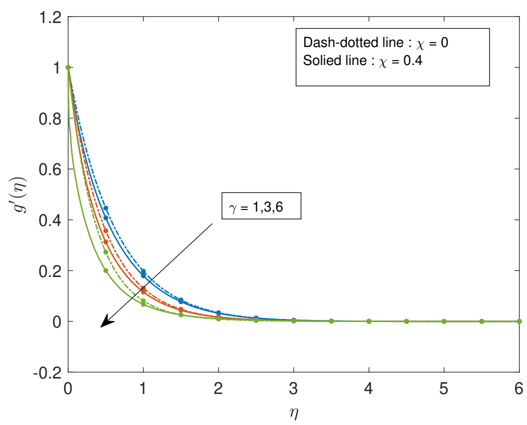

Figure 4.13: Impact of the Williamson, χ, and the porosity parameter, γ, on $g'(\eta)$

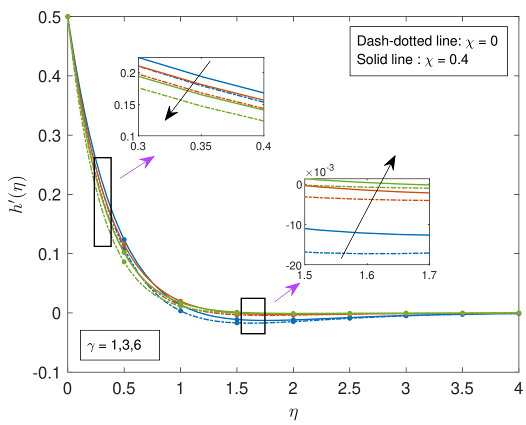

Figure 4.14: Impact of the Williamson, χ, and the porosity parameter, γ, on $h'(\eta)$

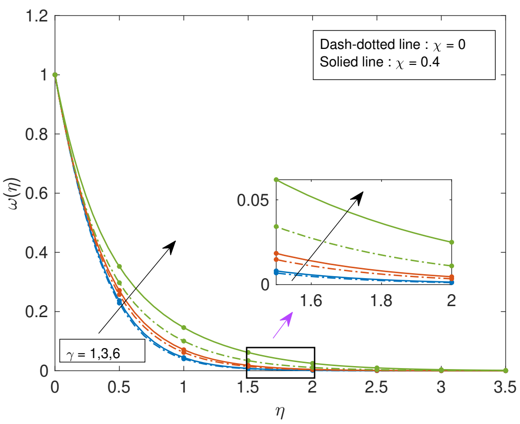

Figure 4.15: Impact of the Williamson, χ, and the porosity parameter, γ, on $\omega(\eta)$

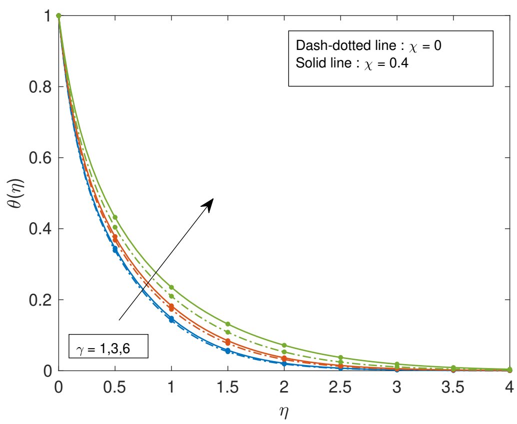

Figure 4.16: Impact of the Williamson, χ, and the porosity parameter, γ, on $\theta(\eta)$

As the porosity parameter, γ, increases, $g'(\eta)$ consistently decreases. This suggests that the presence of the porosity parameter reduces the velocity component in the x-direction. For $\chi = 0$, the $g'(\eta)$ profile remains consistently above that of $\chi = 0.4$, indicating that the shear-thinning properties introduced by the Williamson parameter, χ, have a diminishing effect on the velocity profile. The $h'(\eta)$ profile exhibits a more complex behavior with an initial decrease and subsequent increase as γ increases. This suggests that the y-component velocity initially decreases with higher γ and then increases. For $\chi = 0$, the $h'(\eta)$ profile is below that of $\chi = 0.4$, indicating that the shear-thinning properties enhance the y-direction velocity. The concentration, $\theta'(\eta)$, and the temperature distribution, $\omega(\eta)$, increase with a rise in the porosity parameter, γ. Higher values of γ imply an elevation in temperature and concentration profiles. For $\chi = 0$, the temperature and the concentration profiles are consistently below that of $\chi = 0.4$, indicating that the presence of the Williamson parameter contributes to a higher temperature and concentration. The shear-thinning properties of the Williamson parameter, χ, consistently impact the velocity profiles.

4.4.3 Combined Effects of the Williamson and Chemical Reaction Parameters

Figures 4.17 to 4.20 show the combined effects on $f'(\eta)$, $h'(\eta)$, $\theta(\eta)$, and $\omega(\eta)$, induced by the Williamson parameter and the chemical reaction parameter.

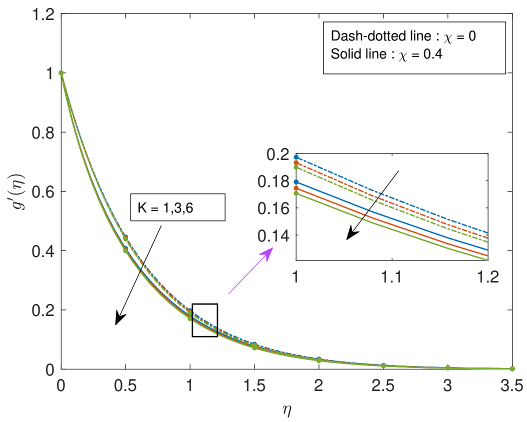

Figure 4.17: Impact of the Williamson, χ, and the chemical reaction parameter, K, on $g'(\eta)$

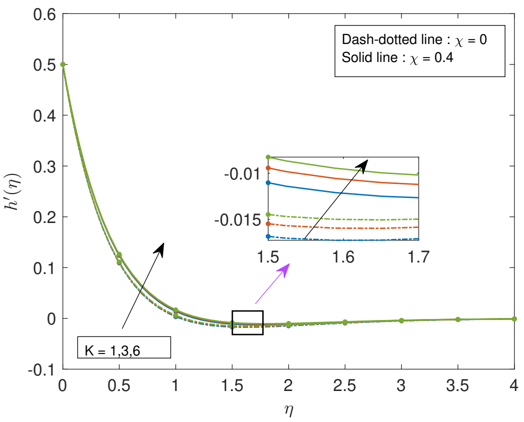

Figure 4.18: Impact of the Williamson, χ, and the chemical reaction parameter, K, on $h'(\eta)$

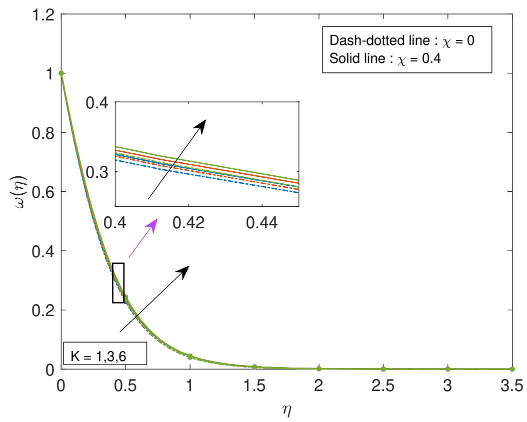

Figure 4.19: Impact of the Williamson, χ, and the chemical reaction parameter, K, on $\omega(\eta)$

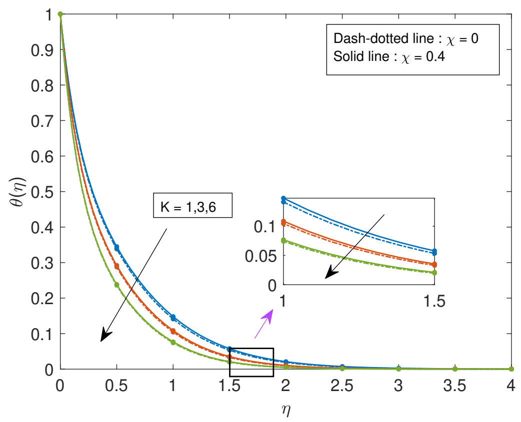

Figure 4.20: Impact of the Williamson, χ, and the chemical reaction parameter, K, on $\theta(\eta)$

The velocity profile, $g'(\eta)$, consistently decreases as the chemical reaction parameter K increases, indicating that higher values of K result in a reduction of the velocity component in the x-direction. For $\chi = 0$, the velocity profiles are consistently above those for $\chi = 0.4$. This suggests that the presence of the Williamson parameter contributes to a diminishing effect on the velocity profiles, especially with an increasing K. The velocity profile, $h'(\eta)$, increases as the chemical reaction parameter, K, increases. This implies that higher values of K lead to an enhancement of the speed along the y-axis. For $\chi = 0$, the velocity profiles are consistently below those for $\chi = 0.4$. This suggests that the shear-thinning properties introduced by the Williamson parameter contribute to an increase in the speed along the y-axis, especially with an increasing K. The temperature distribution, $\omega(\eta)$, increases with an increase in the chemical reaction parameter K. This signifies that higher values of K result in higher temperatures. For $\chi = 0$, the temperature distributions are consistently below those for $\chi = 0.4$. This suggests that the presence of the Williamson parameter contributes to a higher temperature. The concentration, $\theta(\eta)$, decreases as the chemical reaction parameter, K, increases, indicating that higher values of K lead to a reduction in concentration. For $\chi = 0$, the concentration profiles are consistently below those for $\chi = 0.4$. This suggests that the shear-thinning properties introduced by the Williamson parameter, χ, contribute to a lower concentration.

4.4.4 Effect of the Magnetic Parameter

Figures 4.21 to 4.24 display the impact of the magnetic parameter, M, on the velocity profiles, $g'(\eta)$ and $h'(\eta)$, temperature distribution, $\omega(\eta)$, and the concentration profile, $\theta(\eta)$.

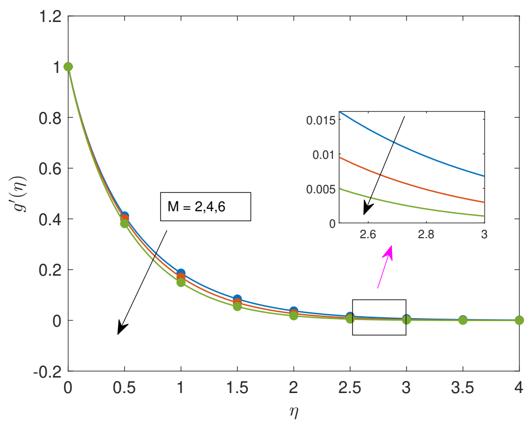

Figure 4.21: The influence of the magnetic parameter, M, on $g'(\eta)$

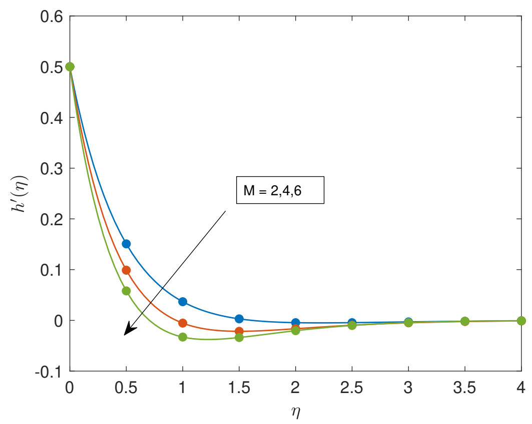

Figure 4.22: The influence of the magnetic parameter, M, on $h'(\eta)$

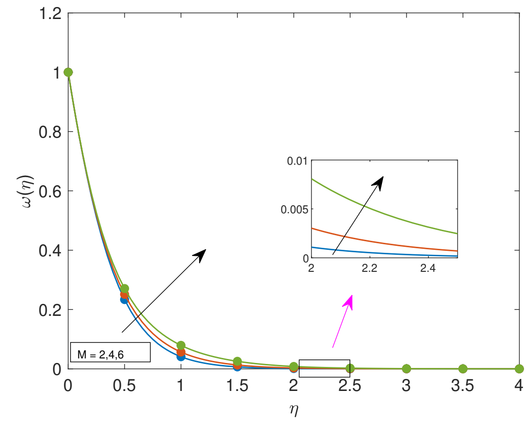

Figure 4.23: The influence of the magnetic parameter, M, on $\omega(\eta)$

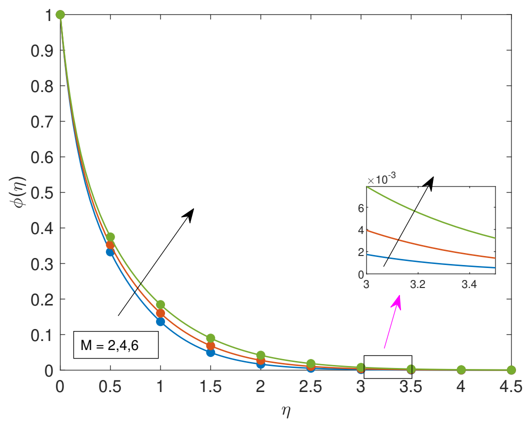

Figure 4.24: The influence of the magnetic parameter, M, on $\theta(\eta)$

A higher value of the magnetic parameter leads to a reduction in the velocity profiles, $g'(\eta)$ and $h'(\eta)$. The decrease in the velocity profiles implies that stronger forces limit the movement of the fluid. The increased magnetic parameter can result in stronger forces that limit the velocity of fluid particles in both the x and y directions. The increase of the magnetic parameter results in simultaneous rises in both the concentration, $\theta(\eta)$, and the temperature distribution, $\omega(\eta)$. The increased magnetic force results in the generation of heat, which in turn raises the temperature. Additionally, a strong magnetic force promotes the concentration of nanoparticles.

4.5 Summary

This study investigates the analysis of magnetohydrodynamic (MHD) Williamson-nanofluid flow across an exponentially stretched surface. The similarity transformation was applied to transform the governing equations into highly non-linear ODEs. The OMD-PQLM is subsequently utilized to solve these non-linear differential equations. It is noteworthy to mention that the OMD-PQLM yields several combinations. However, in this study, the most efficient combination of the OMD-PQLM is chosen to generate results. The obtained results highlight the efficacy of the method in resolving the MHD Williamson-nanofluid flow over an exponentially stretched surface. The study expands its investigation to examine the impact of several parameters on the system, such as the Hall parameter, chemical reaction parameter, thermophoresis particle parameter, Brownian motion parameter, and magnetic parameter, among others. Moreover, the study presents and thoroughly discusses the impact of various parameters. The analysis of the fluid model reveals that the Williamson parameter, χ, exerts a significant influence on various aspects of the system, particularly in shaping velocity profiles, temperature distribution, and concentration. The shear-thinning properties introduced by χ lead to a distinct decrease in the velocity component in the x-direction, and an increase in the y-direction. Additionally, the presence of χ consistently contributes to higher temperature distribution, $\omega(\eta)$, and concentration, $\theta(\eta)$, across different investigations involving varying values of the Hall parameter, β, porosity parameter, γ, and the chemical reaction parameter, K. This indicates that the shear-thinning effects of the Williamson fluid play a crucial role in influencing the overall fluid dynamics and thermal and mass transfer attributes of the system.

Chapter 5

Conclusion

This study presented a novel technique called the overlapping multi-domain paired quasilinearization method (OMD-PQLM) as an effective method for solving both general ordinary differential equations (ODEs) and partial differential equations (PDEs). The effectiveness of the method was proven by thorough evaluations, showcasing its accuracy and capacity to converge. OMD-PQLM has been proven to outperform the standard paired quasilinearization method (PQLM) in terms of accuracy and convergence, as demonstrated by comparative analyses.

Chapter 2 illustrated the application of OMD-PQLM to a system of ODEs, showing its notable accuracy and faster convergence in comparison to the PQLM. The results of this comparative assessment confirm the efficiency of the OMD-PQLM in solving systems of ODEs. It was observed that the combination of equations with increased levels of non-linearity led to a faster convergence rate and improved accuracy. The observed effect can be attributed to the increased use of quasilinearization in these specific combinations of equations. In a larger domain, the PQLM does not achieve convergent and precise results. However, all the OMD-PQLM cases yield convergent and accurate results, even in a large domain.

In Chapter 3, the application of the OMD-PQLM was expanded to include systems of PDEs. The OMD-PQLM demonstrated higher accuracy and convergence characteristics compared to the PQLM, as evidenced by a thorough comparison. A combination of equations exhibiting greater levels of nonlinearity was found to yield a faster convergence rate and improved accuracy. In these particular combinations of equations, the observed result can be attributed to the higher application of quasilinearization. When the temporal domain is expanded, case 1 of the PQLM demonstrated high accuracy, while cases 2 and 3 of the PQLM show deficiencies in providing accurate solutions. However, in all three cases, the OMD-PQLM consistently demonstrated greater efficiency while exhibiting higher accuracy.

Chapter 4 of the study investigated the impact of physical parameters on the flow of MHD Williamson-nanofluid across a model of an exponentially extending surface. The OMD-PQLM was utilized to produce results to analyze the influence of different parameters on the flow patterns. Based on the evidence and results obtained, we can fairly conclude that the method is highly effective in solving equations that characterize flow properties.

The findings obtained in this study suggest that the computational schemes presented are easy to apply and produce higher accuracy and faster convergence. They demonstrate efficiency by requiring a smaller number of collocations and overlapping grids to produce accurate results. The OMD-PQLM's efficiency was evident in its requirement for fewer collocation points compared to the PQLM. Moreover, as the size of the problem domain increased, the OMD-PQLM adapted effectively, converging within shorter computational times, thus offering a scalable solution for complex problems. These findings hold significant implications for practical applications, especially in fields where accurate solutions across large parameter spaces are crucial. The OMD-PQLM's ability to maintain high accuracy and speedy convergence in large domains makes it a valuable tool for engineers, scientists, and researchers tackling real-world problems with complex dynamics. In conclusion, the research establishes the OMD-PQLM as a superior alternative to traditional methods, showcasing its ability to achieve fast convergence, and high accuracy, in large problem domains. By offering efficient and scalable solutions, the OMD-PQLM emerges as a promising approach for addressing complex computational challenges across various domains of science and engineering. The computational simplicity of this method is particularly remarkable because it eliminates the need for a large dense matrix to attain accuracy. Furthermore, the method's adaptability can further its investigation in solving complex problems that are modelled using elliptic equations, and fractional differential equations, among others.

Bibliography

[1] B.V. Norkin. "Mathematical models for insurance business optimization". *Cybernetics and Systems Analysis* 47.1 (2011), pp. 117–133. DOI: https://doi.org/10.1007/s10559-011-9295-5.

[2] A. Quarteroni. "Mathematical models in science and engineering". *Notices of the American Meteorological Society* 56.1 (2009), pp. 10–19. DOI: https://doi.org/10.1007/978-3-030-96166-4.

[3] J.T. Ottesen, M.S. Olufsen, and J.K. Larsen. *Applied mathematical models in human physiology*. Society for Industrial and Applied Mathematics, Philadelphia, (2004). DOI: https://doi.org/10.1137/1.9780898718287.

[4] C. Molina-París and G. Lythe. *Mathematical models and immune cell biology*. Springer Science & Business Media, New york, (2011). DOI: https://doi.org/10.1007/978-1-4419-7725-0.

[5] M. Roger and S. Moreau. "Extensions and limitations of analytical airfoil broadband noise models". *International Journal of Aeroacoustics* 9.3 (2010), pp. 273–305. DOI: https://doi.org/10.1260/1475-472x.9.3.273.

[6] R. Raghavan, J.D.T. Scorer, and F.G. Miller. "An investigation by numerical methods of the effect of pressure-dependent rock and fluid properties on well flow tests". *Society of Petroleum Engineers Journal* 12.03 (1972), pp. 267–275. DOI: https://doi.org/10.2118/2617-pa.

[7] E. Isaacson and H.B. Keller. *Analysis of numerical methods*. Courier Corporation, New York, (1994). DOI: https://doi.org/10.2307/2003280.

[8] B.C. Brookes. "Numerical methods of bibliographic analysis". *Graduate School of Library and Information Science. University of Illinois* (1973). DOI: https://doi.org/10.2307/40321804.

[9] C. Paniconi, A.A. Aldama, and E.F. Wood. "Numerical evaluation of iterative and noniterative methods for the solution of the nonlinear Richards equation". *Water Resources Research* 27.6 (1991), pp. 1147–1163. DOI: https://doi.org/10.1029/91wr00334.

[10] H.H. Goldstine. *A History of Numerical Analysis from the 16th through the 19th Century*. Springer Science & Business Media, New York, (2012). DOI: https://doi.org/10.1007/978-1-4684-9472-3.

[11] M. Benzi. "Key moments in the history of numerical analysis". *Numerical Mathematics* 5 (2009). DOI: https://doi.org/10.1002/nla.815.

[12] I. Todhunter. *A History of the Mathematical Theories of Attraction and the Figure of the Earth from the Time of Newton to that of Laplace*. Vol. 1. Macmillan and Company, Macmillan, (1873). DOI: https://doi.org/10.2307/2003799.

[13] W. Gautschi. "Leonhard Euler: his life, the man, and his works". *SIAM review* 50.1 (2008), pp. 3–33. DOI: https://doi.org/10.1137/070702710.

[14] H. Pulte. "Joseph Louis Lagrange, Méchanique analitique, (1788)". In: *Landmark Writings in Western Mathematics 1640-1940*. Elsevier, (2005), pp. 208–224. DOI: https://doi.org/10.1016/b978-044450871-3/50097-8.

[15] T. Molale. "Mathematical Foundation of Public Key Cryptosystems". *Citeseer* (2005). DOI: https://doi.org/10.1142/9789811208058_0007.

[16] R.S. Calinger. *Leonhard Euler: Mathematical genius in the enlightenment*. Princeton University Press, New Jersey, (2015). DOI: https://doi.org/10.1515/9781400866632-fm.

[17] V. Thomée. "From finite differences to finite elements A short history of numerical analysis of partial differential equations". In: *Numerical Analysis: Historical Developments in the 20th Century*. Elsevier, (2001), pp. 361–414. DOI: https://doi.org/10.1016/b978-0-444-50617-7.50016-1.

[18] R. Courant, K. Friedrichs, and H. Lewy. "On the partial difference equations of mathematical physics". *IBM journal of Research and Development* 11.2 (1967), pp. 215–234. DOI: https://doi.org/10.1147/rd.112.0215.

[19] K.J. Marfurt. "Accuracy of finite-difference and finite-element modeling of the scalar and elastic wave equations". *Geophysics* 49.5 (1984), pp. 533–549. DOI: https://doi.org/10.1190/1.1441689.

[20] G. Birkhoff. "Solving elliptic problems: 1930–1980". In: *Elliptic problem solvers*. Elsevier, (1981), pp. 17–38. DOI: https://doi.org/10.1016/b978-0-12-632620-8.50007-3.

[21] W.R. Wasow. "The accuracy of difference approximations to plane Dirichlet problems with piecewise analytic boundary values". *Quarterly of Applied Mathematics* 15.1 (1957), pp. 53–63. DOI: https://doi.org/10.1090/qam/88800.

[22] J. Crank and P. Nicolson. "A practical method for numerical evaluation of solutions of partial differential equations of the heat-conduction type". In: *Mathematical proceedings of the Cambridge philosophical society*. 43.1. Cambridge University Press. Cambridgeshire, (1947), pp. 50–67. DOI: https://doi.org/10.1007/bf02127704.

[23] P.L. Butzer and R. Weis. "On the Lax equivalence theorem equipped with orders". *Journal of Approximation Theory* 19.3 (1977), pp. 239–252. DOI: https://doi.org/10.1016/0021-9045(77)90055-7.

[24] P. Jamet. "A finite difference scheme and an existence theorem for a nonlinear hyperbolic system of differential equations". *Society for Industrial and Applied Mathematics Journal on Numerical Analysis* 8.3 (1971), pp. 524–535. DOI: https://doi.org/10.1137/0708050.

[25] G. Birkhoff. "Piecewise analytic interpolation and approximation in triangulated polygons". In: *The Mathematical Foundations of the Finite Element Method with Applications to Partial Differential Equations*. Elsevier, (1972), pp. 363–385. DOI: https://doi.org/10.1016/b978-0-12-068650-6.50018-6.

[26] A. Boada, C. Paolini, and J.E. Castillo. "High-order mimetic finite differences for anisotropic elliptic equations". *Computers Fluids* 213 (2020). DOI: https://doi.org/10.1016/j.compfluid.2020.104746.

[27] J.C. Strikwerda. *Finite difference schemes and partial differential equations*. Society for Industrial and Applied Mathematics, Philadelphia, (2004). DOI: https://doi.org/10.1137/1.9780898717938.

[28] P.K. Pandey and S.S.A. Jaboob. "A finite difference method for a numerical solution of elliptic boundary value problems". *Applied Mathematics and Nonlinear Sciences* 3.1 (2018), pp. 311–320. DOI: https://doi.org/10.21042/amns.2018.1.00024.

[29] R.D. Russell and L.F. Shampine. "A collocation method for boundary value problems". *Numerische Mathematik* 19.1 (1972), pp. 1–28. DOI: https://doi.org/10.1007/bf01395926.

[30] B. Guo. *Spectral methods and their applications*. World Scientific, Shanghai, (1998). DOI: https://doi.org/10.47340/mjellt.v1i2.2.2020.

[31] M.Y. Hussaini and T.A. Zang. "Spectral methods in fluid dynamics". *Annual Review of Fluid Mechanics* 19.1 (1987), pp. 339–367. DOI: https://doi.org/10.1007/978-3-642-84108-8.

[32] B. Shizgal. "Spectral methods in chemistry and physics". *Scientific Computation, Springer* (2015). DOI: https://doi.org/10.1007/978-94-017-9454-1.

[33] L He. "Spectral Heat Transfer Coefficient for convection". *International Journal of Heat and Mass Transfer* 216 (2023). DOI: https://doi.org/10.1016/j.ijheatmasstransfer.2023.124557.

[34] Y. Sun, J. Ma, and B. Li. "Chebyshev collocation spectral method for three-dimensional transient coupled radiative–conductive heat transfer". *AMSE journal of Heat and Mass Transfer* (2012). DOI: https://doi.org/10.1115/1.4006596.

[35] M.E. Elyashberg, Y.Z. Karasev, E.R. Martirosian, H. Thiele, and H. Somberg. "Expert systems as a tool for the molecular structure elucidation by spectral methods. Strategies of solution to the problems". *Analytica Chimica Acta* 348.1-3 (1997), pp. 443–463. DOI: https://doi.org/10.1016/s0003-2670(97)00229-8.

[36] H. Schamel and K. Elsässer. "The application of the spectral method to nonlinear wave propagation". *Journal of Computational Physics* 22.4 (1976), pp. 501–516. DOI: https://doi.org/10.1016/0021-9991(76)90046-2.

[37] C.E. Larsen and T. Irvine. "A review of spectral methods for variable amplitude fatigue prediction and new results". *Procedia Engineering* 101 (2015), pp. 243–250. DOI: https://doi.org/10.1016/j.proeng.2015.02.034.

[38] I.M. Park, E.W Archer, N. Priebe, and J.W. Pillow. "Spectral methods for neural characterization using generalized quadratic models". *Advances in Neural Information Processing Systems* 26 (2013).

[39] L.N. Trefethen. *Finite difference and spectral methods for ordinary and partial differential equations*. Mathematics, Cornell University, New York, (1996).

[40] S.M. Schmalholz, Y.Y. Podladchikov, and D.W. Schmid. "A spectral/finite difference method for simulating large deformations of heterogeneous, viscoelastic materials". *Geophysical Journal International* 145.1 (2001), pp. 199–208. DOI: https://doi.org/10.1046/j.0956-540x.2000.01371.x.

[41] M.N. Özişik, H.R.B. Orlande, J.M. Colaço, and R.M. Cotta. *Finite difference methods in heat transfer*. CRC press, Boca Raton, (2017). DOI: https://doi.org/10.1201/9781315168784.

[42] L.N. Trefethen. *Spectral methods in MATLAB*. Society for Industrial and Applied Mathematics, Mathematics, Cornell University, New York, (2000). DOI: https://doi.org/10.1137/1.9780898719598.

[43] E. Tadmor. "Convergence of spectral methods for nonlinear conservation laws". *SIAM Journal on Numerical Analysis* 26.1 (1989), pp. 30–44. DOI: https://doi.org/10.1137/0726003.

[44] S.S. Motsa, Z.G. Makukula, and S. Shateyi. "Spectral local linearisation approach for natural convection boundary layer flow". *Mathematical Problems in Engineering* 2013 (2013). DOI: https://doi.org/10.1155/2013/765013.

[45] S.S. Motsa. "A new spectral relaxation method for similarity variable nonlinear boundary layer flow systems". *Chemical Engineering Communications* 201.2 (2014), pp. 241–256. DOI: https://doi.org/10.1080/00986445.2013.766882.

[46] X. Yu, W. Weng, P.A. Taylor, and D. Liang. "Relaxation factor effects in the non-linear mixed spectral finite difference model of flow over topographic features". *Boundary-layer Meteorology* 140 (2011), pp. 23–35. DOI: https://doi.org/10.1007/s10546-011-9601-9.

[47] C. RamReddy, P.L. Narayana, and S.S. Motsa. "A spectral relaxation method for linear and non-linear stratification effects on mixed convection in a porous medium". *Applied Mathematics and Computation* 268 (2015), pp. 991–1000. DOI: https://doi.org/10.1016/j.amc.2015.07.007.

[48] S.S. Motsa, P.G. Dlamini, and M. Khumalo. "Spectral relaxation method and spectral quasilinearization method for solving unsteady boundary layer flow problems". *Advances in Mathematical Physics* 2014 (2014). DOI: https://doi.org/10.1155/2014/341964.

[49] K. Gangadhar, T. Kannan, G. Sakthivel, and K K. DasaradhaRamaiah. "Unsteady free convective boundary layer flow of a nanofluid past a stretching surface using a spectral relaxation method". *International Journal of Ambient Energy* 41.6 (2020), pp. 609–616. DOI: https://doi.org/10.2478/s11534-013-0182-8.

[50] S.S. Motsa, P.G. Dlamini, and M. Khumalo. "Solving hyperchaotic systems using the spectral relaxation method". In: *Abstract and Applied Analysis*. Hindawi, London. (2012). DOI: https://doi.org/10.1155/2012/203461.

[51] S.R.M Venkata, K. Gangadhar, and P.L.N. Varma. "A spectral relaxation method for three-dimensional MHD flow of nanofluid flow over an exponentially stretching sheet due to convective heating: an application to solar energy". *Indian Journal of Physics* 92.12 (2018), pp. 1577–1588. DOI: https://doi.org/10.1007/s12648-018-1226-0.

[52] S. Shateyi, S.S. Motsa, and Z. Makukula. "On spectral relaxation method for entropy generation on a MHD flow and heat transfer of a Maxwell fluid". *Journal of Applied Fluid Mechanics* 8.1 (2014), pp. 21–31. DOI: https://doi.org/10.36884/jafm.8.01.20273.

[53] R.E. Bellman and R.E Kalaba. *Nonlinear Boundary-Value Problems*. American Elsevier Publishing Co., Inc, New York, (1965). DOI: https://doi.org/10.1145/365474.365523.

[54] M. Magodora, H. Mondal, and P. Sibanda. "Effect of Cattaneo-Christov Heat Flux on Radiative Hydromagnetic Nanofluid Flow between Parallel Plates

using Spectral Quasilinearization Method". *Journal of Applied and Computational Mechanics* (2020). DOI: https://doi.org/10.1108/mmms-01-2019-0028.

[55] I.S. Oyelakin, S. Mondal, and P. Sibanda. "Nonlinear radiation in bioconvective Casson nanofluid flow". *International Journal of Applied and Computational Mathematics* 5 (2019), pp. 1–20. DOI: https://doi.org/10.1007/s40819-019-0705-0.

[56] O. Otegbeye. "On decoupled quasi-linearization methods for solving systems of nonlinear boundary value problems". MSc dissertation. (2014).

[57] S.S. Motsa. "A new spectral local linearization method for nonlinear boundary layer flow problems". *Journal of Applied Mathematics* 2013 (2013). DOI: https://doi.org/10.1155/2013/423628.

[58] S.S. Motsa and I.L. Animasaun. "Paired quasi-linearization analysis of heat transfer in unsteady mixed convection nanofluid containing both nanoparticles and gyrotactic microorganisms due to impulsive motion". *Journal of Heat Transfer* 138.11 (2016). DOI: https://doi.org/10.1115/1.4034039.

[59] O. Otegbeye and S.S. Motsa. "A paired quasilinearization method for solving boundary layer flow problems". In: *American Institute of Physics Conference Proceedings*. 1975.1. American Institute of Physics Publishing LLC. (2018). DOI: https://doi.org/10.1063/1.5042190.

[60] M. Trivedi, O. Otegbeye, M.S. Ansari, and S.S. Motsa. "A paired quasi-linearization on magnetohydrodynamic flow and heat transfer of Casson nanofluid with Hall effects". *Journal of Applied and Computational Mechanics* 5.5 (2019), pp. 849–860. DOI: https://doi.org/10.1166/jon.2019.1691.

[61] O. Otegbeye, S.S. Motsa, and M.S Ansari. "An application of paired quasi-linearization on double-diffusive convection flow over a cone embedded in a porous medium in the presence of nanoparticles". *Heat Transfer—Asian Research* 48.4 (2019), pp. 1413–1439. DOI: https://doi.org/10.1002/htj.21439.

[62] O. Otegbeye and S.S. Motsa. "A paired spectral-finite difference approach for solving boundary layer flow problems". *Afrika Matematika* 30.3 (2019), pp. 433–458. DOI: https://doi.org/10.1007/s13370-019-00658-3.

[63] O. Otegbeye. "On paired decoupled quasi-linearization methods for solving nonlinear systems of differential equations that model boundary layer fluid flow problems." PhD thesis. (2018).

[64] V.M. Magagula, S.S. Motsa, and P. Sibanda. "A Multi-Domain Bivariate Pseudospectral Method for Evolution Equations". *International Journal of Computational Methods* 14.04 (2017). DOI: 10.1142/S0219876217500414.

[65] S.S. Motsa and C.H. RamReddy. "Non-similarity solution for Soret effect on natural convection over the vertical frustum of a cone in a nanofluid using new bivariate pseudo-spectral local linearisation method". *Applied Mathematics and Computation* 314 (2017), pp. 439–455. ISSN: 0096-3003. DOI: https://doi.org/10.1016/j.amc.2017.07.001.

[66] V.M. Magagula, S.S. Motsa, and P. Sibanda. "Multidomain bivariate pseudospectral quasilinearization method for systems of nonlinear partial differential equations". *Computational and Mathematical Methods* 2.4 (2020). DOI: https://doi.org/10.1002/cmm4.1096.

[67] S. Mutua. "Computational and numerical analysis of differential equations using spectral based collocation method". PhD thesis. (2019).

[68] M.P. Mkhatshwa, S.S. Motsa, and P. Sibanda. "Overlapping multi-domain spectral method for conjugate problems of conduction and MHD Free convection flow of nanofluids over flat plates". *Mathematical and Computational Applications* 24.3 (2019). DOI: https://doi.org/10.3390/mca24030075.

[69] M.P. Mkhatshwa, S.S. Motsa, and P. Sibanda. "Overlapping Multi-Domain Spectral Method for MHD Mixed Convection Slip Flow Over an Exponentially Decreasing Mainstream with Nonuniform Heat Source/Sink and Convective Boundary Conditions". *International Journal of Computational Methods* 18.05 (2021). DOI: https://doi.org/10.1142/s0219876221500043.

[70] M.P. Mkhatshwa, S.S. Motsa, and P. Sibanda. "Overlapping multi-domain bivariate spectral method for systems of nonlinear PDEs with fluid mechanics applications". In: *Advances in Fluid Dynamics: Selected Proceedings of ICAFD 2018*. Springer. (2021), pp. 685–699. DOI: https://doi.org/10.1007/978-981-15-4308-1_54.

[71] S. Nzama. "On multivariate overlapping grid spectral quasilinearization methods for problems in cavity flow." MSc dissertation. (2022).

[72] R.E. Bellman, R.E. Kalaba, and L.E Payne. "Quasilinearization and nonlinear boundary-value problems". *American Elsevier* (1965). DOI: https://doi.org/10.2307/2313669.

[73] V.B. Mandelzweig and F. Tabakin. "Quasilinearization approach to nonlinear problems in physics with application to nonlinear ODEs". *Computer Physics Communications* 141.2 (2001), pp. 268–281. DOI: https://doi.org/10.1016/s0010-4655(01)00415-5.

[74] R. Krivec and V.B. Mandelzweig. "Numerical investigation of quasilinearization method in quantum mechanics". *Computer Physics Communications* 138.1 (2001), pp. 69–79. DOI: https://doi.org/10.1016/s0010-4655(01)00191-6.

[75] R.E. Bellman, j. Jacquez, R.E. Kalaba, and S. Schwimmer. "Quasilinearization and the estimation of chemical rate constants from raw kinetic data". *Mathematical Biosciences* 1.1 (1967), pp. 71–76. DOI: https://doi.org/10.1016/0025-5564(67)90027-2.

[76] N. Shazad and A.S. Vatsala. "Extension of the method of generalized quasilinearization for second order boundary value problems". *Applicable Analysis* 58.1-2 (1995), pp. 77–83. DOI: https://doi.org/10.1080/00036819508840363.

[77] B. Ahmad, J.J. Nieto, and N. Shahzad. "The Bellman–Kalaba–Lakshmikantham quasilinearization method for neumann problems". *Journal of Mathematical Analysis and Applications* 257.2 (2001), pp. 356–363. DOI: https://doi.org/10.1006/jmaa.2000.7352.

[78] J.J. Nieto. "Generalized quasilinearization method for a second order ordinary differential equation with Dirichlet boundary conditions". *Proceedings of the American Mathematical Society* 125.9 (1997), pp. 2599–2604. DOI: https://doi.org/10.1090/s0002-9939-97-03976-2.

[79] B. Ahmad, J.J. Nieto, and N. Shahzad. "Generalized quasilinearization method for mixed boundary value problems". *Applied Mathematics and Computation* 133.2-3 (2002), pp. 423–429. DOI: https://doi.org/10.1016/s0096-3003(01)00243-0.

[80] V. Lakshmikantham, N. Shahzad, and J.J. Nieto. "Methods of generalized quasilinearization for periodic boundary value problems". *Nonlinear Analysis* 27.2 (1996), pp. 143–152. DOI: https://doi.org/10.1016/0362-546x(95)00021-m.

[81] V. Lakshmikantham. "An extension of the method of quasilinearization". *Journal of Optimization Theory and Applications* 82 (1994), pp. 315–321. DOI: https://doi.org/10.1007/bf02191856.

[82] T. Kohno, H. Kotakemori, H. Niki, and M. Usui. "Improving the modified Gauss-Seidel method for Z-matrices". *Linear Algebra and its Applications* 267 (1997), pp. 113–123. DOI: https://doi.org/10.1016/s0024-3795(97)80045-6.

[83] M. Usui, H. Niki, and T. Kohno. "Adaptive Gauss-Seidel method for linear systems". *International Journal of Computer Mathematics* 51.1-2 (1994), pp. 119–125. DOI: https://doi.org/10.1080/00207169408804271.

[84] J.P. Milaszewicz. "Improving jacobi and gauss-seidel iterations". *Linear Algebra and Its Applications* 93 (1987), pp. 161–170. DOI: https://doi.org/10.1016/s0024-3795(87)90321-1.

[85] M. Beghini, L. Bertini, and P. Raffaelli. "Numerical analysis of plasticity effects in the hole-drilling residual stress measurement". *Journal of Testing and Evaluation* 22.6 (1994), pp. 522–529. DOI: https://doi.org/10.1520/jte11856j.

[86] F. Wang and H. Wu. "Enhanced oil droplet detachment from solid surfaces in charged nanoparticle suspensions". *Soft Matter* 9.33 (2013), pp. 7974–7980. DOI: https://doi.org/10.1039/c3sm51425k.

[87] S. Gogoi and S.B. Gogoi. "Review on microfluidic studies for EOR application". *Journal of Petroleum Exploration and Production Technology* 9 (2019), pp. 2263–2277. DOI: https://doi.org/10.1007/s13202-019-0610-4.

[88] A. Raees, H. Xu, Q. Sun, and I. Pop. "Mixed convection in gravity-driven nano-liquid film containing both nanoparticles and gyrotactic microorganisms". *Applied Mathematics and Mechanics* 36.2 (2015), pp. 163–178. DOI: https://doi.org/10.1007/s10483-015-1901-7.

[89] G.D. Fulford. "The flow of liquids in thin films". In: *Advances in Chemical Engineering*. (1964), pp. 151–236. DOI: https://doi.org/10.1016/s0065-2377(08)60008-3.

[90] F. Wang and H. Wu. "Molecular dynamics studies on spreading of nanofluids promoted by nanoparticle adsorption on solid surface". *Theoretical and Applied Mechanics Letters* 3.5 (2013). DOI: https://doi.org/10.1063/2.1305406.

[91] N. Guy, G. Enchéry, and G. Renard. "Numerical modeling of thermal EOR: Comprehensive coupling of an AMR-based model of thermal fluid flow and geomechanics". *Oil & Gas Science and Technology–Revue d'IFP Energies Nouvelles* 67.6 (2012), pp. 1019–1027. DOI: https://doi.org/10.2516/ogst/2012052.

[92] A.V. Kuznetsov and D.A. Nield. "Natural convective boundary-layer flow of a nanofluid past a vertical plate". *International Journal of Thermal Sciences* 49.2 (2010), pp. 243–247. DOI: https://doi.org/10.1016/j.ijthermalsci.2009.07.015.

[93] J. Buongiorno. "Convective transport in nanofluids". *American Society of Mechanical Engineers Journal of Heat and Mass Transfer* (2006). DOI: https://doi.org/10.1115/1.2150834.

[94] D.A. Nield and A.V. Kuznetsov. "The Cheng–Minkowycz problem for natural convective boundary-layer flow in a porous medium saturated by a nanofluid". *International Journal of Heat and Mass Transfer* 52.25-26 (2009), pp. 5792–5795. DOI: https://doi.org/10.1016/j.ijheatmasstransfer.2009.07.024.

[95] T. Hayat, A. Aziz, T. Muhammad, and A. Alsaedi. "Active and passive controls of Jeffrey nanofluid flow over a nonlinear stretching surface". *Results in Physics* 7 (2017), pp. 4071–4078. DOI: https://doi.org/10.1016/j.rinp.2017.10.028.

[96] T. Hayat and M. Qasim. "Effects of thermal radiation on unsteady magnetohydrodynamic flow of a micropolar fluid with heat and mass transfer". *Zeitschrift für Naturforschung A* 65.11 (2010), pp. 950–960. DOI: https://doi.org/10.1515/zna-2010-1107.

[97] A.C. Eringen. “Theory of micropolar fluids”. *Journal of Mathematics and Mechanics* (1966), pp. 1–18. DOI: https://doi.org/10.21236/ad0469176.

[98] S.K. Jena and M.N. Mathur. “Similarity solutions for laminar free convection flow of a thermomicropolar fluid past a non-isothermal vertical flat plate”. *International Journal of Engineering Science* 19.11 (1981), pp. 1431–1439. DOI: https://doi.org/10.1016/0020-7225(81)90040-9.

[99] G. Lukaszewicz. *Micropolar fluids: theory and applications*. Springer Science & Business Media, Warszawa, (2012).

[100] G.S. Guram and A.C. Smith. “Stagnation flows of micropolar fluids with strong and weak interactions”. *Computers & Mathematics with Applications* 6.2 (1980), pp. 213–233. DOI: https://doi.org/10.1016/0898-1221(80)90030-9.

[101] C. Fetecau, C. Fetecau, M. Kamran, and D. Vieru. “Exact solutions for the flow of a generalized Oldroyd-B fluid induced by a constantly accelerating plate between two side walls perpendicular to the plate”. *Journal of Non-Newtonian Fluid Mechanics* 156.3 (2009), pp. 189–201. DOI: https://doi.org/10.1016/j.jnnfm.2008.06.005.

[102] T. Hayat, M. Nawaz, M. Sajid, and S. Asghar. “The effect of thermal radiation on the flow of a second grade fluid”. *Computers & Mathematics with Applications* 58.2 (2009), pp. 369–379. DOI: https://doi.org/10.1016/j.camwa.2009.01.040.

[103] M. Husain, T. Hayat, and C. Fetecau. “A note on decay of potential vortex in an Oldroyd-B fluid through a porous space”. *Nonlinear Analysis: Real World Applications* 10.4 (2009), pp. 2133–2138. DOI: https://doi.org/10.1016/j.nonrwa.2008.03.021.

[104] A. Ishak. “Thermal boundary layer flow over a stretching sheet in a micropolar fluid with radiation effect”. *Meccanica* 45 (2010), pp. 367–373. DOI: https://doi.org/10.1007/s11012-009-9257-4.

[105] N.A. Yacob and A. Ishak. “Flow over a stretching sheet in micropolar fluid with radiation effect”. *Journal of Quality Measurement and Analysis (JQMA)* 6.1 (2010), pp. 85–93.

[106] S. Nadeem, M. Hussain, and M. Naz. "MHD stagnation flow of a micropolar fluid through a porous medium". *Meccanica* 45 (2010), pp. 869–880. DOI: https://doi.org/10.1007/s11012-010-9297-9.

[107] H.S. Takhar, R. Bhargava, R.S. Agrawal, and A.V.S. Balaji. "Finite element solution of micropolar fluid flow and heat transfer between two porous discs". *International Journal of Engineering Science* 38.17 (2000), pp. 1907–1922. DOI: https://doi.org/10.1016/s0020-7225(00)00019-7.

[108] C. Chang. "Numerical simulation of micropolar fluid flow along a flat plate with wall conduction and buoyancy effects". *Journal of Physics D: Applied Physics* 39.6 (2006), pp. 1132–1140. DOI: https://doi.org/10.1088/0022-3727/39/6/019.

[109] S. Liao. "General boundary element method: an application of homotopy analysis method". *Communications in Nonlinear Science and Numerical Simulation* 3.3 (1998), pp. 159–163. DOI: https://doi.org/10.1016/s1007-5704(98)90007-7.

[110] S. Liang and D.J. Jeffrey. "Comparison of homotopy analysis method and homotopy perturbation method through an evolution equation". *Communications in Nonlinear Science and Numerical Simulation* 14.12 (2009), pp. 4057–4064. DOI: https://doi.org/10.1016/j.cnsns.2009.02.016.

[111] S. Liao. *Homotopy analysis method in nonlinear differential equations*. Springer, Shanghai, (2012). DOI: https://doi.org/10.1007/978-3-642-25132-0_3.

[112] S. Liao. *Advances in the homotopy analysis method*. World Scientific, Shanghai, (2013). DOI: https://doi.org/10.1142/8939.

[113] T. Fan and X. You. "Optimal homotopy analysis method for nonlinear differential equations in the boundary layer". *Numerical Algorithms* 62 (2013), pp. 337–354. DOI: https://doi.org/10.1007/s11075-012-9587-5.

[114] K. Vajravelu and G.R. Van. *Nonlinear flow phenomena and homotopy analysis*. Springer, Berlin Heidelberg, (2013). DOI: https://doi.org/10.1007/978-3-642-32102-3_2.

[115] R.V. Williamson. "The flow of pseudoplastic materials". *Industrial & Engineering Chemistry* 21.11 (1929), pp. 1108–1111. DOI: https://doi.org/10.1021/ie50239a035.

[116] B.M.J. Rana, S.M. Arifuzzaman, S. Islam, S.K. Reza-E-Rabbi, A. Al-Mamun, M. Mazumder, K.C. Roy, and M.S. Khan. "Swimming of microbes in blood flow of nano-bioconvective Williamson fluid". *Thermal Science and Engineering Progress* 25 (2021). DOI: https://doi.org/10.1016/j.tsep.2021.101018.

[117] U.Z. Khan, A. Zaib, A.W., I. Waini, Z. Raizah, and A.M. Galal. "Features of magnetic field on biological Williamson fluid in radiated blood flow induced by gold particles through a curved moving surface with buoyancy effect". *International Journal of Modern Physics B* 37.03 (2023). DOI: https://doi.org/10.1142/s0217979223500212.

[118] I. Haider, U. Nazir, M. Nawaz, S.O. Alharbi, and Khan i. "Numerical thermal study on performance of hybrid nano-Williamson fluid with memory effects using novel heat flux model". *Case Studies in Thermal Engineering* 26 (2021). DOI: https://doi.org/10.1016/j.csite.2021.101070.

[119] R. Ali, M.R. Khan, A. Abidi, S. Rasheed, and A.M. Galal. "Application of PEST and PEHF in magneto-Williamson nanofluid depending on the suction/injection". *Case Studies in Thermal Engineering* 27 (2021). DOI: https://doi.org/10.1016/j.csite.2021.101329.

[120] S. Nadeem and N.S. Akbar. "Numerical solutions of peristaltic flow of Williamson fluid with radially varying MHD in an endoscope". *International Journal for Numerical Methods in Fluids* 66.2 (2011), pp. 212–220. DOI: https://doi.org/10.1002/fld.2253.

[121] S. Nadeem and S.T. Hussain. "Flow and heat transfer analysis of Williamson nanofluid". *Applied Nanoscience* 4 (2014), pp. 1005–1012. DOI: https://doi.org/10.1007/s13204-013-0282-1.

[122] R.S.R. Gorla and B.J. Gireesha. "Dual solutions for stagnation-point flow and convective heat transfer of a Williamson nanofluid past a stretching/shrinking sheet". *Heat and Mass Transfer* 52 (2016), pp. 1153–1162. DOI: https://doi.org/10.1007/s00231-015-1627-y.

[123] S.U.S. Choi. "Nanofluids: from vision to reality through research". *American Society of Mechanical Engineers Journal of Heat and Mass Transfer* (2009). DOI: https://doi.org/10.1115/1.3056479.

[124] M.P. Mkhatshwa, S.S. Motsa, M.S. Ayano, and P. Sibanda. "MHD mixed convective nanofluid flow about a vertical slender cylinder using overlapping multi-domain spectral collocation approach". *Case Studies in Thermal Engineering* 18 (2020). DOI: https://doi.org/10.1016/j.csite.2020.100598.

[125] S.A. Shehzad, A. Rauf, T. Hayat, M.A. Meraj, and A A. Alsaedi. "MHD stagnation point flow of micro nanofluid towards a shrinking sheet with convective and zero mass flux conditions". *Bulletin of the Polish Academy of Sciences: Technical Sciences* (2017), pp. 155–162. DOI: https://doi.org/10.1515/bpasts-2017-0019.

[126] D. Srinivasacharya and M. Shiferaw. "Magnetohydrodynamic flow of a micropolar fluid in a circular pipe with hall effects". *The ANZIAM Journal* 51.2 (2009), pp. 277–285. DOI: https://doi.org/10.21914/anziamj.v51i0.1835.

[127] S.E. Ahmed, M.A. Mansour, A.M. Rashad, and Z. Morsy. "MHD free convection and sinusoidal heating in a wavy cavity filled with a heat-generating porous medium using cu-water nanofluids". *Computational Thermal Sciences: An International Journal* 12.3 (2020). DOI: https://doi.org/10.1615/computthermalscien.2020030316.

[128] M. Nawaz, S. Rana, I.H. Qureshi, and T. Hayat. "Three-dimensional heat transfer in the mixture of nanoparticles and micropolar MHD plasma with Hall and ion slip effects". *American Institute of Physics Advances* 8.10 (2018). DOI: https://doi.org/10.1063/1.5050670.